PROLIFERATION RISK ASSESSMENT OF A PEBBLE-BED REACTOR

A Dissertation

by

DANY MULYANA

Submitted to the Graduate and Professional School of
Texas A&M University
in partial fulfillment of the requirements for the degree of

DOCTOR OF PHILOSOPHY

Chair of Committee,	Sunil S. Chirayath
Committee Members,	Pavel V. Tsvetkov
	John R. Ford, Jr
	Rupak K. Mahapatra
Head of Department,	Michael Nastasi

August 2021

Major Subject: Nuclear Engineering

ABSTRACT

An analysis of a pebble bed reactor (PBR) system has been completed to assess its proliferation resistance (PR) against multiple special nuclear material-SNM (uranium and plutonium) diversion scenarios. The PR assessment uses data generated using Monte Carlo N-particle (MCNP) code simulations on infinite lattice and full core PBR models. The PR assessment is based on multi-attribute utility analysis (MAUA) technique. A combined intrinsic and extrinsic barriers PR assessment is done using proliferation resistance analysis and evaluation tool for observed risk (PRAETOR) code using 68 attributes. In addition, an intrinsic PR assessment method is developed by utilizing only four attributes: spontaneous fission neutrons, heat load, radiation load, and Rossi-α. Compared to PRAETOR, the new method is more capable to differentiate PR of Pu diversion scenarios with respect to PBR operations.

This study finds that the spent fuel of PBR is more attractive for proliferation if the fuel has a higher ^{235}U enrichment and/or lower burnup level. A full core modeling and simulation on a one-batch refueling scheme shows that if HTR-10, a PBR-type is rescaled to 250 MWth, it would yield 1.9 significant quantity (SQ) of plutonium and 1.73 SQ of low enriched uranium (LEU) per year with a fissile plutonium quantity of 82.9% at a fuel burnup of 65.9 GWd/MTU. A once-through-then-out (OTTO) refueling scheme enables the fuel to reach a higher burnup level, resulting in less leftover ^{235}U and fissile Pu content in the spent fuel compared to the one-batch refueling scheme. A 3-pass refueling scheme discharges fuel with 5.6% less fissile plutonium content (at 0.0414 g per pebble) and 3.1%

total plutonium content (at 0.0532 g per pebble) than the OTTO, but it leaves slightly higher ^{235}U by 0.3% (at 0.357 g per pebble). At fuel burnup of 80 GWd/MTU, the intrinsic PR of the 3-pass refueling scheme is 0.3109 ± 0.004 that is practically the same as the OTTO refueling scheme (0.3037 ± 0.0044).

The PBR system has a lower intrinsic PR than the current technology of Pressurized Water Reactor (PWR). An intrinsic PR comparison on integrated PWR (iPWR) and PBMR-400 designs at a same rated output power of 500 MWth with a one-batch refueling scheme is performed using the new methodology. In terms of Pu diversion, the PR of PWR system (0.345 ± 0.002) is higher than the PBR (PBMR-500) system (0.282 ± 0.001) while both reactors have a similar PR of U diversion (PWR: 0.263 ± 0.001 vs. PBR: 0.261 ± 0.001).

This study showed that the PRAETOR code formalism is comparatively less useful in differentiating between SNM diversion scenarios in PBR' case, if a large number of intrinsic and extrinsic attributes (such as 68 used in this study) are utilized, compared to the new four-intrinsic-attribute method developed.

DEDICATION

To my parents, my wife, and my children

ACKNOWLEDGEMENTS

Allah is my only superior, who put me at this point.

I would like to thank my committee chair, Dr. Sunil Chirayath who never gave up on me, and my committee members, Dr. Pavel Tsvetkov, Dr. John Ford, and Dr. Rupak Mahapatra, for their guidance and support throughout the course of this research. Also, thanks to Ms. Kelly Ragusa who always got my back for any of my English matter.

Thanks also to my friends, my colleagues, and faculty and staff members in the Department of Nuclear Engineering at Texas A&M University for making my time at the university a great experience.

Last, but not the least, thanks to my mother and father for their strong encouragement even though from remote, to my wife, Siska, and to my cute and cheerful children, Luthfia and Lintang for their support, patience, love and for moments that we passed together during this period with tears and cheers.

CONTRIBUTORS AND FUNDING SOURCES

Contributors

This work was supervised by a dissertation committee consisting of Professor Sunil S. Chirayath, Professor Pavel V. Tsvetkov, and Professor John R. Ford, Jr of the Department of Nuclear Engineering and Professor Rupak Mahapatra of the Department of Physics.

The proliferation resistance assessment methodology presented in Chapter 2 was under guidance of Professor Sunil S. Chirayath. All other work conducted for the dissertation was completed by the student independently.

Funding Sources

Graduate study was supported by a fellowship from The Ministry of Research and Technology of Indonesia through RisetPro Initiative and was also supported by Texas A&M internal funds managed by Dissertation Committee Chair, Prof. Chirayath.

NOMENCLATURE

FFP	Fresh Fuel Pebble
HEU	Highly Enriched Uranium
HTGR	High Temperature Gas-cooled Reactor
HTR	High Temperature Reactor with pebble fuel
IAEA	International Atomic Energy Agency
iPWR	Integrated Pressurized Water Reactor
KMP	Key Measurement Point
LEU	Low Enriched Uranium
LWR	Light Water Reactor
MAUA	Multi-Attribute Utility Analysis
MBA	Material Balance Area
MBP	Material Balance Period
MCNP	Monte Carlo N-Particle code
MUF	Material Unaccounted For
OTTO	Once-Through-Then-Out
PBMR	Pebble Bed Modular Reactor
PBR	Pebble Bed Reactor
PR	Proliferation Resistance
PRAETOR	Proliferation Resistance Analysis and Evaluation Tool for Observed Risk

PWR	Pressurized Water Reactor
R	Proliferation Risk
SFP	Spent Fuel Pebble
SMP	Strategic Measurement Point
SMR	Small Modular Reactor
SNM	Special Nuclear Material
SQ	Significant Quantity

TABLE OF CONTENTS

LIST OF FIGURES

Page

LIST OF TABLES

Page

1. INTRODUCTION

1.1. Topic and context

The pebble bed reactor (PBR) is one of the generation IV reactor designs that offers improvements for most safety issues in comparison to previous reactor generations. It uses graphite as a neutron moderator, helium as a coolant and working fluid, and pebble-type enriched uranium fuel. Each pebble contains thousands of tri-isotropic (TRISO) coated uranium spheres and is capable of keeping the fuel and its fission products intact given the high-temperature operation scenario. The pebble-type fuel also enables refueling to maximize the fuel burnup. With the proper refueling scheme, the fuel can reach up to 90 GWd/MTU or more, which is about twice that of light water reactor (LWR) spent fuel.

The PBR design originated in 1947 at Oak Ridge national laboratory (Simnad 1991). Its development was successfully demonstrated in Germany through the arbeitsgemeinschaft versuchsreactor (AVR) in 1967. The AVR is a 46 MWth test reactor producing a 15 MWe output that successfully operated for 21 years. It was followed by the development of the General Atomics 330 MWe power reactor at Fort St. Vrain, USA in 1974 and the thorium high temperature reactor (THTR), a 300 MWe designed in Germany in the 1980s (Ion, et al. 2004). The General Atomic design used a hexagonal fuel design instead of pebble fuel. Unfortunately, these reactor developments were abandoned due to some rising mechanical issues and the coincidence with the Chernobyl accident.

China has been proceeding with the PBR's development and commissioned a 10 MWth high-temperature test reactor (HTR-10) project in development since the early

1990s. The HTR-10 was intended to be a test reactor ready for upscaling to a higher power reactor with a modular design called the high temperature reactor pebble-bed module (HTR-PM). The reactor has a working fluid with a temperature inlet of approximately 350 ^{o}C and an outlet of 700 ^{o}C, resulting in a thermal efficiency of approx. 50% (Wu, Lin and Zhong 2002). This gives it an economic benefit for co-generation purpose in addition to its use for generating electricity. It was followed by the pebble bed modular reactor (PBMR) project in South Africa with a 400 MWth power reactor design (PBMR-400). Slightly different from the HTR-PM design, the PBMR-400 has a central graphite structure as a reflector to produce higher power; however, both reactors use the same pebble fuel design with different uranium enrichments.

The PBR selected for this dissertation study utilizes low enriched uranium (LEU) in the form of TRISO-coated spheres with a diameter of 0.091 mm. Around 7,000 to 15,000 TRISOs containing 5 to 9 g of uranium are loaded into a pebble with a diameter of 6 cm (Wu, 2002; Dudley, et. al, 2008; IAEA-TECDOC-1694). The space between the TRISOs and the 1 cm thickness of the outer radius are filled by graphite as neutron moderator. Approximately 29,000 pebbles are loaded into the core of the HTR-10 loads to produce a 10 MWth power (Wu, 2002). Approximately 451,530 mixed pebbles are loaded into the core of the PBMR-400 to produce 400 MWth (Dudley, et al. 2008). They have the same pebble design but different fissile loading settings in the pebble. The HTR-10 uses 17wt% initial ^{235}U enrichment with 5 g uranium per pebble (Wu, 2002; IAEA-TECDOC-1694) while the PBMR-400 uses 9.6wt% UO_2 with 9 g uranium per pebble for a target burnup of 90 GWd/MTU (IAEA-TECDOC-1694). The pebble and TRISO designs

enable fission product retention during and after neutron irradiation in the core and ensure no gases are released during its lifetime.

As with light water reactors (LWR), a portion of the fuel in the PBR must be replaced (refueled) after a certain period. The fuel of the PBR is much smaller than that of the LWR, enabling a higher refueling rate. The refueling can be done without shutting down the reactor, which is termed online refueling. The online refueling enables each pebble to achieve a certain burnup level. In general reactor application, a lower burnup level raises proliferation concerns, as the leftover ^{235}U is high and the produced plutonium would be of weapons grade quality with a larger content of fissile plutonium.

Teuchert and Hass showed that uranium with a higher ^{235}U enrichment mixed with thorium as fuel for the PBR leads to a lower production of plutonium (Teuchert and Haas 1986). They also found that the mass of fissile plutonium isotopes (^{239}Pu and ^{241}Pu) in PBR spent fuel, with an 8 wt% starting ^{235}U enrichment, is 0.17 kg/GW(electric).day compared to 0.578 kg/GW(electric).day in a LWR discharged fuel assembly, with a 3.2 wt% ^{235}U enrichment. The total amount of Pu produced in PBR spent fuel is 1.5% of the initial uranium loading and thus less attractive for proliferation because of the low plutonium quality (the fissile plutonium content is only 45%) compared to LWR spent fuel with a fissile Pu content of 69% (Teuchert and Haas 1986). The Teuchert and Hass study also showed that the amount of ^{238}Pu present in spent fuel could complicate the spent fuel handling due to its decay heat and spontaneous fission neutron rate. Although they described the proliferation benefit of PBR, no details of quantitative methodology to assess proliferation resistance (PR) can be found in their work.

The proliferation risk of advanced reactors must be assessed quantitatively to assure their applicability for peaceful nuclear energy programs. So far, the international atomic energy agency (IAEA) has not been able to finalize a safeguards system to be applied to the PBR design. Hence, there is a risk in moving forward with the deployment of PBRs without incorporating safeguards measures.

The risk of nuclear proliferation (R) is determined by:

$$R = P_A \times P_S \times C. \tag{1}$$

where, P_A is the probability of a state pursuing certain proliferation pathway, the P_S is the probability of a State's success for that pathway, leading to the measurable consequence (C). From an engineering perspective, P_S is the most controllable parameter through the implementation and enforcement of nuclear safeguards measures in order to mitigate the overall risk. The P_S can be minimized through maximizing PR, which are the intrinsic and extrinsic barriers offered by a system (in this study, the PBR). This study focuses on the analysis of the PR metric for a typical PBR to recommend measures to mitigate their proliferation risk.

For a nuclear energy system, PR is defined as any characteristic the system which impedes the diversion, or undeclared production of nuclear material, or misuse of technology by States in order to acquire nuclear weapons or other nuclear explosive devices (IAEA, 2002). The basic principle of PR requires that both intrinsic and extrinsic barriers be implemented throughout the life cycle of an innovative nuclear energy system to ensure that the system will continue to be unattractive as a means of acquiring SNM for use in a nuclear weapons program.

A nuclear system consists of main and supportive sub-systems. A main system is primarily optimized to meet its safety requirements. The supportive systems are optimized to avoid any single point failure that may arise in the main system. The nuclear system must also be optimized to provide its highest PR. PR optimization is based on the intrinsic and extrinsic features of the nuclear system. During its design phase, the intrinsic features can be optimized by changing basic technical parameters. However, once the design phase is complete, there is only a limited possibility to change the intrinsic features of the reactor. The extrinsic features are very likely to take part in the nuclear system once it is designed. Both features must be quantified to obtain an optimal PR of the nuclear system.

A methodology, based on multi-attribute utility analysis (MAUA), had been developed to assess the PR using 68 intrinsic and extrinsic attributes for various nuclear fuel cycles(Charlton, et al. 2007) (Chirayath, Elmore, et al. 2015). The method determines a PR value that can be used to compare various nuclear energy systems. The method, which was coded in Fortran 90, was later named PRAETOR (proliferation resistance analysis and evaluation tool for observed risk).

The PRAETOR code has been used to evaluate the fast breeder reactor fuel cycle with both uniform and expert weights, with and without extrinsic nuclear safeguards measures in place (Metcalf 2009). Special nuclear material (SNM) diversion scenarios for pressurized water reactor (Chirayath, Elmore, et al. 2015) and small modular reactor (Kitcher, 2012) (Kitcher, Performance and Safety Analysis of Generic Small Modular Reactor 2012) were successfully analyzed using PRAETOR to get insights into the facilities' PR characteristics. A PR study of an inert matrix fuel (IMF) in the transuranic

nuclear fuel cycle (NFC) of a high temperature gas reactor prismatic fuel (not pebble fuel) relative to the uranium and plutonium mixed-oxide (MOX) NFC of an LWR was also performed using PRAETOR (Aoki, Chirayath and Sagara 2020). The study was able to recommend a reduced safeguards inspection frequency goal to manage the IMF.

A study on the safeguards approaches for PBR can be found in Durst et. al, 2009 and 2012, which provides a concept based on the LWR safeguards approach. One challenge mentioned in the work is the lack of realistic simulation and modeling of PBR to determine the nuclear material content of core fuel and spent fuel pebbles to design an adequate safeguards system. Designing an appropriate safeguards approach for a certain fuel cycle depends heavily on the intrinsic characteristics of the reactor, especially on the transmutation mechanism is uses to produce the SNM.

The SNM quantity and the quality that define the intrinsic PR are parts of the nuclear reactor design. A lack of practical experience with any advanced reactor design raises some issues in defining its produced SNM quality and quantity. Computational modeling and simulations are the only ways to calculate the SNM production at this stage.

1.2. Focus

This study focuses on the proliferation risk assessment of a PBR system by carrying out an analysis on mitigating proliferation risk. The reactors analyzed in this study are the HTR-10, HTR-PM and PBMR-400, and their various refueling strategies are considered. The risk analysis methodology utilizes an established MAUA method.

A comparative PR analysis of a PBR (an advanced reactor technology) and an LWR (current reactor technology) is the highlight of this study. The data for the analysis was generated using the Monte Carlo N-particle Version 6.1 (MCNP) reactor physics simulation code) (Pelowitz 2013).

1.3. Objectives and Outcomes

The objectives of this dissertation are:

a) To develop a new methodology of assessing the intrinsic PR of the HTR-10 by involving the Rossi-α parameter as a new attribute for PR evaluation.
b) To investigate the significance of various refueling schemes of the HTR-10 on PR.
c) To compare the PR of the PBR with one of the latest PWR designs.
d) To develop a new safeguards approach for the PBR.

The outcomes of the study that could benefit society are:

a) introducing a framework to integrate a safeguards system in PBR design to support the safeguards-by-design approach; and
b) introducing a new algorithm to choose a nuclear energy system with reasonably low proliferation risk.

1.4. Overview of the structure

This dissertation is arranged in five chapters. Chapter 1 introduces the background and objectives of the study. Chapter 2 describes the methodology development for

performing the PR assessment of the PBR using an infinite lattice modeling in MCNP, where the developed PR is compared with PRAETOR's calculated result. Chapter 3 describes the full-core reactor modeling and simulations based on the PBR's refueling schemes that were used to understand how these schemes change the SNM production and the overall intrinsic PR values. Chapter 4 provides an intrinsic PR comparison and analysis between PBR and PWR technologies. Chapter 5 describes a safeguards approach for the PBR system. Chapter 6 provides conclusions of the study.

2. PROLIFERATION RESISTANCE ASSESSMENT METODOLOGY

2.1. Introduction

This chapter describes the PR assessment methodology used for the PBR. The methodology utilizes information on both intrinsic and extrinsic PR attributes and performs a MAUA analysis. The data required to prepare inputs for the MAUA analysis were generated using reactor physics simulations employing the Monte Carlo N-Particle radiation transport code, MCNP 6.1. The simulation uses an infinite lattice reactor model of HTR-10 fuel. The fuel and lattice information for the simulations are derived from HTR-10's technical specification, but the results are extended to HTR-PM, which has a 25 times higher rated power output.

2.2. HTR-10 overview

The 10 MWth high-temperature gas-cooled test reactor (HTR-10) is a modular pebble bed type reactor designed to comply with some advanced design features. It is designed: 1) to use pebble and TRISO structures that are capable of containing fission products up to 1600 ^{o}C; 2) to enable the core to maintain the fuel element temperature under 1600 ^{o}C at any conditions; 3) to have a passive cooling system; 4) to shut down the reactor using control rods only; 5) to use graphite withstanding 1600 ^{o}C; 6) to use helium as a coolant; 7) to avoid the need for a pressure-tight reactor building; and 8) to separate the reactor core from the steam generator installation (Wu, Lin and Zhong 2002).

As an experimental reactor version of the small modular reactor (SMR) PBR design, its small size makes the HTR-10 suitable for both safety and proliferation risk

study. The HTR-10 uses graphite pebbles embedded with low enriched uranium (LEU) TRISO particles as fuel in the core and helium gas as the coolant. The pebble fuel is expected to achieve a maximum temperature of 919 ^{o}C at normal operation. The HTR-10 core has approx. 27,000 graphite pebbles. Each pebble contains 5 g of uranium in the form of enriched uranium dioxide (Wu, Lin and Zhong 2002). The reactor is expected to achieve an average fuel burnup of 80 GWd/MTU, which is achievable by passing the pebbles axially through the core multiple times using gravity. This allows an online refueling capability for continuous, uninterruptable operation. To deal with any excess reactivity, the fuel can be mixed with neutron poisons, such as boron, in the same pebble or separated into different pebbles (Tran and Hoang 2012).

With a volume of 5 m^3, the HTR-10 core can produce 10 MWth of power with a target burnup of 80 GWd/MTU through an online refueling scheme. The uranium oxide density is typically 10.4 g/cm^3 with an ^{235}U enrichment of 17 wt% (IAEA TECDOC 1694). The pebble has a diameter of 6 cm with its inner 5 cm containing the TRISOs. The core itself is 90 cm in radius and 2 m in height. The volumetric filling fraction of the pebbles in the core is approximately 61%.

With the HTR-10 design, each fuel pebble has approximately 8000 to 9000 TRISO particles per pebble. However, this number depends on the amount of the uranium loaded in the pebble. Each TRISO particle has dimensions as shown in Figure 2-1 with an outer diameter of about 0.91 mm (IAEA TECDOC 1694). The buffer layer is filled by graphite with a density of 1.1 g/cm^3. The inner PyC has a density of 1.9 g/cm^3. The SiC has a density of 3.18 g/cm^3, while the outer PyC has a density of 1.9 g/cm^3. The pebble itself

has a radius of 3 cm, of which the inner 2.5 cm of its radius contains the TRISOs. The uranium free zone (the outer 0.5 cm of the radius) in the pebble and the space between the TRISOs in the uranium zone are filled by graphite having a density of 1.73 g/cm^3.

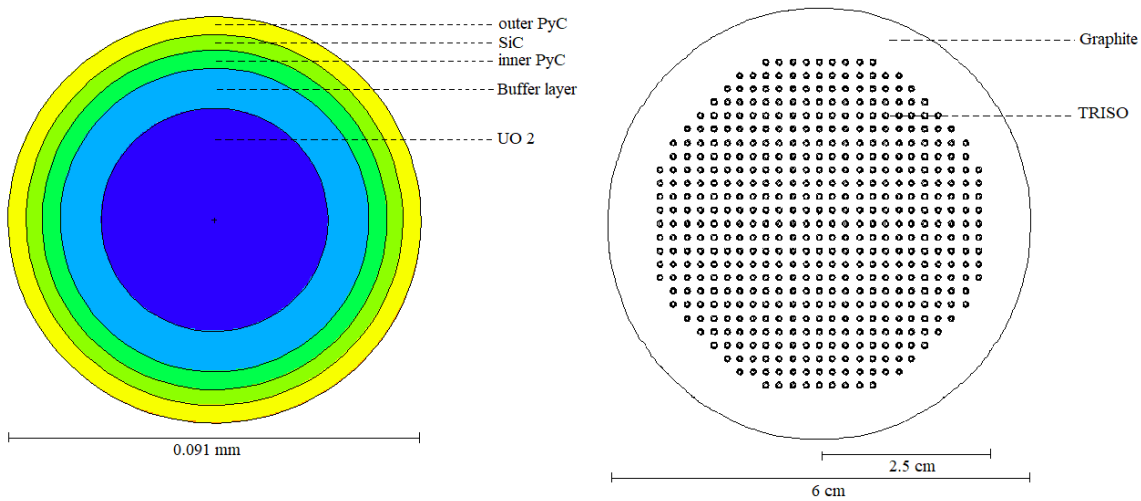

Figure 2-1. TRISO fuel design (left) and a pebble fuel containing the TRISO (right). Sizes are not to scale.

During starting up, the core can be configured with several strategies to achieve criticality safely. This can be done by filling up the core with fuel and pure graphite pebbles to a ratio of 57-43 (IAEA TECDOC 1694). Once it reaches criticality, the reactor is refueled online with the same pebble ratio. To increase the power, the graphite pebbles are gradually replaced with the fuel to increase the fuel to moderator ratio. With a proper reactivity control, the core may also be fully loaded by only fuel pebbles without any pure graphite pebbles. However, the effect of startup on the nuclide production is not the focus of this study. Instead, this proliferation resistance assessment study assumes that the fuel cycle is based on PBR's equilibrium operation at certain fuel burnup target values.

2.3. Methodology

2.3.1. Reactor Physics simulation with MCNP

Assessing the PR of a nuclear system requires detailed information about the material involved in the system. Material quantification can be performed in different ways. In the case where no practical data is available, a numerical transport code can be used to simulate the operation of a reactor. Generally, there are two types of numerical transport codes: deterministic and stochastic. A deterministic code takes less time for simulation but has difficultly in adapting to a complex geometry. Unfortunately, however, a deterministic code for a relatively new reactor design is rarely available. As the PBR is not yet marketed, no code was available for this study.

A stochastic code, such as MCNP, takes a much longer time for reactor physics simulations since it mimics the stochastic nature of radiation transport more realistically. However, MCNP is capable of handling the complex geometry of the reactor. IAEA-TECDOC-1382 provides a comprehensive reactor simulation study using Monte Carlo and diffusion calculations. Wu, et al. (2019) present a burnup computation for HTR-10 employing layer-to-layer movement to simulate the online refueling using a layer-mixed-shell fuel movement model. An MCNP simulation study by Acir and Coskun on the neutronics and fuel burnup of a PBMR-400 fueled by reactor-grade plutonium and minor actinides from the spent fuel of LWR is available (Acir and Coskun 2012). Another MCNP simulation study by Turkmen and Colak reveals that the effect of pebble packing on neutron spectrum and isotopic composition and reported that the effect is less significant (Turkmen and Colak 2012).

This study uses MCNP 6.1 to quantify the nuclide production in a PBR, although some other codes could also have been used. Wang et al. (2013) show criticality calculations on the HTR-10 using SCALE6/CSAS6 and MCNP5 and the same ENDF/B-VII.0 cross section library for both codes. They found a neutron reactivity difference of 680 pcm for high-fidelity models and approx. 200-250 pcm for infinite lattice configurations, but both codes have consistency in their neutron spectra. Therefore, the results may vary based on the choice of different reactor physics simulation computer codes. However, a code comparison is not the focus of this study.

The first step in a reactor physics simulation using MCNP is to define the required geometry of the reactor model. To minimize the simulation resources, this study deploys an infinite lattice simulation of a fuel pebble lattice rather than a full core simulation to calculate neutron multiplication and other reactor dependent parameters. With MCNP, this type of simulation can be performed by applying a reflective boundary condition on all sides of the pebble's lattice to estimate the infinite neutron multiplication factor, k_∞ instead of effective neutron multiplication factor, $k_{\text{eff.}}$ k_∞ is usually higher than k_{eff}. However, the transmutation mechanism of actinides should be the same with the full core simulation.

The lattice configuration used to arrange the TRISOs in a pebble and the pebbles in the core depend on their volumetric packing fraction requirements. In a PBR application, several arrangements can be made (Rosales, et al. 2014). Since packing TRISOs in the ball does not require a tight arrangement, a simple cubic (SC) lattice with a maximum packing fraction of 52.36% is sufficient to arrange the TRISOs in the fuel

ball. Kepisty, et. al. (2016) present that, at a low packing fraction, the Monte Carlo simulations using a SC and a simple hexagonal lattice structure provide similar results.

The space between TRISOs in the pebble is filled with graphite. The SC arrangement for the TRISOs in the pebble can be assigned easily in MCNP through a cubical lattice definition. The total number of TRISOs in the fuel pebble depends on how much uranium is expected in it. It defines the lattice size to be used for the SC. In this study, each pebble is loaded with 5 g of UO_2, making the total uranium in the pebble equal to 4.41 g. Since the diameter of the TRISO is 0.91 mm, the exact number of TRISOs in each pebble is 7345.61, and its optimum number is 7,223 if no clipped TRISOs are included (ref. Figure 2-2). Taking the optimum number, each TRISO has 0.61 mg of UO_2. With this configuration, the cube lattice has a side of 0.1876 cm. The space between TRISOs in the pebble is filled with graphite with a density of 1.73 g/cm^3.

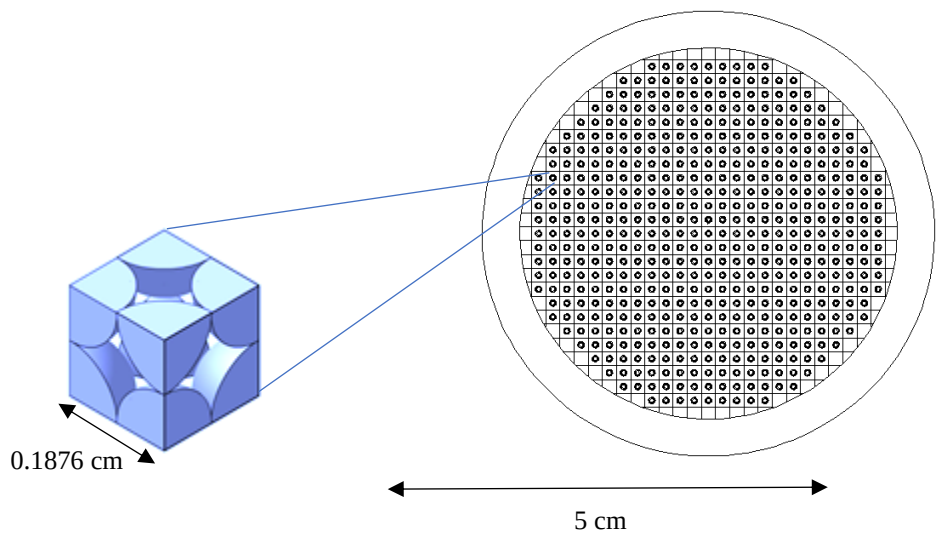

Figure 2-2. A simple cubic (SC) arrangement of TRISOS in a pebble

To arrange the pebbles in the PBR core, a body-centered cubic (BCC) arrangement (ref. Figure 2-3) with a maximum packing fraction of approximately 68% is used, since

both the HTR-10 and the PBMR-400 designs require a packing fraction of about 61%. However, other arrangements, such as a face centered cubic (FCC) or a hexagonal close-packed (HCP) having packing fractions over 70%, may also be used. The BCC arrangement contains two full-volume spheres in a cube lattice. The pebble sphere of the PBR has an outer radius of 3 cm, totaling a volume of 113.1 cm^3. Since the requirement of the packing fraction is 61%, the side of the lattice cube is 7.18 cm. If the packing fraction for BCC is maximized to 68% with the same pebble size, the side of the lattice cube will decrease to 6.93 cm. The space between the pebbles in the cube lattice is filled by helium, which act as coolant and working fluid with a density of 0.00016 g/cm^3. With a packing fraction of 61%, the HTR can contain 29,106 pebbles in total. Therefore, for the core power of 10 MWth, each single fuel pebble is equal to a power of 343 Wth.

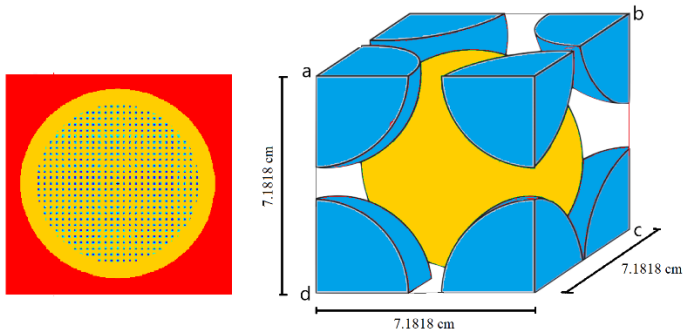

Figure 2-3. Fuel pebble design. TRISO particles inside fuel pebble layout for the MCNP input, where the yellow-colored outer graphite structure housing the TRISO particle dots is surrounded by helium gas in red (left) and a BCC in MCNP input where the yellow is the fuel pebble and the blue is also the same fuel pebble (color differentiation is only for the ease of visualization).

To meet the needs of this proliferation resistance assessment study, there are three main parameters that would affect the target nuclides (uranium and plutonium) depletion

and production: fuel burnup; cooling period; and initial ^{235}U enrichment. Nevertheless, to simplify the analysis, the cooling period is excluded and is fixed at only one year.

The chosen ^{235}U enrichment values for the fuel are 4.95 wt%, 10 wt%, and 17 wt%. The 4.95 wt% represents a common enrichment value used in a typical LWR, while 17 wt% is the enrichment used in the HTR-10. The 10 wt% is chosen as a mid-value between the two. The nuclide quantity data are extracted for burnup values of 5, 10, 25, 35, 45, 65, 75, 80, and 90 GWd/MTU. The highest burnup is slightly higher than the prescribed one for the HTR-10 of 87.7 GWd/MTU (Wu, 2002). Fuel burnup values that are lower than the average are used to represent reactor operations, where the reactor could be misused to produce a high-quality plutonium. This means the system is expected to reach the target fuel burnups of 5, 10, 25, 35, 45, 65, 75, 80, and 90 GWd/MTU within 64, 238, 321, 449, 577, 830, 962, 1026 and 1154 days, respectively.

The MCNP simulations use ENDF/B-VIII.1 nuclear cross-section data at 1200 K for all materials. All the MCNP simulations use a two-node computer cluster holding twenty processors in total. Each simulation uses 3 million (15,000 particles per each of 200 cycles) neutron transport histories to result in a stochastic standard deviation for k_∞ at less than 50 pcm.

Although the reactor model used in this study is an HTR-10 with a power level of only 10 MWth, the simulation result is applicable to any power level by multiplication, provided that the fuel parameters are the same. Since the HTR-PM is an upgraded reactor based on the HTR-10 design, its power of 250 MWth gives a multiplication factor of 25

for all the simulated material quantities using HTR-10 fuel lattice when assuming the fuel parameters do not change, especially for the initial uranium loading.

2.3.2. Proliferation resistance assessment with PRAETOR code

The PR analysis and evaluation tool for observed risk (PRAETOR) was developed within the Nuclear Engineering Department of Texas A&M University. The PRAETOR code performs MAUA analysis in three tiers with different attributes to describe the system being analyzed for PR (ref. Figure 2-4).

PRAETOR code uses sixty-eight attributes as inputs to calculate the PR (Chirayath, 2015). These attributes are grouped into three tiers. The final PR value is the third tier. The second tier is divided into 4 stages (ref. Figure 2-4): Stage 1 (diversion); Stage 2 (transportation); Stage 3 (transformation); and Stage 4 (weaponization), which describe the stages of nuclear material proliferation. Each stage is split into subcategories, and these subcategories represent the first tier, which is comprised of several attributes as inputs. Some attributes in a subcategory may be similar or completely the same as another subcategory of a different stage depending on the assumptions made for each stage.

The reason for utilizing the tiers is to provide an understandable measure for policy makers to analyze the system under management. For policy makers, the system is usually evaluated at tier 3, or as the final PR for calculating the needed resources to mitigate the overall proliferation risk. However, if any system manager needs to trace which area needs optimization, the second and first tiers are the levels that should be evaluated prior to directly finding which attribute needs a detailed optimization.

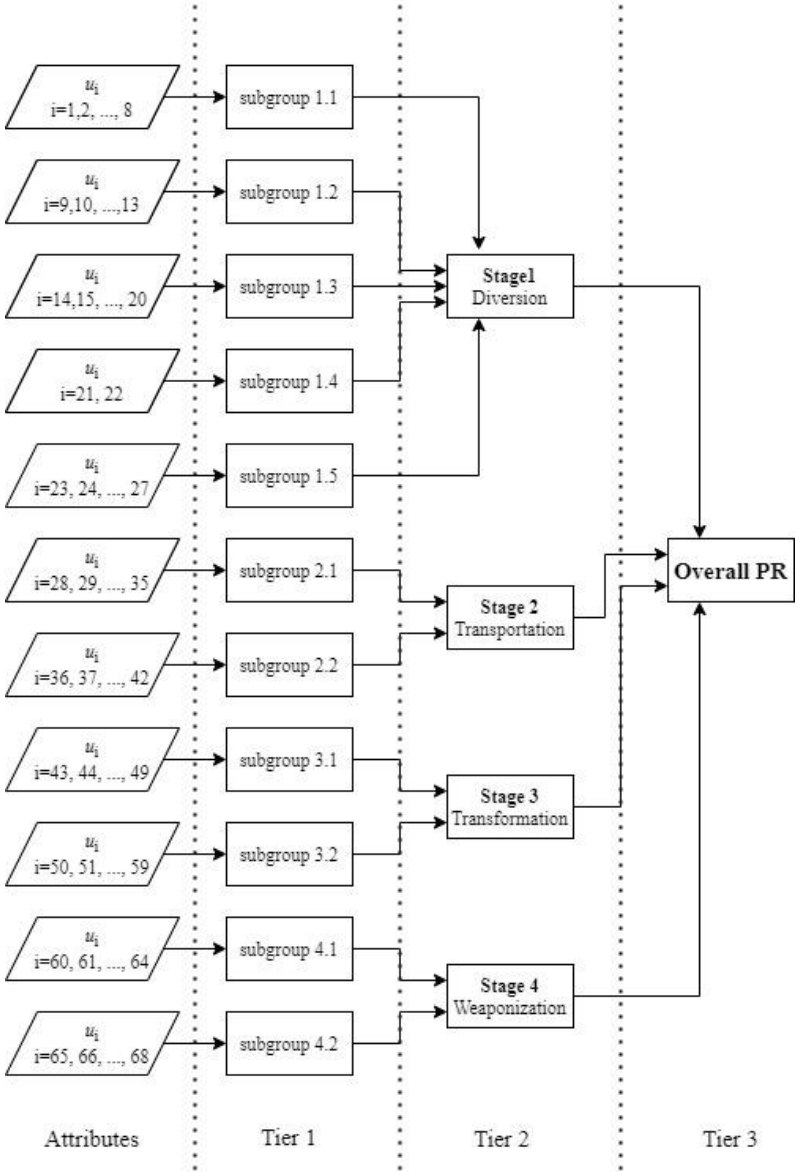

Figure 2-4. PRAETOR tier aggregation scheme

The sixty-eight attributes can generally be classified into intrinsic and extrinsic PR attributes (ref. Table A.1). The intrinsic attributes are those that result from the technical design of nuclear energy systems, while the extrinsic attributes result from supporting or additional sub-systems applied within the system. The extrinsic attributes naturally follow the intrinsic. The attribute optimization is expected to take place in a design phase to

minimize safeguards costs from the operator's and the vendor's perspective. The IAEA encourages a safeguards-by-design concept for simplifying safeguards application on any nuclear facilities.

PRAETOR uses the multi-attribute utility analysis (MAUA) aggregation scheme to calculate the overall PR from the multi-attributes input. MAUA simplifies multi-criteria decision-making, converging into a single criterion by using weighting factors for each of the attributes defined through a survey completed by experts (Chirayath, 2015). PRAETOR employs this weighting scheme for general use (ref. Table A.1).

PRAETOR uses the following two functional forms of the MAUA function (Chirayath, 2015):

$$U(x_1, x_2, \dots, x_n) = \sum_{i=1}^{n} k_i u_i(x_i) \quad \text{(Eq. 2.1)}$$

$$1 + KU(x_1, x_2, \dots, x_n) = \prod_{i=1}^{n} (1 + K k_i u_i(x_i)) \quad \text{(Eq. 2.2)}$$

where U is the overall utility value for a certain tier of all attribute values x_i, while u_i are utility functions normalized from 0 to 1 for each attribute value. The k_i values are weighting factors for each attribute, while K is a scaling parameter.

These two forms (additive and multiplicate MAUA) are the options that can be selected while using PRAETOR code for performing PR assessment. Eq. 2.1 is an additive functional form that is mostly useful and beneficial if the analyst's goal is to find a system that performs well against as many measures of PR, or technological options, as possible. However, this form relies heavily on the weighting factor. If the utility function goes to unity while the weight is low, the overall utility value will be low. Eq. 2.2 is a multiplicative form that allows extreme values of the utility function to affect the result

more heavily. However, the multiplicative form is less sensitive to changes in intermediate values, although it would still serve adequately in comparing two technology options against one another. As this study aims to rely less on the more subjective weighting factors, the multiplicative form is chosen to be performed within PRAETOR.

This study focuses on the intrinsic parameters. Hence, not all of the sixty-eight attributes within PRAETOR are determined quantitatively. Although there are nineteen attributes considered as intrinsic attributes included in PRAETOR related directly to nuclear and radiation properties, only twelve of them need to be quantified through MCNP simulations: κ_1, κ_2, …, κ_{12} (ref. Table A.1). The seven others can be derived from some of the other twelve. Most quantities in Table A.1 are normalized to 1 significant quantity (SQ) of Special Nuclear Material. For a low enriched uranium (LEU), 1 SQ is equal to a 75 kg of ^{235}U. For plutonium, however, 1 SQ is 8 kg regardless of its isotopic composition. During stage 4, the weaponized spent LEU fuel becomes a sphere of HEU changing the SQ to 25 kg of ^{235}U. There are also other intrinsic characteristics that are not computable using MCNP, since they are qualitatively determinable, e.g., attribute number 4, 6, 7, 12, 30, 33, 34, 35, 53, 59, 64, 66, and 67 (ref. Table A.1).

The extrinsic parameters are attribute numbers 9, 10, 11, 13, 16, 17, 18, 19, 20, 21, 22, 23, 24, 25, 26, 27, 42, 43, 51, 52, 55, and 56 (ref. Table A.1). Attribute numbers 14, 15, 40, 41, 44, 45, 46, 47, 48, 49, 50, 54, 63, and 68 are hypothetical attributes based on proliferator's characteristics. These attributes are set to minimum or maximum values, depending on which one leads to the minimum PR. However, it is not viable to set an

extreme value for any hypothetical attribute, so Indonesia is used and assumed to be a "typical country" with average values for these attributes.

The diversion targets considered are leftover ^{235}U and plutonium in spent fuel. The MCNP depletion simulation yields a set of data for all simulated nuclides, including the leftover ^{235}U and plutonium. Mass data for both materials can be extracted directly from the MCNP output. A complete methodology by Chirayath, et al. (2015) on how to perform PRAETOR calculation can be followed.

The mass (κ_1), the volume (κ_2), the number of item (κ_3), and the volume of non-occurring gas (κ_8) are derived directly from the ^{235}U, Pu, and gases masses per spent fuel pebble simulated through MCNP. The radiation dose levels (κ_4) are simulated using MCNP on a single fuel pebble model. The model uses the previously calculated masses. The radiation dose accounts for spontaneous neutrons, (n, γ), and gamma radiation using a ring detector tally of F5 in MCNP. This ring tally is located at 1 m away from the outer surface of the spent fuel. The tally uses 20 million simulated particles to provide a good statistical interference.

When simulating the neutron radiation from SF (spontaneous fission) and photon from neutron capture reaction, the starting particle is specified as "SF" in the source definition input with a proper multiplier for each case. To calculate the gamma from the spontaneous decay, a separate simulation is carried out using photons in the source definition input as the starting particles. The heat load (κ_5) calculation also accounts for the same radiation modes simultaneously but using a different heat deposition estimator, which accounts for the energy deposition within the volume of the pebble.

Since the radiation load coming from the spent fuel pebble is dominated by gamma particles, the shielding thickness needed for the transportation (κ_6) calculation assumes an exponential law for only the gamma ray, since it dominates the radiation within stage 2. A half-value layer (HVL) of 0.578 cm is predicted by MCNP simulations using lead as the shield.

The calculation for the radiation load during transformation (κ_7) assumes that the spent fuel is separated from all the pebble's graphite. It is modeled as a sphere with a radius of 0.45 cm and the same density of 10.4 g/cm^3. The calculation also uses a point estimator at a distance of 1 m away from its outer surface.

The spontaneous fission neutrons (κ_9) value is calculated directly using constants for the isotopic composition calculated by the reactor physics depletion simulation (Stewart 1991). The sphere's radiation load (κ_{10}) can be calculated simultaneously using a point detector estimator at a distance of 1 m from the SNM sphere's surface. The load also represents the radiation level (κ_{12}) with a different unit of Sv.h^{-1}SQ^{-1}. This estimator calculates neutron currents on a surface at radii of 7.03 and 4.58 cm of the HEU and plutonium spheres, respectively. The simulation also uses 20 million particles to provide a good statistical convergence. The starting particle is set as SF in MCNP's SDEF card.

The heat load (κ_{11}) calculation uses MCNP's energy deposition estimator on the SNM's spheres through four separated simulations. One simulation calculates the heat from energy deposited by spontaneous fission neutrons. The second simulation calculates the heat by photons from spontaneous decay. The third one calculates the heat from alpha radiation, and the last one calculates the heat from beta radiation. Energy deposition by

photons as a product of the (n, γ) reaction by spontaneous neutrons is not calculated since it would be less significant.

2.3.3. Simplified MAUA methodology for PR assessment

PR assessment using PRAETOR is comprehensive but may be less conducive for the PBR case. PRAETOR considers four stages of proliferation. In the case of the PBR, one of the attributes, the number items needed to divert 1 SQ of plutonium, biases the results of PRAETOR. This is because the number of items (fuel pebbles) needed is more than 100,000 and may even reach into the millions. In the case of LWRs, this attribute is reasonable, because the total plutonium contained in one assembly is about 5 kg, so the number of items needed to be diverted is only two. This is the motivation behind developing a new methodology with a lower number of attributes for the PBR case, and the objective is to only analyze the intrinsic PR with this new methodology.

The simplified methodology is developed to provide a similar PR assessment function as that of PRAETOR. With its sixty-eight attributes to be input, PRAETOR is a comprehensive PR assessment code. However, since PRAETOR was developed based on the LWR fuel cycle, its application is impractical for a conceptual nuclear system. It also incorporates numerous possible attributes and is not limited to the intrinsic ones. The simplified method focuses solely on the intrinsic parameters of how the reactor breeds the proliferation target material. Also, PRAETOR does not provide uncertainty in the calculated overall PR value, which is important in risk analysis.

Intrinsic safeguards characteristics reflect material attractiveness directly regardless of the presence of any extrinsic barriers. Material attractiveness is one of the

bases for nuclear system design and is usually inversely related to the PR, which will be higher if the material is less attractive. Although the IAEA defines material safeguards based on the total mass of plutonium, material attractiveness is based on the plutonium isotopic composition as well. From the perspective of a highly motivated proliferator, a higher content of fissile isotope(s) in plutonium will simplify the subsequent process of weaponization. Hence, the simplified PR methodology will focus on the plutonium's isotopic composition, which is measurable by existing measurement techniques.

The PR assessment would be simpler if the plutonium isotopes could be measured directly. However, they cannot be inferred directly using any non-destructive measurement. Non-destructive measurements are able only to interrogate the spent fuel to provide interpretable information such as burnup level, cooling time, and initial enrichment (Phillips 1991). Plutonium and uranium isotopes radiate particles, which are useful to assess the intrinsic PR features indirectly. Generally speaking, even number plutonium isotopes and ^{238}U radiate more neutrons from spontaneous fission compared to the fissile isotopes. They also generate more heat, mostly through the alpha decay mechanism. Meanwhile, the fissile plutonium isotopes can be viewed from the reaction kinetics perspective. MCNP can calculate kinetics parameters and reactivity changes through adjoint weighting of tally scores in continuous energy Monte Carlo *k*-eigenvalue calculations (Kiedrowski, Brown and Wilson 2010).

This simplified method uses only four attributes to quantify the PR of plutonium spheres produced from spent PBR fuel at various fuel burnups. The attributes considered are spontaneous fission neutron rate, heating rate, radiation exposure, and Rossi-α.

Spontaneous fission neutrons correlate directly to either plutonium or uranium isotope composition and can be measured straightforwardly through total neutron counting (Stewart 1991) and neutron coincidence counting (Ensslin 1991). Principally, the heat rate of a plutonium weapon can be determined through an ordinary calorimeter measurement. In addition, a radiation exposure measurement is a very common and straightforward routine that may account for all kinds of radiation, mostly neutrons and gamma.

Rossi-α relates to the kinetics of a nuclear explosive device (NED). In a NED, the system does not depend heavily on delayed neutrons because of their longer neutron mean generation time (Λ). But, in nuclear reactors it is very useful because delayed neutrons aid in better reactor control and safety, and their lower energy at birth contributes to neutron economy. In a NED, the reaction is expected to occur in a very short time. Faster is better. Since the kinetics of this process depend heavily on the material composition, the quality of plutonium isotopes defined by its composition for the NED material is the key to making a good NED. Therefore, weapons-grade plutonium is categorized differently from reactor-grade plutonium.

When detonated, an NED is expected to achieve prompt criticality as fast as possible rather than achieving a delayed criticality like in a reactor. In a prompt criticality, the system only needs one prompt neutron to maintain its criticality.

The relationship between prompt and delayed criticality can be obtained from their neutron multiplication factors by the following:

$$k'_{eff} = k_{eff} - \beta_{eff} \qquad \text{(Eq. 2.3)}$$

where β_{eff} is the effective delayed neutron fraction, the k'_{eff} is the neutron multiplication factor with only prompt neutrons, and k_{eff} is when delayed neutrons are also considered.

The prompt neutron lifetime is approximately equal to its mean generation when a system is at a critical state because the role of delayed neutrons is negligible. At its critical state, the number of fissions is proportional to the number of absorptions occurring per cm^3.s at time *t* and can be estimated by (Lamarsh and Baratta 2001)

$$\frac{dN_F(t)}{dt} \cong \frac{k-1}{\Lambda} N_F(t) \qquad \text{(Eq. 2.4)}$$

With $N_F(0)$ as the number of fissions at $t = 0$ or at prompt critical, its solution is:

$$N_F(t) = N_F(0) \exp\left(\frac{k-1}{\Lambda} t\right) \qquad \text{(Eq. 2.5)}$$

where, $N(0)$ is the fission rate at time, $t = 0$, k is the neutron multiplication factor, Λ is the prompt removal lifetime, and the term $\frac{k-1}{\Lambda}$ is like a growth or decay constant, commonly termed as Rossi-α (Lamarsh and Baratta 2001). If α is positive, the fission rate increases exponentially with time and vice versa if it is negative. This means an attractive material for NEDs should have a Rossi-α value≥ 0.

Rossi-α can be measured by employing a subcritical assembly of LWR spent fuel to quantify its Pu content (Kaplan, et al. 2014). In this study, the α is computed using MCNP simulations with its criticality calculation mode (KCODE mode). From the KCODE simulation, one would get the values of *k* (as an effective multiplication factor) and Λ (as prompt removal lifetime). If the system is a subcritical assembly, the value is expected to be negative.

Using the MAUA methodology of Equations 2.1 and 2.2, the intrinsic PR can be calculated with only the four afore-described attributes: spontaneous fission neutron rate; the radiation exposure rate; the heat load; and the Rossi-α. A uniform weighting scheme is used for these attributes.

The MAUA requires utility functions for all the four attributes involved. The utility functions are employed to convert the attribute input values supplied by the user into a scale ranging from 0 to 1. The set of equations 2.6 are the utility functions for the radiation load (u_{rad}), the spontaneous fission neutron rate (u_{SF}), and the heat load (u_{heat}), which are the same as those used in PRAETOR (Chirayath, Elmore, et al. 2015).

$$u_{rad} = 0; \quad \text{if} \quad h_{rad} < 0.00001 \text{ [R/h]}$$

$$u_{rad} = 0.05157 \ln(h_{rad}) + 0.6438; \quad \text{if} \quad 0.00001 \leq h_{rad} \leq 1000 \text{ [R/h]}$$

$$u_{rad} = 1; \quad \text{if} \quad h_{rad} > 1000 \text{ [R/h]}$$

$$u_{SF} = 1 - e^{-3.5(\frac{h_{SF}}{2700})^{1.8}}$$

$$u_{heat} = 1 - e^{-3(\frac{h_{heat}}{171})^{0.8}} \qquad \text{(Eq. 2.6)}$$

A minor modification on the lower limit of the radiation load has been changed from the original PRAETOR value of 0.01001 R/h to 0.00001 R/h. This change is to take into consideration the fact that radiation load at 1 m away from the plutonium sphere can be lower than 0.01001 R/h.

The utility function (u_α) for Rossi-α describes that any α equal to or greater than 0 per second leads to a minimum utility value (U_α) of 0. For any other value $u_\alpha$is given by

$$u_\alpha = 1 - \exp\,(h_\alpha t) \qquad \text{(Eq. 2. 7)}$$

where α is the Rossi-α and t is the reaction time of 59 shakes (1 shake = 10^{-8} seconds). This value of t is defined by analyzing a set of simulations proving that a sphere of pure ^{239}Pu metal without any reflector approaches its criticality with a mass of 9.94 kg leading to the minimum utility value of 0 (at α ≅ 0) and when its k approaches zero (at α approx. -1.1 × 10^7 s^{-1}) with a zero-approaching mass leading to the maximum utility value of 1. h represents the value of each of the four respective parameters.

Since the simulated material's uncertainty is not provided by MCNP, the propagated uncertainty for the final simplified PR values only comes from all the corresponding MCNP predicted stochastic errors. Based on Eq. 2.1 and 2.2, the respective uncertainties associated with the overall PR are as follows:

$$\sigma_{PR+} = k\sqrt{({\sigma_{rad}}^2 + {\sigma_{SF}}^2 + {\sigma_{heat}}^2 + {\sigma_\alpha}^2)} \qquad \text{(Eq. 2.8)}$$

$$\sigma_{PR*} = |PR|\sqrt{\left(\frac{\sigma_{rad}}{u_{rad}}\right)^2 + \left(\frac{\sigma_{SF}}{u_{SF}}\right)^2 + \left(\frac{\sigma_{heat}}{u_{heat}}\right)^2 + \left(\frac{\sigma_\alpha}{u_\alpha}\right)^2} \qquad \text{(Eq. 2.9)}$$

Figure 2-5 shows the workflow performed in this study. The reactor model referred to in this study is the pebble fueled HTR-10, since the simulation is an infinite lattice. The optimizations are not performed in this study, but the flow chart shows that an optimization may be carried out to optimize the overall design. PRAETOR, with its 68 attributes, enables the optimization to be taken on both the intrinsic and extrinsic parameters. Meanwhile, the simplified method only enables an optimization to the intrinsic parameters that can be tweaked through design or operation modification.

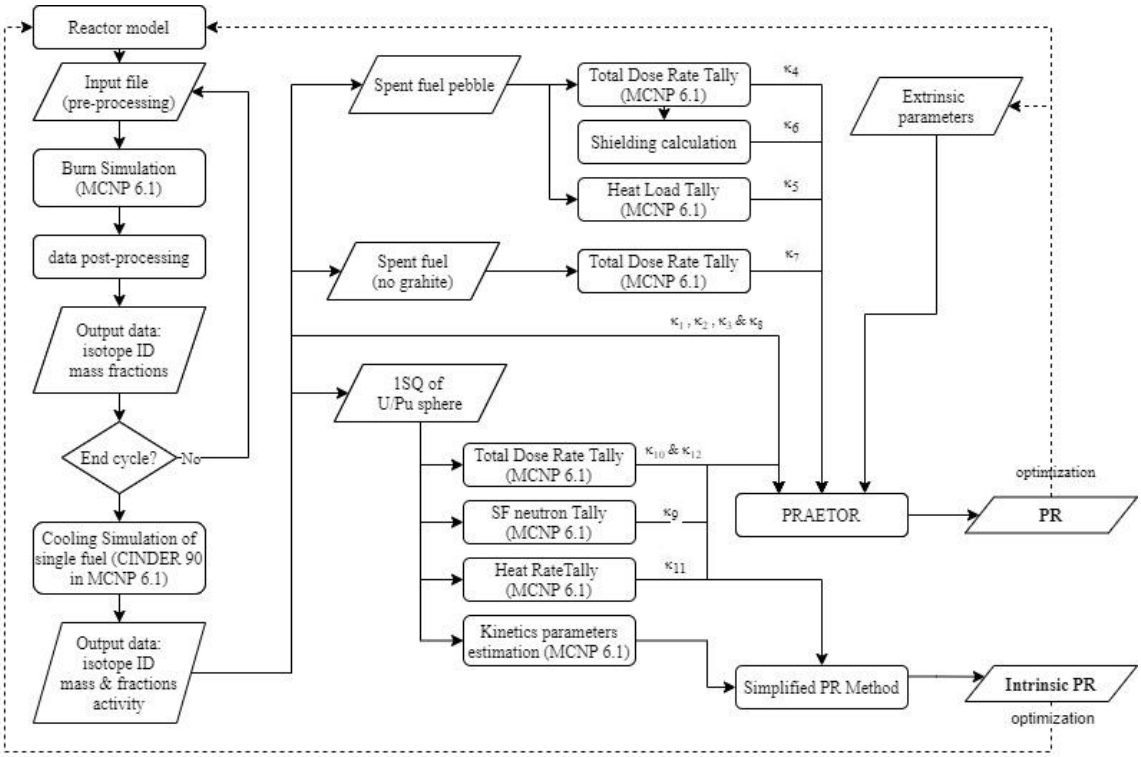

Figure 2-5. Workflow to calculate PR using PRAETOR and the simplified method.

2.4. Results and Discussion

As mentioned earlier, three MCNP simulations are performed on an infinite cube lattice containing two identical fuel pebbles. They are based on three different fuel types having different uranium enrichments of 4.95 wt%, 10 wt%, and 17 wt%. Figure 2-6 shows the neutron multiplication factor (k_{eff}) Vs fuel burnup correlation as well as fuel burnup Vs time of irradiation for each simulation. The time Vs fuel burnup correlations for all simulations are identical. All simulations show xenon and other poison effects on k_{eff} for the beginning period of about 2 days.

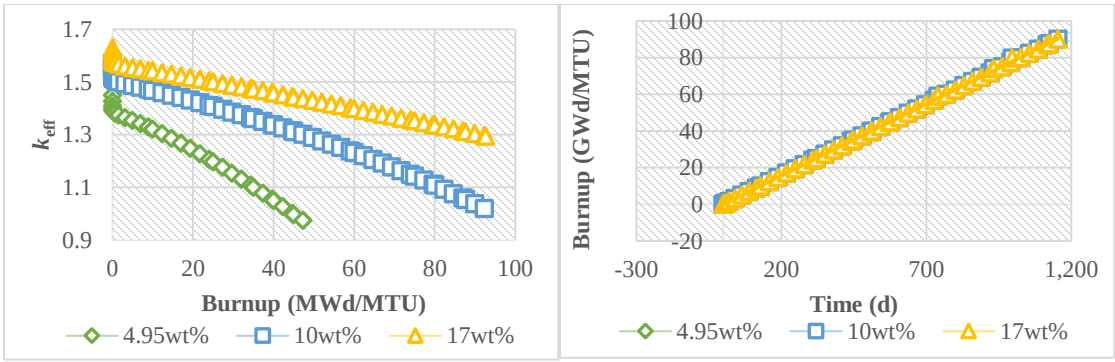

Figure 2-6. Neutron multiplication factor for all simulations (left); and their time-burnup correlation (right)

With the 4.95 wt% ^{235}U enriched fuel, the system reaches subcriticality at a fuel burnup of about 45 GWd/MTU, which is equivalent to 575 days. As expected, the 4.95 wt% fuel cannot attain a fuel burnup of 80 GWd/MTU due to its lack of sufficient fissile content. The system with 10 wt% reaches subcriticality at a fuel burnup of about 95 GWd/MTU, which is equivalent to 1214 days. The 17 wt% system reaches subcriticality at a fuel burnup of about 180 GWd/MTU, or the equivalent of 2300 days. However, the 17 wt% fuel does not reach its attainable burnup since the target burnup of all simulations is only 80 GWd/MTU. The highest simulated burnup is 90 GWd/MTU.

As the energy is extracted from all fuel types at their respective higher burnups, ^{239}U and ^{237}U production becomes higher as the fuel enrichment is lower. The quantity of ^{238}U and the same thermal power assumption causes the lower enrichment fuel to have a higher neutron flux. As the flux value rises, the nuclide transmutation rate becomes faster. ^{239}U production is due to the neutron capture reaction of ^{238}U, while ^{237}U is produced from the (n,2n) reaction of the ^{238}U and from the (n,γ) reaction of ^{236}U, which is also produced through the (n,γ) reaction of ^{235}U. These mechanisms produce a higher plutonium content

at a lower enrichment, which then contributes to the overall energy production, especially from the ^{239}Pu.

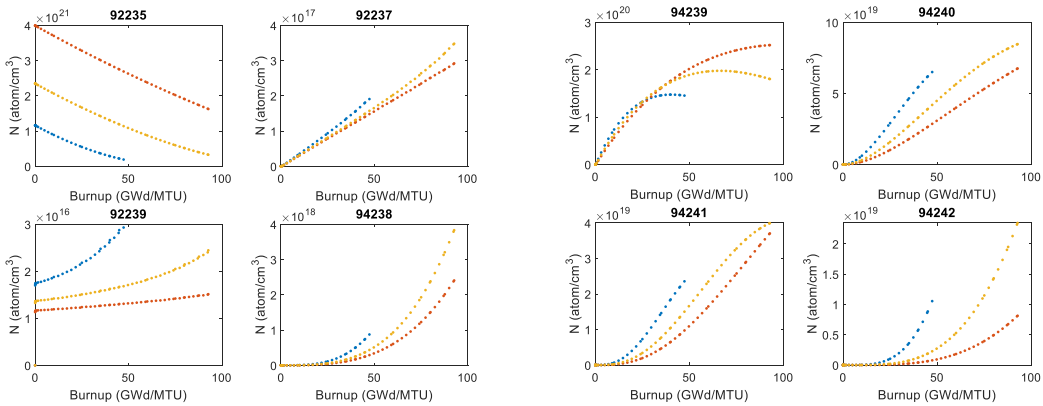

Figure 2-7. MCNP calculated densities of uranium and plutonium isotopes in pebble fuel vs. burnup

The concave downward curve of ^{239}Pu (ref. Figure 2-7) means the system may not only experience ^{239}Pu loss by neutron capture reaction to produce a higher mass of plutonium isotopes but may also by fission. As with the 4.95 wt%, the 10 wt% fuel also encounters ^{239}Pu depletion at higher burnups. With the 10 wt%, this phenomenon takes place after reaching approximately 70 GWd/MTU. This depletion is significant in both types after the ^{235}U content is less than approximately 3%. Since the 17 wt% has much more ^{235}U, the ^{239}Pu depletion will contribute significantly to the power production at higher burnup values only beyond the limit of the simulation performed in this study. The total Pu produced by all fuel enrichment types relative to the initial uranium loading per fuel pebble is similar (ref. Figure 2-8). The lower enrichment yields slightly higher total Pu at the respective low burnup values. However, the fissile (odd number) and fertile (even number) plutonium isotopes produced in each fuel type are clearly distinguishable.

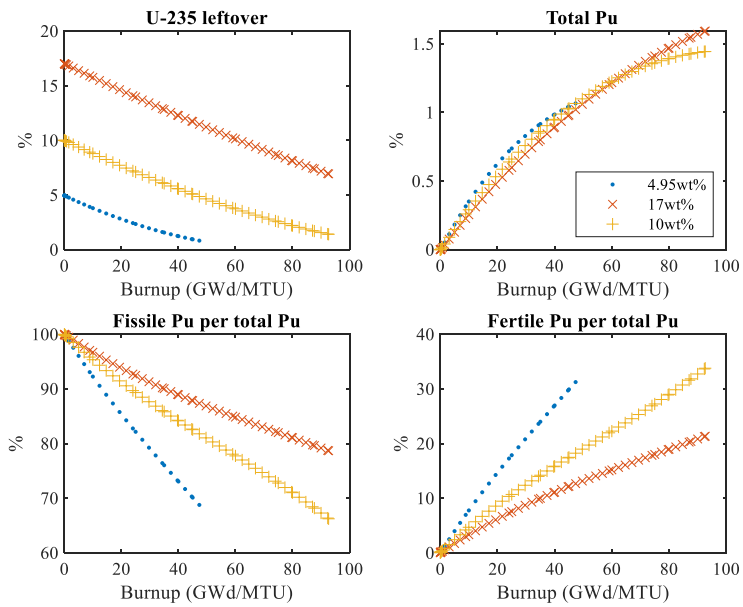

Figure 2-8. Simulated SNM per single fuel pebble of 5 g UO2 without cooling

Since the PR analysis is performed for a one-year cooled spent fuel, the resulting data shown in Figures 2-7 and 2-8 are further extended by simulating the decay for the cooling period. Figure 2-9 shows the leftover ^{235}U and total Pu masses in percentage for each fuel enrichment type after the cooling. As expected, both uranium and plutonium content do not change significantly. Figure 2-10 shows the fissile plutonium mass and percentage per total plutonium of the one-year cooled spent fuel. The fissile mass is dominated by ^{239}Pu, which is higher by an order of tens compared to the ^{241}Pu mass (ref. Table 2.1). The fissile isotopes within the spent fuel of PBR is higher than 60% (ref. Figure 2-10). The quality of plutonium is more attractive for proliferation at lower burnup level and/or at higher ^{235}U enrichment.

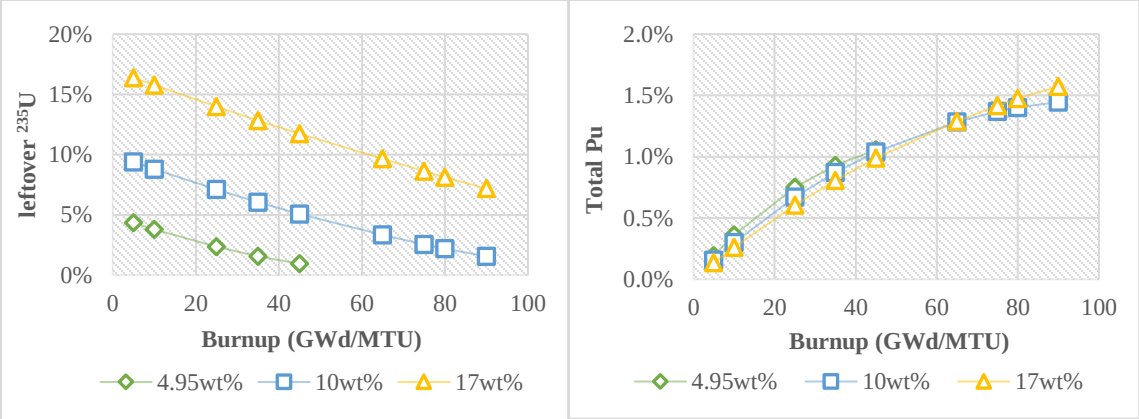

Figure 2-9. Simulated SNM after 1 y cooling. ^{235}U leftover (left) and plutonium (right)

Table 2-1. Simulated plutonium isotopes weight fraction from a 1-y cooled spent pebble fuel

^{235}U Enrichment	Burnup (GWD /MTU)	^{235}U (g)	Pu (g)	^{238}Pu	^{239}Pu	^{240}Pu	^{241}Pu	^{242}Pu	^{241}Am*
4.95 wt%	5	0.192	0.009	0.002%	96.060%	3.731%	0.203%	0.004%	0.010%
	10	0.167	0.016	0.008%	91.697%	7.460%	0.799%	0.037%	0.039%
	25	0.103	0.033	0.066%	78.389%	16.888%	4.050%	0.607%	0.200%
	35	0.069	0.042	0.156%	69.789%	21.794%	6.559%	1.702%	0.323%
	45	0.042	0.048	0.308%	61.811%	25.527%	8.680%	3.673%	0.427%
10 wt%	5	0.415	0.008	0.001%	97.637%	2.265%	0.096%	0.001%	0.005%
	10	0.387	0.013	0.005%	95.082%	4.519%	0.386%	0.009%	0.019%
	25	0.313	0.030	0.039%	87.344%	10.363%	2.116%	0.139%	0.104%
	35	0.267	0.038	0.084%	82.243%	13.590%	3.704%	0.379%	0.183%
	45	0.224	0.046	0.156%	77.231%	16.388%	5.426%	0.799%	0.267%
	65	0.148	0.057	0.403%	67.714%	20.898%	8.633%	2.353%	0.425%
	75	0.113	0.060	0.611%	62.901%	22.823%	9.981%	3.683%	0.491%
	80	0.097	0.062	0.738%	60.602%	23.641%	10.531%	4.488%	0.518%
	90	0.069	0.064	1.047%	56.116%	25.059%	11.311%	6.466%	0.556%
17 wt%	5	0.722	0.006	0.001%	98.333%	1.607%	0.059%	0.000%	0.003%
	10	0.695	0.012	0.004%	96.551%	3.205%	0.237%	0.003%	0.012%
	25	0.616	0.027	0.029%	91.213%	7.365%	1.341%	0.052%	0.066%
	35	0.566	0.036	0.062%	87.710%	9.677%	2.413%	0.139%	0.119%
	45	0.517	0.044	0.109%	84.279%	11.684%	3.642%	0.286%	0.180%
	65	0.425	0.057	0.259%	77.761%	14.935%	6.238%	0.807%	0.307%
	75	0.380	0.062	0.375%	74.466%	16.354%	7.578%	1.228%	0.373%
	80	0.358	0.065	0.443%	72.897%	16.980%	8.206%	1.475%	0.404%
	90	0.316	0.069	0.602%	69.832%	18.132%	9.375%	2.059%	0.461%

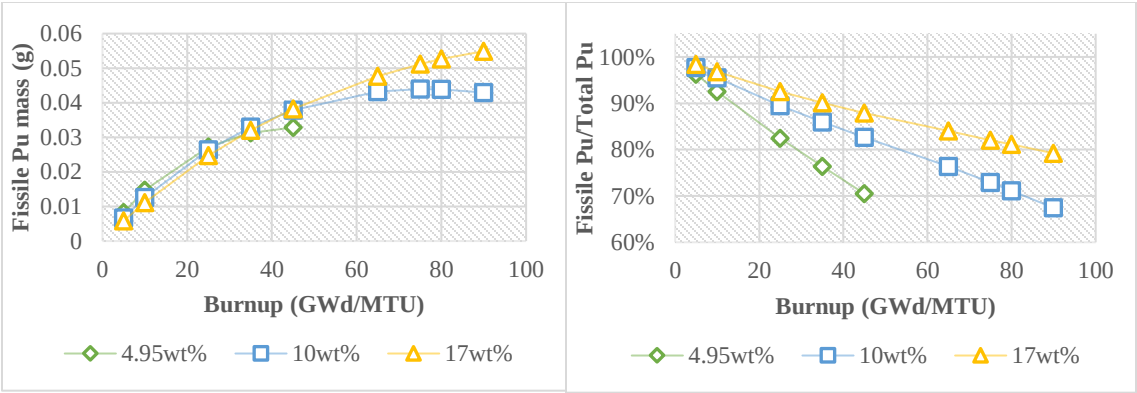

Figure 2-10. Simulated fissile plutonium per single fuel after 1 y cooling.

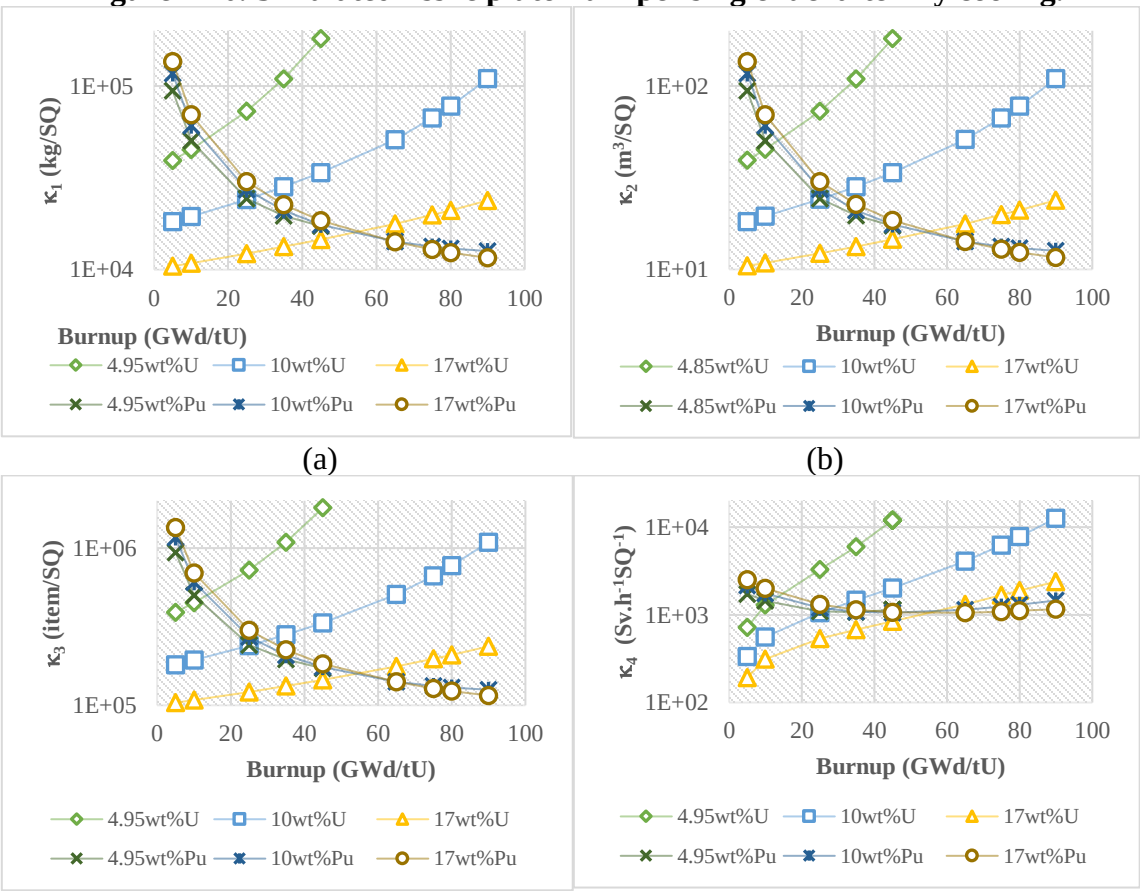

Figure 2-11. SNM intrinsic attributes used for PRAETOR inputs: (a) mass, (b) volume, (c) number of items, (d) radiation dose level,

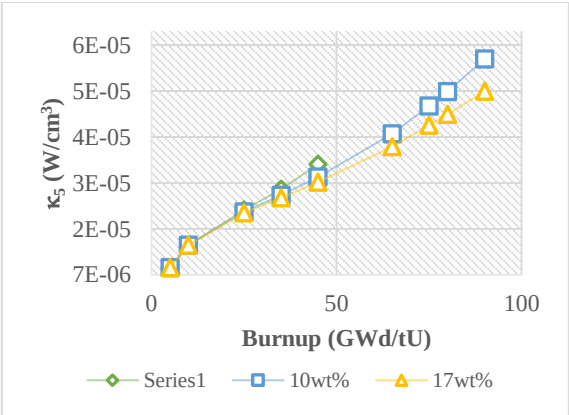

(e)

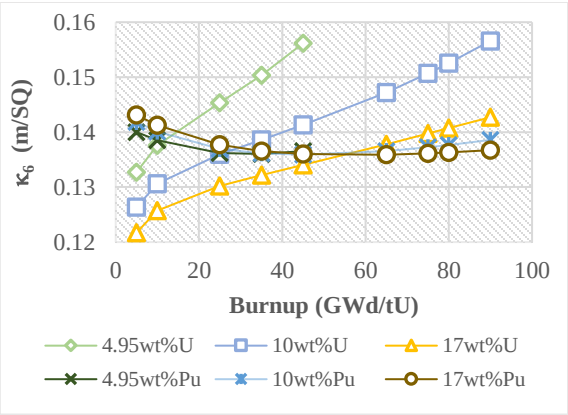

(f)

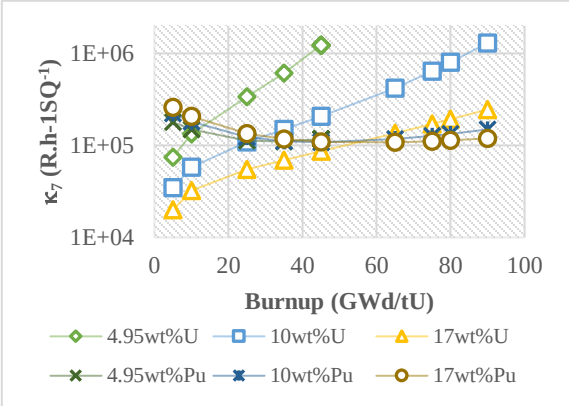

(g)

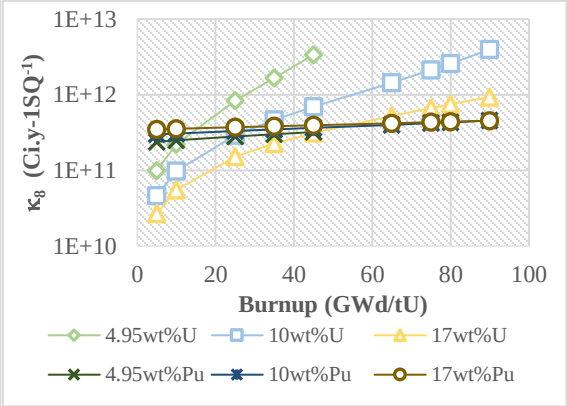

(h)

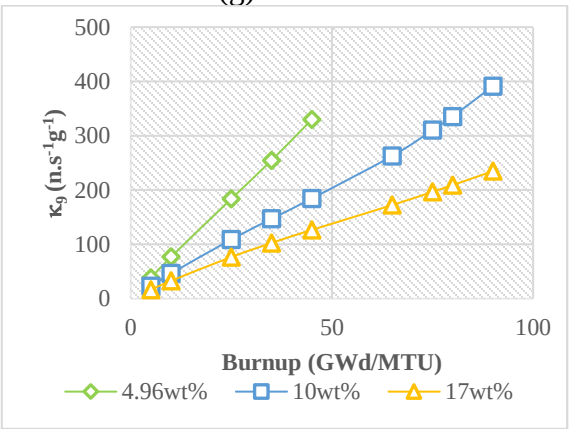

(i)

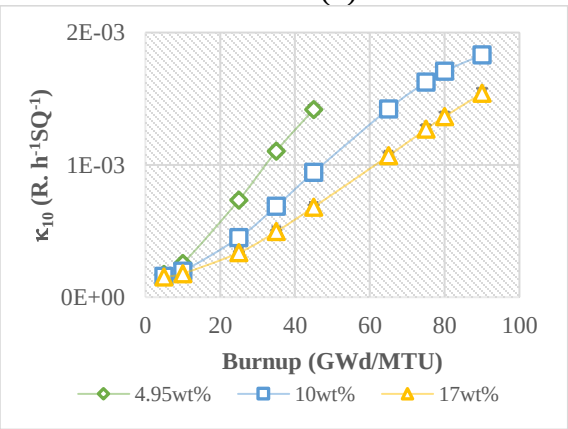

(j)

Figure 2-11 (cont). SNM intrinsic attributes used for PRAETOR inputs: (e) heat load, (f) transportation shielding thickness, (g) transformation radiation load, (h) non-natural occurring gas, (i) Pu sphere spontaneous fission neuron rate, (j) Pu sphere radiation exposure,

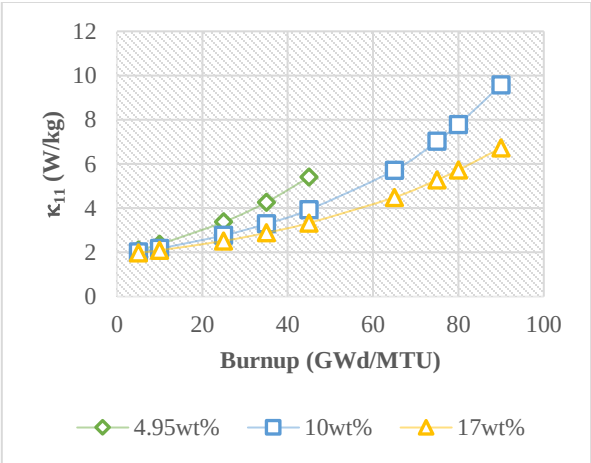

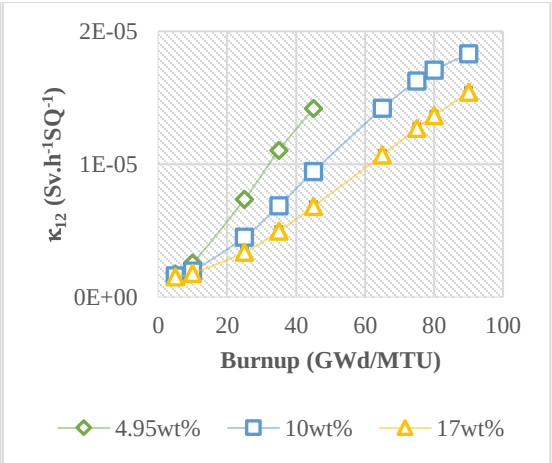

(k) (l)

Figure 2-11 (cont). SNM intrinsic attributes used for PRAETOR inputs: (k) Pu sphere heat load, and (l) Pu sphere radiation dose rate.

Figure 2-11 shows all the attributes generated through MCNP simulation to be used as PRAETOR inputs. The mass (κ_1), volume (κ_2) and number of items (κ_3) have a similar trend curve since they were derived from the same ^{235}U and Pu mass per spent fuel pebble. The radiation dose levels (κ_4), the shielding thickness needed for transportation (κ_6), and the radiation load during transformation (κ_7) also resemble similar profiles to the previous three attributes, which means the number of items to divert 1 SQ of SNM dominates these attributes.

In the weaponization stage, where the calculation considers only pure SNM sphere, the nuclides composition dominates the overall profile in the spontaneous fission neutron rate (κ_9), radiation exposure (κ_{10} and κ_{12}), and heat rate (κ_{11}). These four attributes in Figure 2-11 are only for plutonium spheres. These results are within a confidence interval of 99%. The standard deviations are not visible on the graph since they are too small. The spontaneous fission neutrons and radiation exposure profiles indicate competing roles for the fissile and fertile plutonium isotopes, but the distinction between different fuel types

and burnup values is clearly visible. The heat rate graphs indicate the number of fertile isotopes in the sphere, since the heat is mostly generated by alpha decay from the fertile ones. Although neutrons and gamma rays contribute to the overall heat deposition, they are too small to make a significant difference.

Since the assumption for ^{235}U weaponization excludes a post-irradiation enrichment process, there is only one value for each of these attributes, assuming the weapons enrichment is 90% regardless of the fuel type and fuel burnup. For 1 SQ of ^{235}U spheres (which becomes 25 kg since it is an HEU sphere), the spontaneous fission neutron rate is 3.55E-03 $\pm$ 2.13E-06 $n.s^{-1}g^{-1}$, the heating load is 6.88E-09 $\pm$ 6.70E-14 W/kg, and the radiation exposure is 1.21E-05 $\pm$ 1.65E-06 $R.h^{-1}SQ^{-1}$ at 1 m away from the HEU sphere.

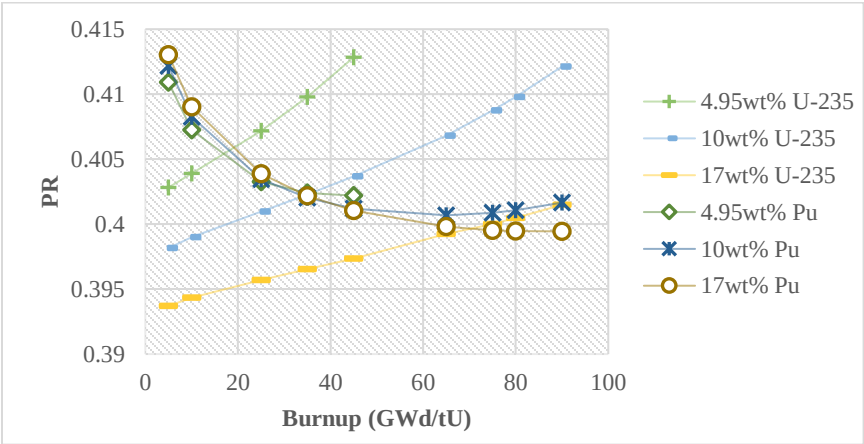

Figure 2-12. PRAETOR-generated PR values for ^{235}U and plutonium diversion using the multiplicative form.

The PR values for both diversion scenarios (uranium and plutonium) at different initial uranium enrichments and at different fuel burnup values are shown in Figure 2-12. The PR profile of the ^{235}U diversion scenario follows the trend of its leftover mass. As

expected, the lower enrichment fuel has a higher PR value due to its lower ^{235}U content. At low burnup values, PR values of the ^{235}U diversion are lower than that of the plutonium diversion scenario due to the higher number of pebbles needed to divert plutonium. The PR of plutonium diversion inversely follows the total plutonium quantity profiles as shown in Figure 2-9.

Although slightly observable, plutonium diversion PR values computed using PRAETOR hardly differentiate the initial ^{235}U enrichment. This is due to the small amount of plutonium per spent fuel pebble. The Stage 1 to 3 attributes rely heavily on the amount of plutonium per pebble, defining the number of pebbles needed to divert 1 SQ of plutonium, which decreases as the burnup value increases. A high number of items needed for diversion drives some key attributes beyond their utility value limits. This causes the PR values in the first three stages to become barely distinguishable. The PR values are heavily distorted by the quantity of the pebbles. The high quantity can be considered as a proliferation barrier. However, since SNM diversion is more likely to be undertaken by a State rather than a group of terrorists or a single person, as in nuclear security, this type of barrier may not be effective in the PBR case. The mass of the diverted item or the number of items to be diverted may not be an issue for a State-level actor. With a good quality plutonium, PBR offers an attractive spent fuel for a nuclear proliferator. Therefore, PRAETOR is not suitable to quantify the PR of plutonium diversion for the PBR, although it can distinguish the PR of ^{235}U diversion very well.

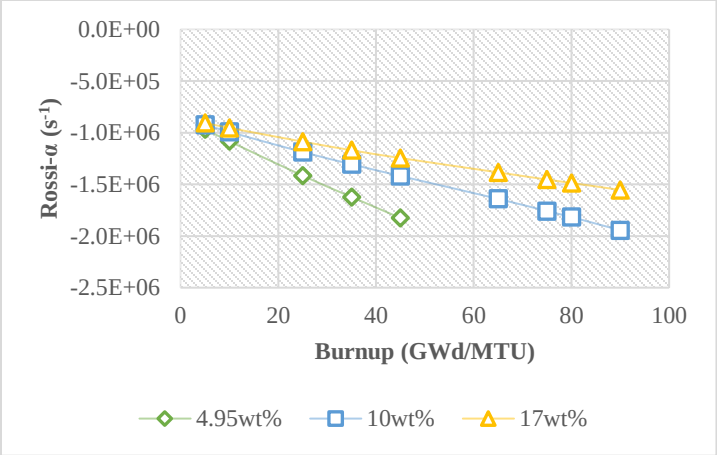

Figure 2-13. Simulated Rossi-α of 1 SQ plutonium sphere.

To remedy this situation, PRAETOR is simplified to use only four parameters, which were discussed previously. Figure 2-13 shows MCNP simulation results of the kinetic parameters (Rossi-α) on a 1 SQ of plutonium sphere. These results are within a confidence interval of 99%, which are not visible on the graph since they are too small. The Rossi-α profiles from the simulation are showing negative values, indicating that the system is within subcritical conditions. The overall trends follow a straight line. This is because the Rossi-α is a linear coefficient between the effective delayed neutron fraction and the prompt neutron lifetime. These parameters are computed using MCNP and are depicted in Equation 2.5.

Using both multiplicative and additive forms of MAUA, the PR profile using the simplified method is shown in Figure 2-14. The multiplicative form yields slightly higher PR. It uses a same weighting factor of 0.3 and a scaling factor of 4.268E-04. This simplified PR profile is easier for risk interpretation compared to PRAETOR's result on plutonium's PR.

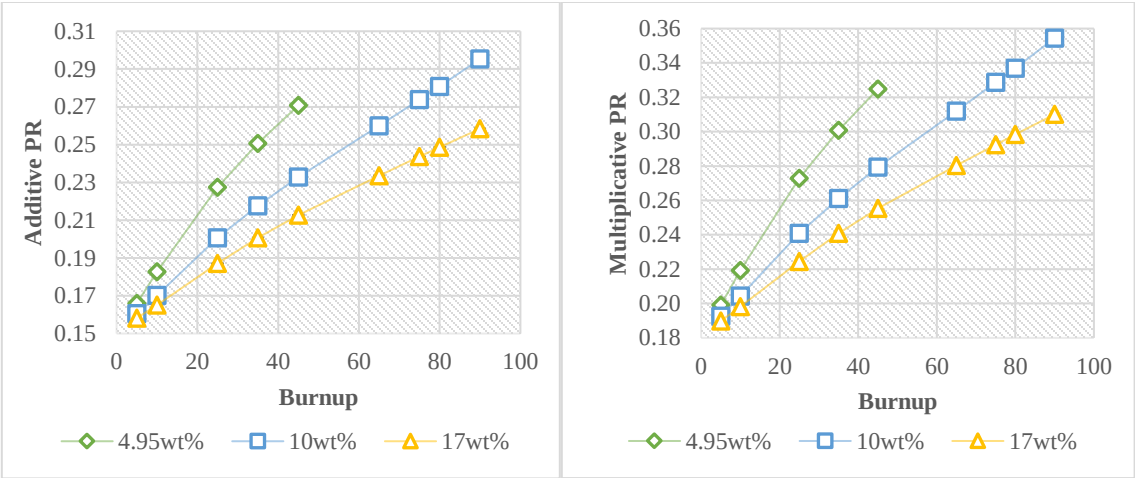

Figure 2-14. Simplified PR values of 1 SQ plutonium sphere.

Since the standard deviation is too small to be visible in the graph, the PR values and their standard deviation can be found in Table 2.2. The overall trend by the simplified method is obvious and distinguishable between different fuel types and burnup values. The PR is clearly higher with a lower initial uranium enrichment and higher burnup. These profiles represent the competing effect from both the fissile and fertile plutonium isotopes.

The simplified PR assessment method is less applicable to quantify PR for the ^{235}U diversion scenario assuming a single post-irradiation enrichment value. As shown in Figure 2-12, PRAETOR is able to assess the ^{235}U diversion in PBR sufficiently. However, this does not exclude the possibility of using the simplified method for ^{235}U diversion.

Table 2-2. PR values calculated by the simplified method within a confidence interval of 99%.

Additive

Burnup (GWd/MTU)	Initial ^{235}U enrichment								
	4.95wt%			10wt%			17wt%		
5	1.66E-01	±	8.02E-04	1.61E-01	±	5.63E-04	1.58E-01	±	5.15E-04
10	1.83E-01	±	5.19E-04	1.70E-01	±	4.87E-04	1.65E-01	±	8.33E-04
25	2.27E-01	±	6.05E-04	2.01E-01	±	5.62E-04	1.87E-01	±	5.36E-04
35	2.51E-01	±	6.54E-04	2.18E-01	±	5.84E-04	2.01E-01	±	5.55E-04
45	2.71E-01	±	7.37E-04	2.33E-01	±	6.11E-04	2.13E-01	±	5.84E-04
65				2.60E-01	±	6.69E-04	2.34E-01	±	6.00E-04
75				2.74E-01	±	7.57E-04	2.44E-01	±	6.26E-04
80				2.81E-01	±	7.98E-04	2.49E-01	±	6.16E-04
90				2.95E-01	±	8.15E-04	2.58E-01	±	6.57E-04

Multiplicative

Burnup (GWd/MTU)	Initial ^{235}U enrichment								
	4.95wt%			10wt%			17wt%		
5	1.99E-01	±	3.36E-03	1.93E-01	±	2.30E-03	1.90E-01	±	4.66E-04
10	2.19E-01	±	2.73E-03	2.04E-01	±	2.20E-03	1.98E-01	±	3.41E-03
25	2.73E-01	±	4.01E-03	2.41E-01	±	3.22E-03	2.24E-01	±	2.70E-03
35	3.01E-01	±	4.88E-03	2.61E-01	±	3.75E-03	2.41E-01	±	3.12E-03
45	3.25E-01	±	5.49E-03	2.79E-01	±	4.10E-03	2.55E-01	±	3.51E-03
65				3.12E-01	±	5.01E-03	2.80E-01	±	4.10E-03
75				3.29E-01	±	5.51E-03	2.92E-01	±	4.30E-03
80				3.37E-01	±	5.80E-03	2.98E-01	±	4.53E-03
90				3.54E-01	±	6.36E-03	3.10E-01	±	4.91E-03

3. PEBBLE BED REACTOR REFUELLING SCHEME SIGNIFICANCE ON PROLIFERATION RESISTANCE

3.1. Introduction

PBR can be refueled using at least three different schemes. The first is a one-batch scheme where all of the fuel pebbles in the core are refueled after the reactor reaches its sub-criticality. From now on, this scheme will be referred to as the once-through-then-out (OTTO), or single-pass, scheme. In contrast, in a multi-pass refueling scheme both fresh fuel insertion and used fuel re-insertion is performed, allowing the fuel to be passed multiple times through the core to reach a specific target burnup. The one-batch scheme is suitable for a small modular reactor (SMR) PBR type that is intended to be placed in a remote place to accommodate a long period of refueling time without the online refueling. The latter allows for better neutron flux distribution in the core. One another known scheme is a *peu-a-peu*, or little-by-little, scheme where a small portion of fuel is added step-by-step to reach criticality (Tran, 2012). However, this scheme is not a part of this study since it emphasizes the reactor operation within the startup, or pre-equilibrium, stage and turns into the OTTO, or multi-pass, after criticality is achieved for a defined power level.

The isotopic composition of the spent fuel material will be affected primarily by the fuel residence time and its position in the core. Both parameters relate directly to the neutron flux that the irradiating fuel experiences within the core, which also defines the fuel burnup. With the online refueling in place, the nuclide production and loss mechanism

within the pebble in the core may vary radially and axially. Pebble positioning depends on the refueling method applied in the operation. Hence, this will directly affect the plutonium production and the ^{235}U burning mechanism, causing the plutonium isotope composition to vary with position. Due to this, the SNM's quality can be engineered for a proliferation effort. Therefore, the PBR can be optimized to maximize SNM production. The change of refueling scheme within a declared operation should also be carefully surveilled for PBR safeguards. There can be manipulations made by the operator to generate the needed amount and quality of SNM by engineering the refueling scheme without the need of any design modifications.

In this study, the three refueling schemes are evaluated to analyze the quantity and the quality of the SNM in the spent fuel through a full core reactor physics modeling using a high-fidelity HTR-10 model. The modeling and simulation use the Monte Carlo N-particle (MCNP) 6.1 code to simulate the core physics and the nuclide production and loss mechanisms. MCNP 6.1 is integrated with CINDER90, meaning it automatically passes the neutron flux information to calculate the nuclide production and loss mechanism using the Bateman equation (Fensin, et al, 2015; Fensin and Umbel, 2015). The simulation results are further used to generate proliferation resistant (PR) values using the PRAETOR code or the simplified PR assessment method.

The PR quantification of PBR with online refueling within this study is limited to its equilibrium operation only. The equilibrium stage is a condition where the operation is continuous, and it ideally uses same refueling method repeatedly.

The purpose of this chapter is to provide an analysis methodology that can be used to optimize the proliferation resistance in the PBR operation. The information may be used to design a proper and suitable safeguards strategy and approach. The PR will be calculated by PRAETOR and the simplified MAUA method to compare the applicability of the two methods.

3.2. Methodology

To investigate the significance of refueling schemes on PR, three sets of Monte Carlo simulations are carried out to model the nuclides produced by one batch, OTTO, and multi-pass schemes in the core and in the discharged fuel pebble. The simulations use MCNP 6.1 on a full core HTR-10 model (IAEA-TECDOC-1694). The small size of the HTR-10 allows for the use of a high-fidelity model in Monte Carlo simulation. The simulation results are used to calculate the PR of leftover ^{235}U and Pu on the discharged spent fuel pebble (SFP) using PRAETOR and the simplified MAUA methodology described in Chapter 2.

The core of the HTR-10 has a volume of 5 m^3 with a diameter of 1.8 m and a height of 1.97 m. It also has a conical region followed by a smaller cylindrical region at the bottom of the core, where the fuel pebbles are discharged for recirculation or ultimate disposal based on the fuel burnup measurement (Ref. Fig. 3-1). The graphite structures of the reactor use the same material of carbon with various densities (IAEA-TECDOC-1694).

As in Chapter 2, the pebble fuel configuration in the core has a 61% packing fraction with BCC configuration, where each lattice contains two fuel pebbles without any graphite pebble. The TRISO configuration in the pebble is a simple cubic. The initial ^{235}U

enrichment of fuel is 17 wt%. Including the fuel discharge region at the bottom of the core, the total number of fuel pebbles in the core is 29,106, which is equivalent to 128.28 kg of uranium (21.9 kg of ^{235}U which is less than one SQ of LEU). The model excludes any possible clipped lattice in the core to avoid calculation inaccuracy. Each pebble is defined to contain 5 g UO_2 with a density of 10.4 g/cm^3. One of the features of MCNP, URAN, enables the random sampling of TRISO particles in a pebble and the random sampling of the pebble itself in the core for a more realistic simulation (Brown and Martin 2004).

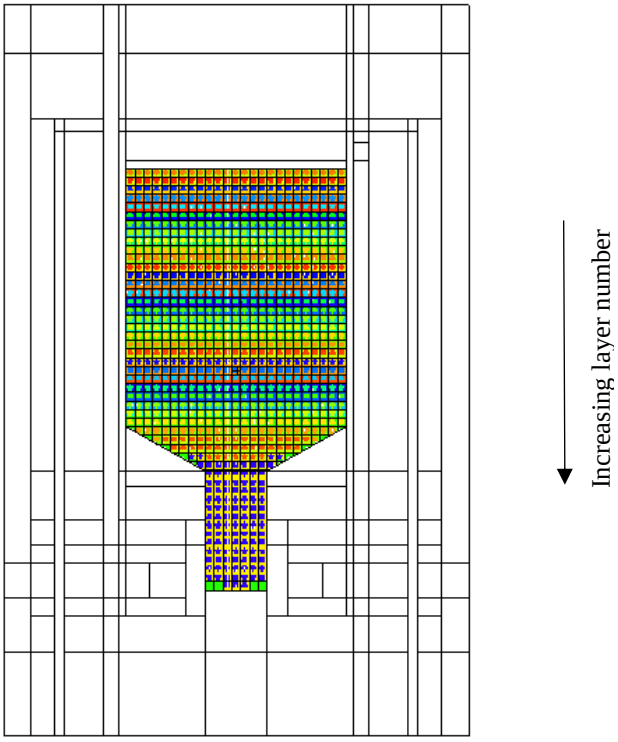

Figure 3-1. HTR-10 reactor model (IAEA-TECDOC-1694). The 1st layer is the top position whilst the 33rd is the bottom position. The noncolored parts are the graphite structures.

Based on a preliminary optimization study for the required neutronic simulation, a history of 5 million neutrons (25,000 particles per each of 200 iterations) is deployed for

the criticality and fuel depletion or burnup calculations using MCNP. The calculation reached a standard deviation close to 40 pcm (within a confidence interval of 68%) for the effective multiplication factor (k_{eff}). The temperature used in this calculation is uniform at 1200 ^{o}K for the fuel and the coolant, but the other reactor materials are at 600 ^{o}K. The nuclear data used in the simulation is ENDF/B-VIII.

3.2.1. One-batch scheme

The one batch scheme is the simplest, since the refueling rate is very low without online refueling. The reactor is operated until it reaches its subcriticality prior to the discharge of the full core. Refueling is done for the whole irradiated fuel regardless of the individual burnup level of each pebble.

The core operation is simulated for 1154 days, which is equivalent to the target burnup of 90 GWd/MTU assuming a constant power of 10 MWth, without control rod insertion and a capacity factor of 100%. However, this target burnup value is not expected to be achieved, since the fuel depletions in the core are not uniform.

3.2.2. Single-pass or One-Through-Then-Out (OTTO) scheme

In the OTTO refueling scheme, the HTR-10 core is divided into 33 fuel zones axially as layers (ref. Fig. 3-1). Each layer contains 882 fuel pebbles in 441 lattices (2 pebbles per lattice). All layers use the same BCC configuration with a 61% packing fraction. In the simulation, no graphite pebbles are modeled, and no control rod insertion is accounted for. The capacity factor is also assumed to be 100%.

Each of the 33 fuel layers moves downward through the axial layers. There is no fuel recirculation into the core once the fuel pebbles are discharged. The fresh pebbles are

inserted at the top layer of the core (the 1st layer). The fuel pebbles at the bottom-most layer (33rd) are discharged and labelled as spent fuel pebbles (SFP). This means 3% of the total fuel is replaced in each cycle. The interval at which each layer moves down in a refueling period is simply referred to as a cycle.

The refueling periods are calculated to achieve burnup values of 75, 80, and 90 GWd/MTU in three independent simulations. With the given amount of uranium (128.28 kg) in the core and a constant power of 10 MWth, these burnup values are expected to be achieved within 962, 1026, and 1154 days, respectively. These suggest the refueling periods become 29, 31, and 35 days, respectively.

Each simulation will be completed for 99 refueling cycles at a constant power (10 MWth) with a capacity factor of 100% (without interruption). This is based on the consideration that after the 34th cycle, the reactor reaches its equilibrium cycle. Therefore, the first 33 cycles of the 99 cycles are considered as the pre-equilibrium phase, and the remaining 66 cycles are considered as the equilibrium phase. The goal for this is to provide a statistical variance in the concentration of nuclides predicted by MCNP, representing the equilibrium phase of the reactor. This is needed because MCNP does not provide uncertainty values for the material concentration that it predicts in tandem with CINDER90. It can be determined by a means proposed by Chirayath, et.al (2021). However, since it has not been coded in MCNP yet, and their study was not available during the early part of this study, the uncertainty is instead determined through this brute force method, which is simpler, although it requires more computational time.

3.2.3. Multi-pass scheme

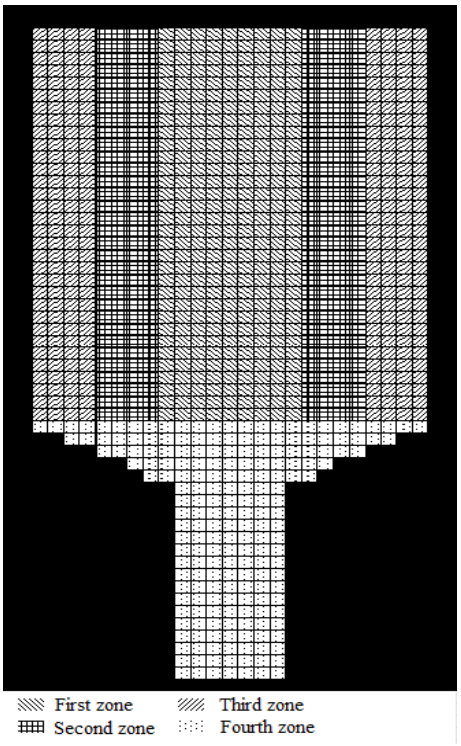

Figure 3-2. In-out fuel shuffling in multi-pass refueling scheme of HTR-10.

The same reactor core model (Fig. 3-1) is used for the multi-pass refueling simulation with a modification. The core is divided radially based on the number of passes, *n*, where *n* is the number of passes of the fuel through the core. Since the chosen number of passes of the pebble is three, the core is radially divided into three zones (ref. Fig. 3-2). This means each pebble will be passed three times through the core to achieve the target burnup. This is expected to be sufficient, since this part of the work aims to provide data for comparing the PR values between the OTTO and the multi-pass schemes.

The simulation is performed only for the target burnup case of 80 GWd/MTU, since the computational time needed to perform the job is more expensive, needing *n*-

times of the computational time in OTTO. The target burnup is expected to be achieved with a refueling period of 10.33 days for each fuel portion, and it is equivalent to the 31 days refueling cycle used in the OTTO refueling scheme.

The three-pass scheme discharges 3% of the fuel pebbles in each cycle. Two-thirds of the discharged fuel is re-inserted into the outer radial position at the top of the core. Hence, only 1% of the fuel is replaced every refueling period. With this in-out refueling pattern, the radial neutron flux in the core's center is expected to be higher than that of the OTTO scheme. An out-in or random refueling pattern may also be performed to obtain different radial neutron flux shapes. However, due to the time limitation for this study, only the previously explained refueling scheme is performed.

Since HTR-10 has a discharging zone at its bottom, the model in this study has four zones. The first three zones are the main zones, while the fourth zone is a discharging zone where the fuel pebbles coming from the main zones are mixed within the cone of the fourth zone and discharged further through a smaller cylinder. The pebble positioning within the fourth zone is expected to be random. However, it is not modelled as a random positioning to simplify the study.

In Fig.3.1, the first, the second, and the third zones contain 30 layers each. Each layer in each zone contains 294 fuel pebbles. This is the same number of pebbles being discharged at the bottom of the fourth zone and of the fresh pebbles being inserted at the top position of the first zone. There are 2,646 pebbles in the fourth zone grouped in 9 layers. Hence, for this 3-pass scheme, there are total 99 layers in the core.

Using MCNP, each refueling cycle is simulated and its output is fed to the next refueling cycle. The total performed simulation is 220 cycles, where 99 of them are the pre-equilibrium cycles. A similar and simpler online refueling study using MCNPX based on material homogenization can achieve faster equilibrium phase and requires less computational resources (Wu et al., 2019). However, a homogenization may change the physics. This study is instead using a higher fidelity modeling to provide more detailed fuel pathway information and fuel residence history based on its position in the core.

3.2.4. PR calculation

The PR calculation is performed on the discharged fuel only to compare the different refueling schemes. The calculation methodology uses the one described in Chapter 2. Both the PRAETOR and the simplified methodology for PR assessments are performed and their results compared.

3.3. Results and Discussion

3.3.1. One-batch refueling scheme

Figure 3-3 shows the simulation result for the HTR-10 with the one-batch refueling scheme. Using this scheme, the subsequent refueled profile will be completely the same, since the core is replaced totally using fresh fuel pebbles (FFP). The initial k_{eff} was 1.202, but then it dropped significantly by about 350 pcm in two days due to the buildup of ^{135}Xe and other neutron poisons. The k_{eff} decreased constantly and reached near subcriticality (k_{eff}=1.000) in 845 days, which is equal to an average burnup of only 65.91 GWd/MTU (ref. Fig. 3-3). Hence, it cannot reach the targeted operation time of 1154 days, as expected because of the one-batch refueling scheme.

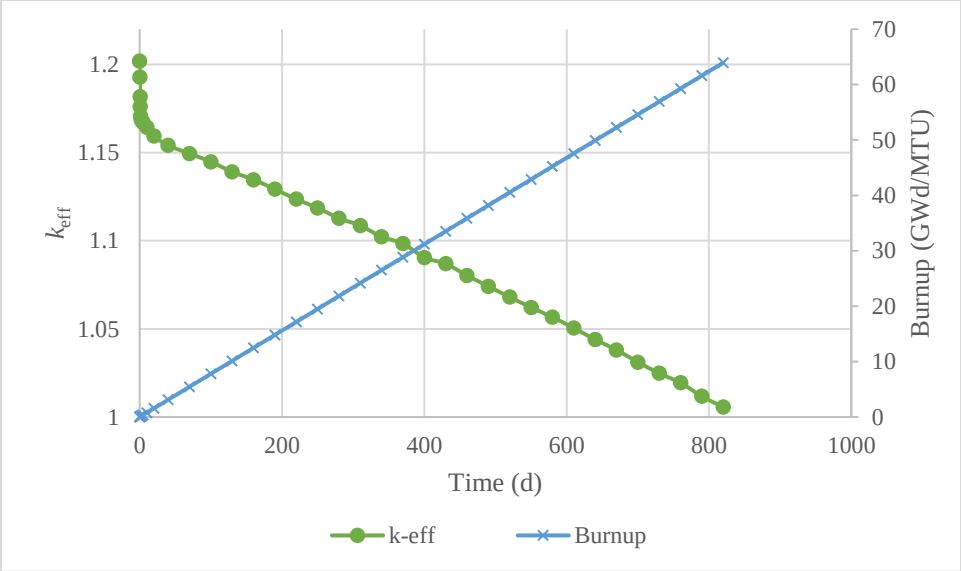

Figure 3-3. Effective neutron multiplication factor and burnup history over time for the one-batch refueling scheme.

After reaching a subcritical state, 1.42 kg of plutonium (much less than 1 SQ of plutonium) and 116.35 kg of uranium is in the core. This means the (core averaged) spent fuel contains plutonium of 1.1 wt% (ref. Fig. 3) and uranium of 90.7 wt% relative to the initial uranium loading of 128.28 kg. Approx. 10.36 wt% (12.06 kg) of the total uranium left in the core is ^{235}U (Mulyana and Chirayath 2019). This amount is less than 1 SQ value for LEU which is 75 kg of ^{235}U. The percentage of plutonium content is comparable to that found in typical commercial LWR spent fuel, which is 1.39 wt% at 70 GWd/MTU and 0.9% at 45 GWd/MTU (Nakano and Okubo 2011).

Using HTR-10 with a one-batch refueling scheme, a proliferator might need 6 (rounded up from 5.52) cycles, which is approximately 5070 days, to get 1 SQ of plutonium and 7 (rounded up from 6.22) cycles, which is approximately 5912 days, to get 1 SQ of LEU. We might find this PBR system to be proliferation-proof and conclude that

its fresh fuel only poses the proliferation concern, not its spent fuel. Its fresh fuel contains 21.81 kg of ^{235}U, and hence a proliferator could divert 1 SQ of LEU from fresh fuel in 4 cycles. However, the HTR-10 is an experimental reactor with a small fissile load producing only 10 MW thermal (Wu, 2002). To meet the market's needs for electricity generation in the future, the HTR-10 is meant to be rescaled to be a modular reactor producing 250 MWth per module, which the HTR-PM is intended for.

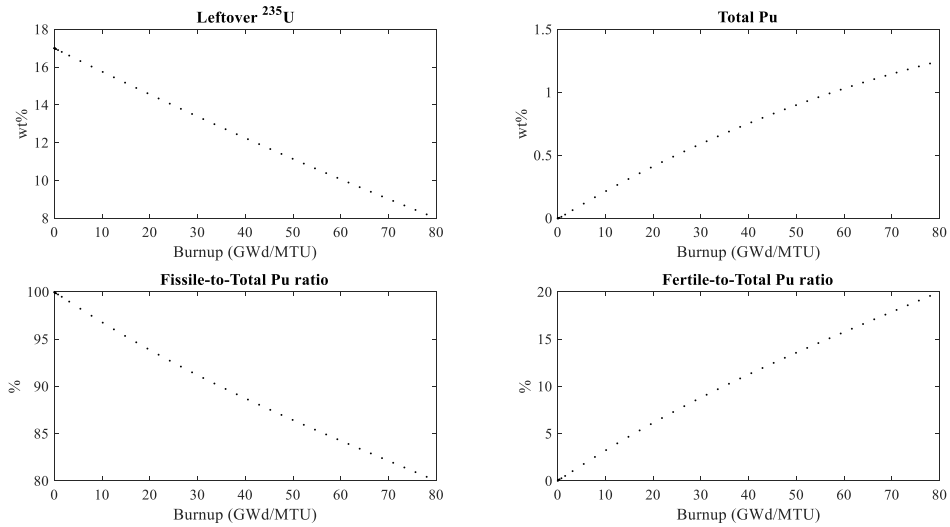

Figure 3-4. ^{235}U leftover (top-left) and total plutonium (top-right) mass in percentages relative to initial uranium loading; fissile (bottom-left) and fertile (bottom-right) plutonium percentages relative to total plutonium produced in one-batch scheme.

If the reactor module is rescaled and its cycle period of 845 days is preserved, a 250 MWth core will be loaded with 3,206.9 kg of uranium. Assuming the same 17wt% uranium enrichment and 5 g of UO_2 per pebble, the fresh fuel contains 7.27 SQ of LEU per module per cycle. Taking the same nuclide percentage of HTR-10, the upscaled module would produce approximately 35.27 kg (1.1wt% of initial U) of plutonium per year (with a burnup of 65.91 GWd/MTU) and would leave 2,908.6 kg of the remaining

LEU with 10.36wt% of ^{235}U. These are equal to 3.14 SQ of plutonium and 4.01 SQ of LEU per module per cycle or 1.9 SQ of plutonium and 1.73 SQ of LEU per module per year. Suppose that a power plant needs to produce 1000 MWe; it will yield 19 SQ of plutonium and 17.3 SQ of LEU per year assuming the reactor's thermal efficiency is 40%.

The quality of the plutonium is quite good from a nuclear weaponization perspective. At 65.91 GWd/MTU, using the one-batch scheme, the average fissile content of the plutonium in the core is 82.9% of the total plutonium. This is significantly higher than that of the LWR which is 62.7% at 70 GWd/MTU and 61.1% at 45 GWd/MTU (Nakano and Okubo 2011). This high fissile plutonium content is obviously a proliferation concern. The fissile content would be much more if the refueling cycle were shorter than 845 days, which also means a lower burnup value (ref. Fig. 3-4). This must be noted when applying any safeguards approach, because the total plutonium produced will be lower, which implies a longer period to get 1 SQ of plutonium, and that can be mistakenly implied to be a lower proliferation risk.

3.3.2. One-Through-Then-Out (OTTO) refueling scheme

Three independent simulations of the OTTO refueling scheme are completed with 99 cycles each. Fig. 3-5 shows the k_{eff} as a function of time for all three target burnup values of 75, 80, and 90 GWd/MTU, indicated by their respective refueling period of 29 days, 31 days, and 35 days. For each burnup value, each of the reactivity swings indicates that the refueling is carried out. The largest swing in effective neutron multiplication factor is at the very first cycle and is caused by the neutron poisons, especially by ^{135}Xe and ^{149}Sm. The swings within the pre-equilibrium phase are smaller, since the core, before

refueling, still has more fissile uranium than in the equilibrium phase. As the operation is approaching the equilibrium phase, the swings are more consistent and vary at a range of 49 to 77 pcm, 63 to 87 pcm, and 75 to 103 pcm for the burnup case of 75, 80, and 90 GWd/MTU, respectively.

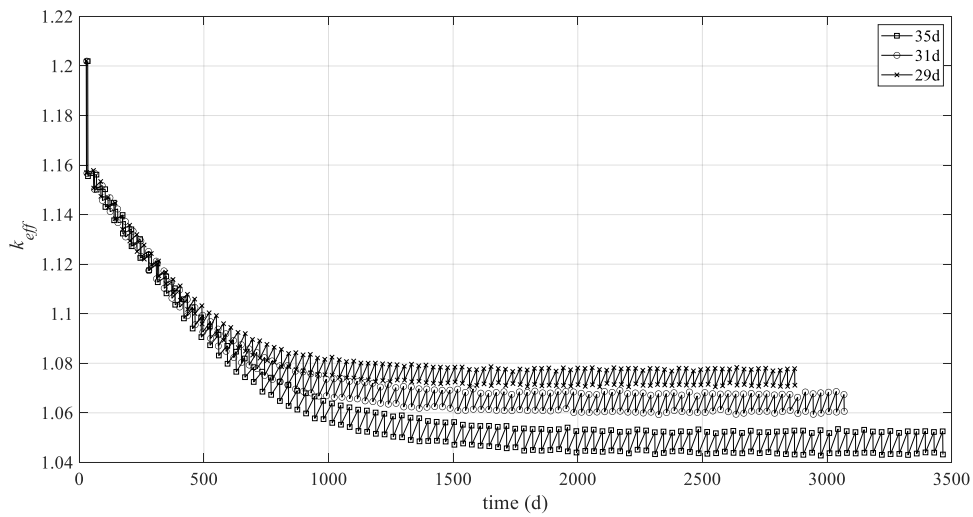

Figure 3-5. Effective neutron multiplication factor for the refueling period of 29, 31, and 35 days.

After the insertion of the 34th refueling pebble, the discharge burnup starts to reach equilibrium and its mean values are 75.33 ± 0.10, 82.94 ± 0.15, and 94.11 ± 0.23 GWd/MTU for the refueling periods of 29, 31, and 35 days, respectively. The results are showing that all simulations successfully reach all the target values of 75, 80, and 90 GWd/MTU. The pebbles can be burned longer than the 35-day refueling period to achieve a higher target burnup than 90 GWd/MTU, since the k_{eff} in the equilibrium phase is approximately 400 pcm higher than the critical point. From the three simulations, the maximum attainable burnup for the 17wt% pebble fuel can be approximated as nearly 118

GWd/MTU. This maximum value can be increased by adding more fissile content in the pebble, either its initial enrichment or in the number of TRISO per pebble assuming constant densities.

The atomic density of some key nuclides as a function of time obtained from MCNP simulations of different fuel burnup targets are shown in Fig. 3-6. Each nuclide identity is ZZAAA, where ZZ is the atomic number and AAA is the atomic mass number. MCNP nearly produced all possible nuclides, depending on the availability of the used nuclear data, by using its tier 2 option of the burnup simulation. As expected, at a higher fuel burnup, ^{235}U is burnt more, and more ^{238}U is converted, yielding more ^{237}U and ^{239}U. These also increase plutonium isotope production linearly. The less leftover ^{235}U and fissile plutonium (refer to Fig. 3-8) at higher burnup values would lead to a higher PR, although the total plutonium amount becomes higher, as expected. These effects are due to the higher total neutron flux in the core with higher burnup values, which also means longer refueling periods, given the power is constant (refer to Fig. 3-7). This behavior of the flux provides an insight for reactor safeguards design that any refueling period modification will also change the flux, and this should be detectable using an in-core power measurement.

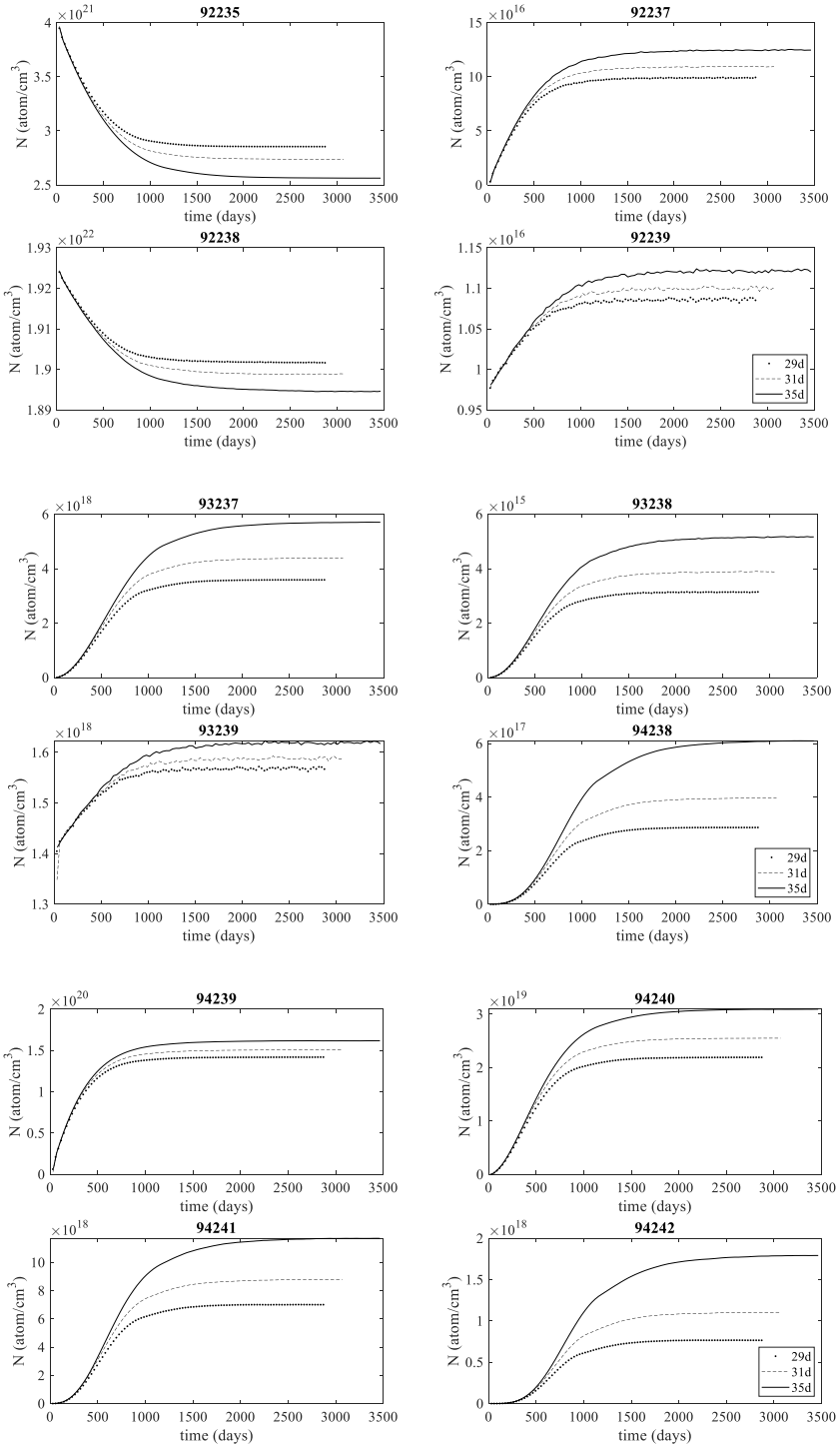

Figure 3-6. Mean value of some key nuclide densities produced in the core (without cooling) by OTTO scheme.

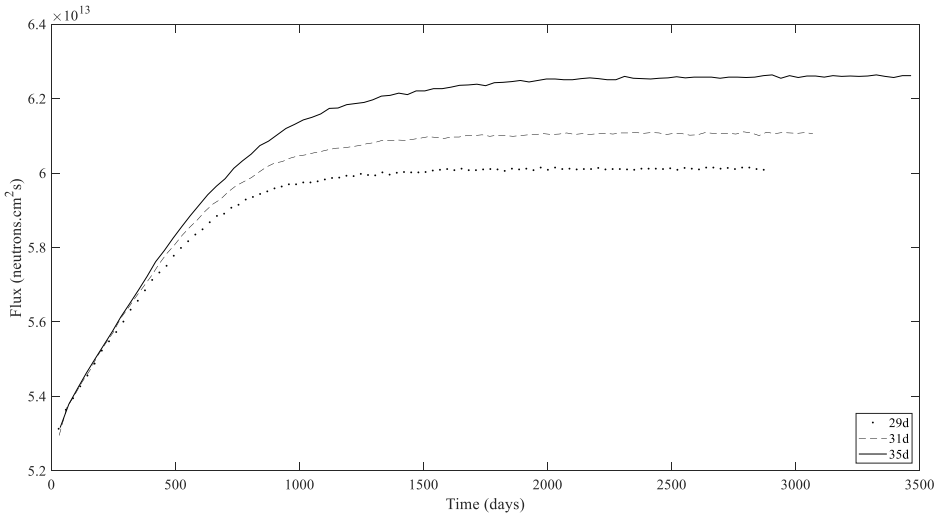

Figure 3-7. Total neutron flux history over different refueling periods with the OTTO scheme.

The average quantity of plutonium and ^{235}U leftover in the core are somewhat different from the one-batch scheme. At 75 GWd/MTU, the relative percentage of total plutonium over the initial uranium loading is 0.74% ± 0.01%. The ^{235}U in the leftover uranium becomes 12.19wt% ± 0.06wt%. With a 10 GWd/MTU higher burnup, it leaves ^{235}U 17.7%, higher than the one-batch scheme. This will shorten the required time to collect 1 SQ of LEU. Conversely, the total plutonium percentage is 32.7% lower, which will require more time to collect 1 SQ of plutonium. However, the average fissile plutonium content in the core is 86.70% ± 0.18% over the total plutonium (ref. Fig. 3-8), which is 4.6% higher than the one-batch scheme. This number is decreased to 84.03% ± 0.27% when the burnup is 90 GWd/MTU, but the total plutonium increases to 0.89wt% ± 0.01wt% (ref. Fig. 3-8). Therefore, the core inventory of the OTTO can be inferred as

having a higher proliferation risk than the one-batch scheme. Note that this is the data for all the pebbles in the core and that the discharged pebbles may be somewhat different.

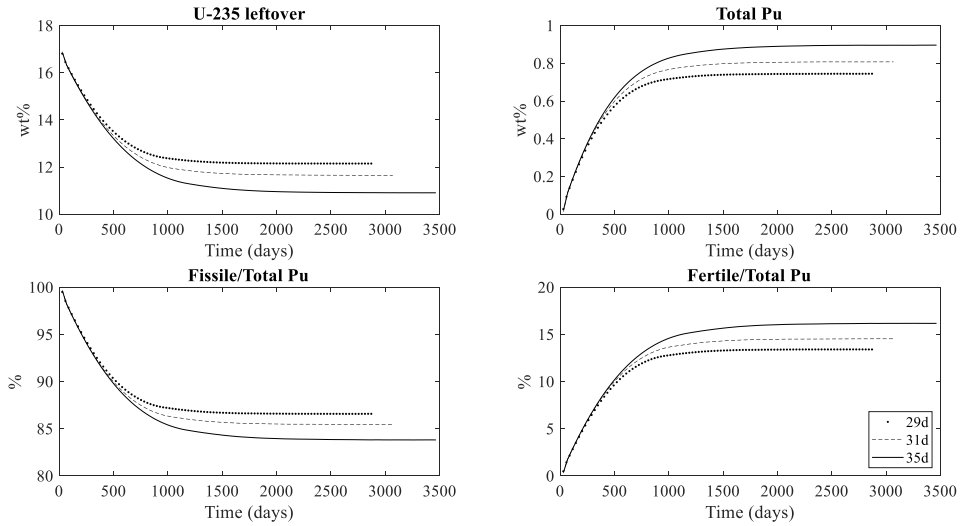

Figure 3-8. Mean value of nuclide percentage in the core by the OTTO scheme: leftover ^{235}U (top-left) and total plutonium (top-right) mass in percentages relative to initial uranium loading; fissile (bottom-left) and fertile (bottom-right) plutonium isotopes in percentages relative to total plutonium produced.

The radial neutron flux shape does not vary significantly with different refueling periods in the OTTO schemes, since the scheme assumes that the fuel position does not change radially. Fig. 3-9 shows the flux shape of layer 15 from the top when the core is in the equilibrium phase, exactly seven years after the core starts operating. The thermal group neutron flux energy ranges from 0 to 0.625 eV, while the intermediate group neutron flux energy ranges from 0.625 eV to 100 keV, and the fast group neutron flux energy is anything above 100 keV. The mean value of the thermal neutron flux of the longest refueling period (35 d) is slightly higher at all radial positions, but its shape is not significantly different compared to others.

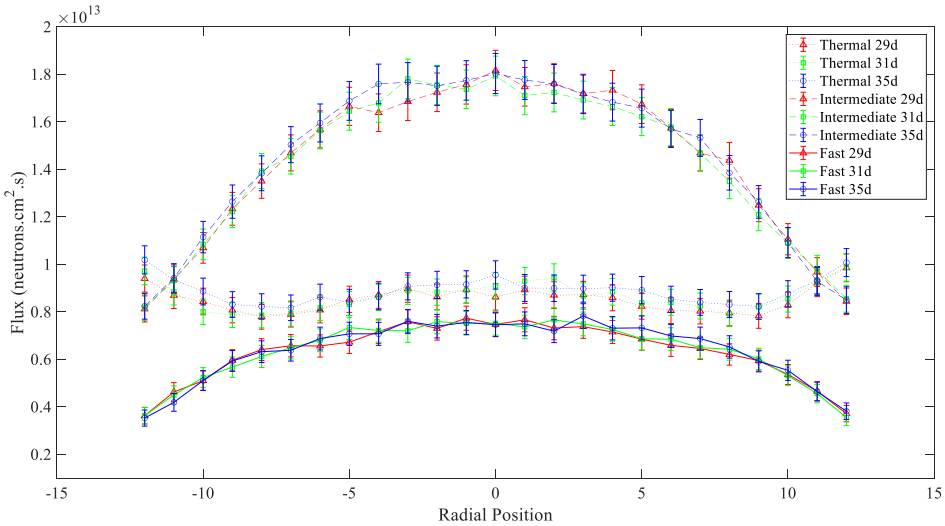

Figure 3-9. Radial neutron flux distribution in the core center over different refueling periods with the OTTO schemes at time of 7 years after starting up.

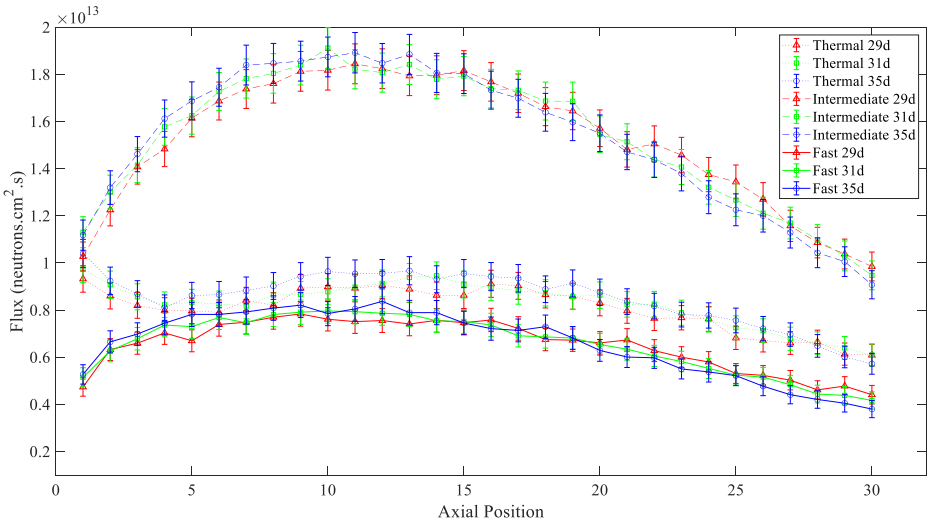

Figure 3-10. Axial neutron flux distribution in the core center over different refueling periods with OTTO scheme at time of 7 years after starting up (position 0 is the top).

Meanwhile, the axial neutron flux shape, especially of the intermediate and the fast energy neutrons, changes observably with the varying burnup (ref. Fig. 3-10). These

higher energy neutrons are higher at the upper core position and smaller at the lower core position when the refueling period is longer. This is as expected because, with a longer refueling period, the fuel resides longer at any position. As the fuel moves downward, it is losing more ^{235}U, causing the ^{235}U mass difference between the newly inserted fuel at the top and the longer residing fuel to increase. However, the axial thermal flux shapes do not vary with the different refueling periods, and they are different only by their overall intensities. This is because the total thermal neutron loss and production rates do not change axially when the refueling period changes.

The proliferation resistance assessment in this study is assuming that the diversion is taking place on a one-year cooled spent fuel, which also assumes that the fuel handling is much safer since the radiation load is lower. This assumes that the assessment is only made on the discharged spent fuel, which is going to be stored in the spent fuel inventory. To account for this, the simulated average data is then fed into another MCNP simulation for calculating the mass of all nuclides after one year of cooling. The mass input to the cooling simulation comes from only the bottom layer of the core (i.e., the 33rd) within cycle 50th through 99th to represent the discharged spent fuel within these cycles. Table 3.1 shows all uranium and plutonium isotope mean masses after one year of cooling averaged within the equilibrium phase. As expected, at higher burnups, the total plutonium produced (up to 1.33%) in this scheme relative to its initial uranium loading is higher than the value of the same parameter in the one-batch scheme, which is 1.13%.

Table 3-1. Average value of uranium and plutonium nuclide masses per Spent Fuel Pebble within the equilibrium phase of three refueling periods (after one-year cooling). All values are within a confidence interval of 99%.

nuclide	29 days (75 GWd/MTU)	31 days (80 GWd/MTU)	35 days (90 GWd/MTU)
^{235}U (g)	3.87E-01 ± 1.62E-03	3.56E-01 ± 2.43E-02	3.18E-01 ± 3.10E-02
^{238}Pu (g)	1.77E-04 ± 2.83E-06	2.39E-04 ± 4.59E-06	3.58E-04 ± 1.03E-06
^{239}Pu (g)	3.89E-02 ± 8.58E-05	3.99E-02 ± 9.83E-05	4.08E-02 ± 4.95E-05
^{240}Pu (g)	9.04E-03 ± 5.64E-05	1.02E-02 ± 7.55E-05	1.18E-02 ± 1.02E-04
^{241}Pu (g)	3.19E-03 ± 3.28E-05	3.82E-03 ± 4.54E-05	4.77E-03 ± 6.27E-05
^{242}Pu (g)	5.08E-04 ± 8.98E-06	7.06E-04 ± 1.49E-05	1.09E-03 ± 2.86E-04
^{241}Am (g)	5.08E-04 ± 8.98E-06	3.58E-04 ± 5.16E-06	4.78E-04 ± 1.06E-06
Total Pu (g)	5.14E-02 ± 1.30E-03	5.51E-02 ± 1.40E-03	5.83E-02 ± 1.50E-03
Total Pu*	1.18wt%	1.25wt	1.33wt%
Total ^{235}U leftover*	8.86wt%	8.18wt%	7.21wt%
Number of cycles for 1 SQ of Pu**	175.0 ± 1.1 (4943.6 ± 31.0 days)	165.3 ± 1.2 (4668.4 ± 37.2 days)	154.3 ± 1.1 (4358.8 ± 39.2 days)
Number of cycles for 1 SQ of LEU**	219.8 ± 2.8 (6210.6 ± 78.1 days)	238.7 ± 4.0 (7399.1 ± 124.3 days)	272.1 ± 7.1 (9523.9 ± 250.1 days)

*relative to initial uranium based on the mean values.
**For HTR-10

3.3.3. Multi-pass refueling scheme

Figure 3-11 shows that the k_{eff} of the multi-pass (3-passes) is higher than that of the OTTO (1-pass) scheme at any given time of irradiation, which is expected because, in the multi-pass refueling scheme, the fuel pebble is not only shuffled axially, but also radially. The smaller swing in k_{eff} for the multi-pass is due to the shorter refueling period. The pre-equilibrium phase is assumed to be 99 cycles, or equal to one full pass of each pebble through the entire core, and the flattening of the k_{eff} curve can be observed in Figure 3-11 after approximately 1,000 days (10.3 days per cycle x 99 cycles for one full pass) of irradiation. Since this study focuses on the continuous online refueling, the mass of the nuclides of interest within the equilibrium stage are averaged.

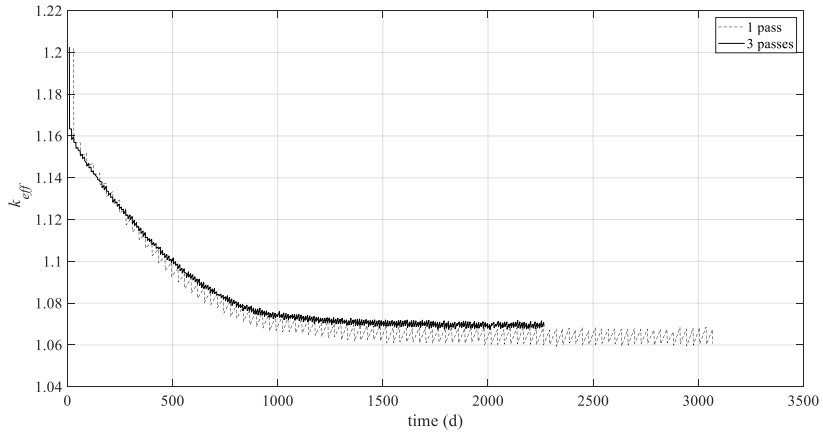

Figure 3-11. Effective neutron multiplication factor for the 3-passes and 1-pass (OTTO) refueling schemes targeting a same fuel burnup of 80 GWd/MTU.

After reaching its equilibrium (cycle 100th and after), the 10.3 days refueling period per cycle of 3-pass scheme yields spent fuel pebbles with an average discharge burnup of 81.38 ± 1.48 GWd/MTU achieving the intended target burnup of 80 GWd/MTU. However, since the performed multi-pass scheme is passing each fuel pebble to the three main core zones, the attainable burnup can also be grouped into three zones by excluding the fourth zone. Spent fuel attains burnup differently among different core zones due to the neutron flux radial variation. Through the first zone it attains 30.73 ± 0.51 GWd/MTU, through the second zone it attains 27.09 ± 0.29 GWd/MTU, and through the third zone it attains 24.95 ± 0.27 GWd/MTU, which all are within a confidence interval of 99%.

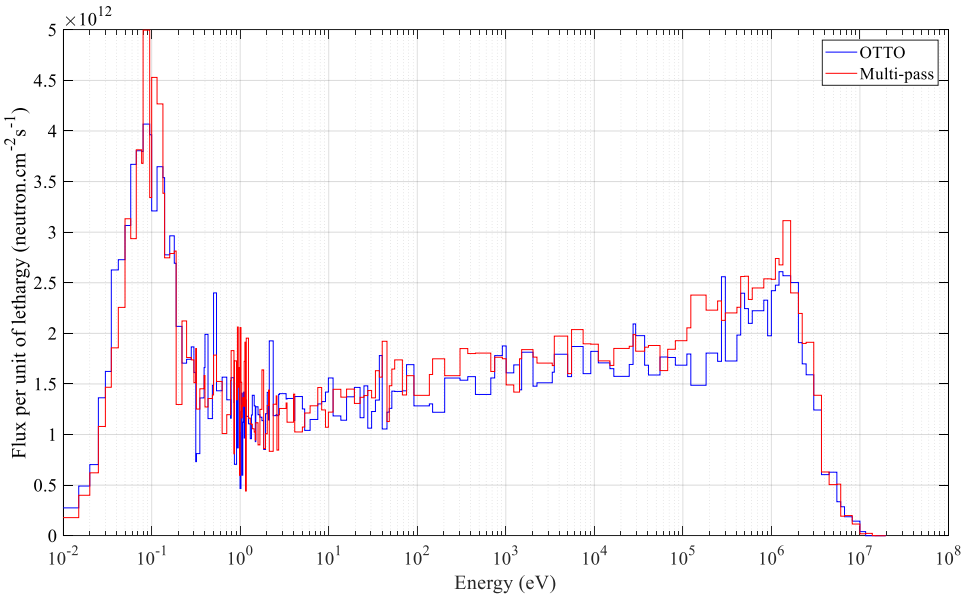

Figure 3-12. Neutron Spectra comparison of OTTO and multi-pass refueling schemes at the center of the core with a confidence interval of 99%.

Figure 3-12 shows the neutron spectrum at the center of the core, axially and radially. The neutron flux levels are high for the multi-pass refueling scheme because of less fissile material content in the core compared to the OTTO refueling scheme, which means that if the same power has to be drawn it will lead to a higher neutron flux.

Radially, the highest attainable burnup is within the center of the core, since the deployed refueling is an in-out pattern where the fresh fuel is always be at the center since more ^{235}U is available. This will differ with the transmutation processes, especially with ^{238}U, at different radial positions in the core.

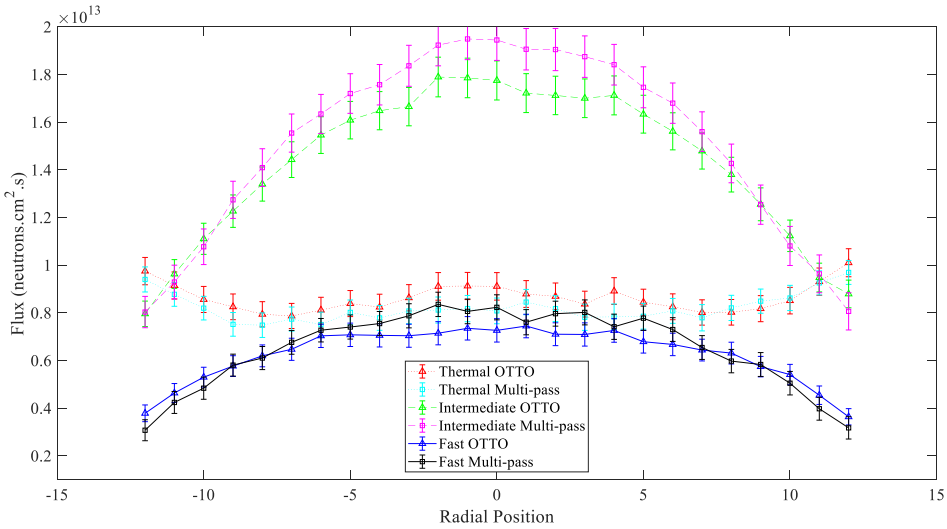

Figure 3-13. Radial neutron flux distribution at core center of the OTTO Vs multi-pass refueling schemes after 6 years of reactor startup.

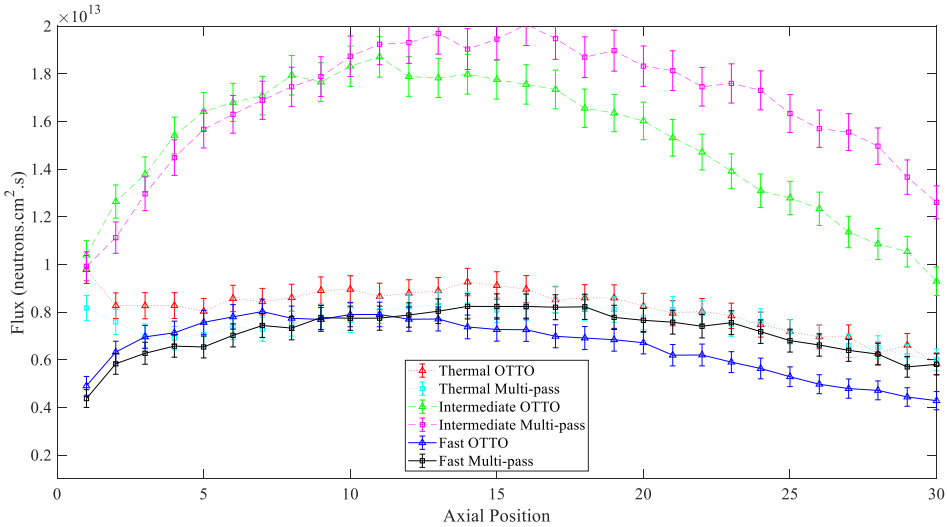

Figure 3-14. Axial neutron flux distribution at core center of the OTTO Vs multi-pass refueling schemes after 6 years of reactor startup.

The axial neutron distribution in the core with the multi-pass refueling scheme is not higher at the upper core like with the OTTO (ref. Fig. 3-14). All the neutron energy group fluxes with the multi-pass refueling scheme peak more to the axial center. This is

because the fresh fuel in the multi-pass is less and flattens down the flux shape at the upper core. The higher ^{235}U content in the top core makes the OTTO produce more fissions within the zone. The multi-pass reduces this effect, reshapes the neutron flux, and hence peaks at a relatively lower axial zone than the OTTO.

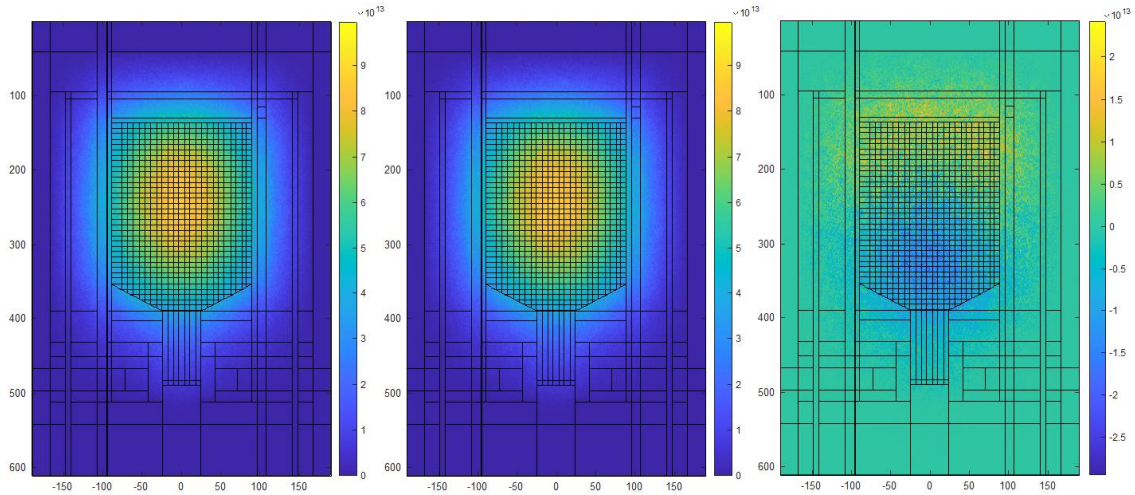

Figure 3-15. Total neutron flux of OTTO (left) Vs multi-pass (center) refueling schemes and the difference between the two (right), where positive values show the OTTO is higher. Vertical axis is the reactor height and horizontal axis is the radial position in cm.

The total neutron flux map of the multi-pass in the core does not seem to be different from of the OTTO. However, the difference map can tell that the OTTO has more neutrons at the upper zone (ref. Fig. 3-15). Conversely, the multi-pass has more neutrons at the lower zone. Due to these, the depletion of ^{235}U will be much more at the upper core with the OTTO, but at the lower core with the multi-pass scheme. This will also affect the amount of transmutation products with a short half-life (e.g., ^{239}U and ^{239}Np) in the core and in the discharged spent fuel, which will directly affect ^{239}Pu inventory.

Fig. 3-16 shows the produced nuclide accumulation in the core of the multi-pass refueling scheme at 80 GWd/MTU with a comparison to the OTTO simulation. Not all the nuclides reach equilibrium masses at the same cycle. However, in general, they all do after approximately 150 cycles. In Fig.3-16 and 3-17, the core average values account for all nuclides in the core at any time, while the discharged values account for only the discharged pebbles at each cycle. In the multi-pass, the discharged pebbles are the 99th layer which is the 9th layer of the fourth zone coming from the 33rd layer of the third zone. Meanwhile, in the OTTO scheme, the discharged pebbles are from the 33rd layer.

In an equilibrium core with a constant power, the multi-pass refueling scheme burns a similar amount of ^{235}U and ^{238}U as the OTTO. However, the multi-pass refueling scheme spares less ^{239}U in the discharged pebbles (ref. Fig. 3-16). ^{238}U is mostly converted to ^{239}U through neutron capture reaction strongly within an intermediate energy range of 7 eV to 20 keV.

Since the multi-pass refueling scheme is using an in-out pattern, once the fresh fuel has passed through the highest neutron flux point in the first zone, it passes through a much lower neutron flux at the upper second zone before it passes through the higher neutron flux points again. This gives the ^{239}U more opportunity to decay to ^{239}Np while the pebble is still in the low neutron flux zone. Furthermore, the ^{239}Np also decays earlier to ^{239}Pu. Both ^{239}U and ^{239}Np have half-lives of 23.45 minutes and 2.356 days, respectively, which is relatively shorter than the refueling period of 10.3 days. This also allows the produced ^{239}Pu earlier in the first zone to contribute to the power generation through fission in the outer radial zone (e.g., the second and the third zones). This causes

the neutron flux at the lower zone to become even higher (ref. Fig 3.15) and allows the discharged ^{239}Pu in the multi-pass's spent fuel to become less than in the OTTO.

The loss of ^{239}Pu may also be caused by neutron captures to yield ^{240}Pu and other higher atomic mass isotopes. Again, since the multi-pass refueling has a higher neutron flux at the lower core, the rate of these reactions is slightly faster, so the ^{240}Pu, ^{241}Pu, and ^{242}Pu are slightly higher than of the OTTO, although some of the ^{241}Pu also contributes to the power generation through fission as well. The same phenomenon is also responsible for converting more ^{238}Pu into ^{239}Pu in the multi-pass refueling scheme.

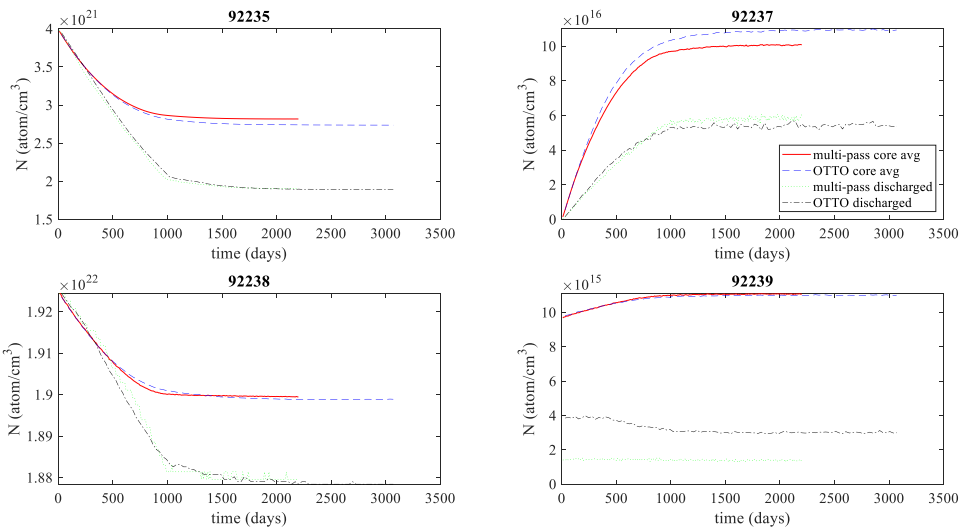

Figure 3-16. Some key nuclides produced in the core (cooling not considered) by multi-pass in comparison with the OTTO refueling scheme.

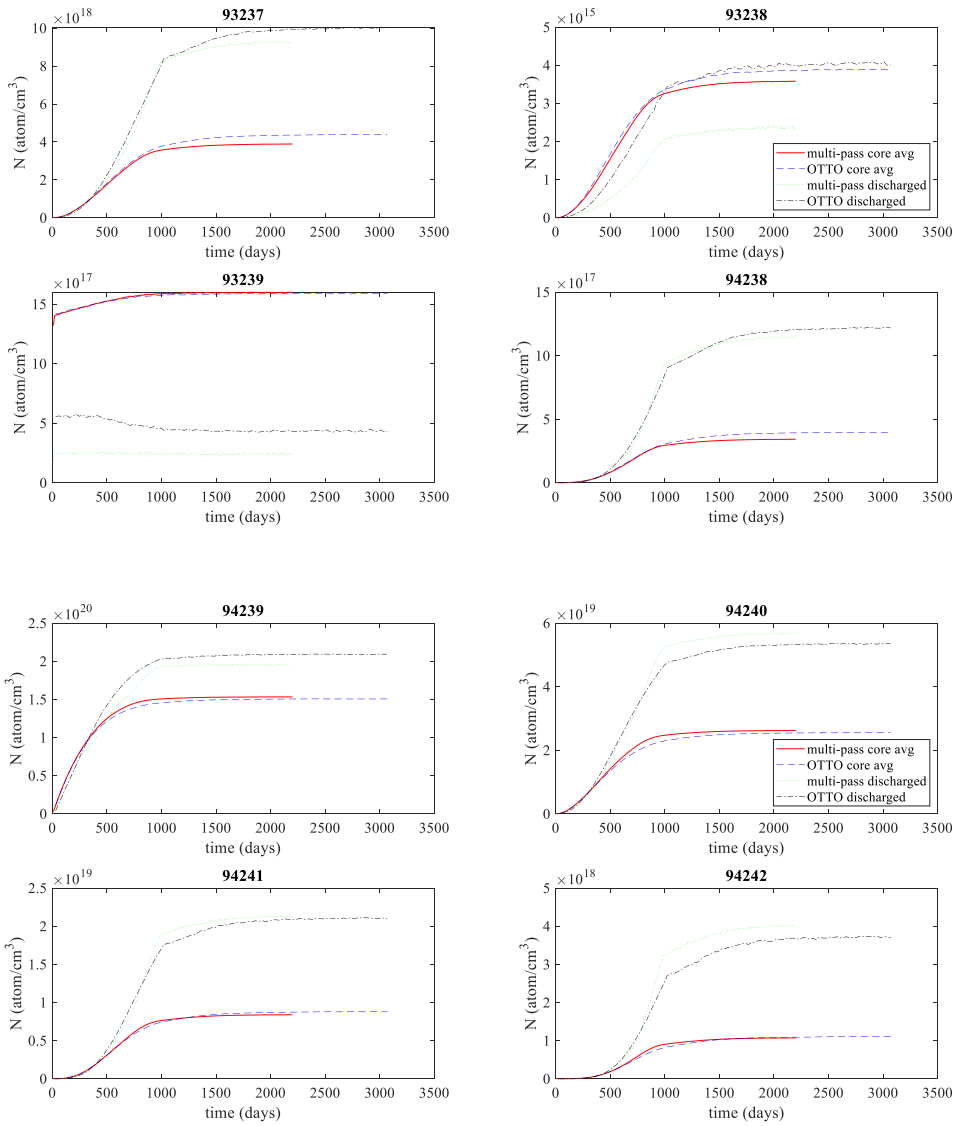

Figure 3-16 (cont.). Some key nuclides produced in the core (cooling not considered) by multi-pass in comparison with the OTTO refueling scheme.

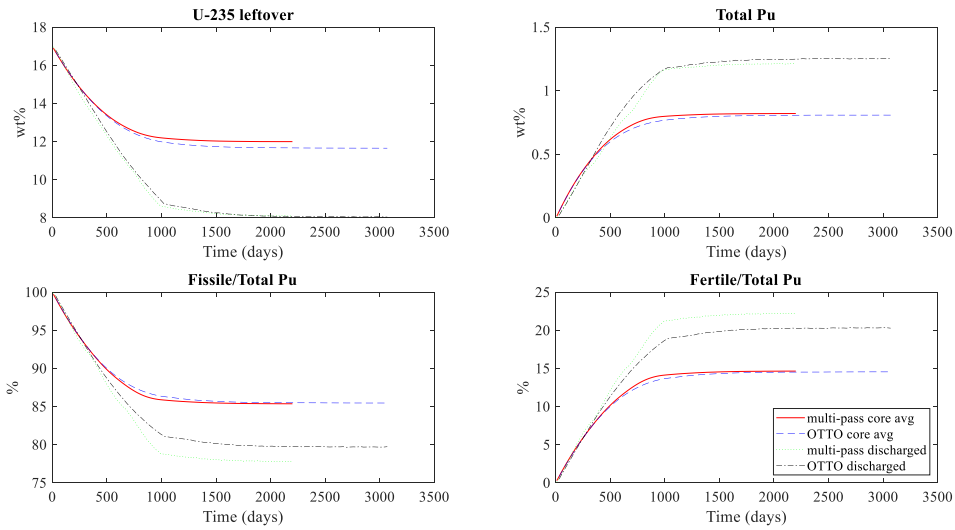

Figure 3-17. ^{235}U leftover (top-left) and total plutonium (top-right) mass in percentages relative to initial uranium loading; and fissile (bottom-left) and fertile (bottom-right) isotopes in percentages relative to total plutonium produced by the multi-pass in comparison with the OTTO refueling scheme.

Like the OTTO simulation, to prepare the PR assessment, the discharged spent fuel is further simulated for a one-year cooling period. After the cooling, each spent fuel pebble has 3.57E-01 ± 5.85E-04 g of leftover ^{235}U. This value is statistically the same as the 31-day OTTO simulation, which is 3.56E-01 ± 2.43E-02 grams. This is because both simulations are targeting the same fuel burnup value of 80 GWd/MTU. However, as mentioned previously, both simulations produce quite different plutonium isotope compositions (ref. Table 3.2). The fissile Pu (^{239}Pu and ^{241}Pu) isotope percentages by the 3-pass method are lower by 5.6%, while the total Pu isotopes are lower by 3.1%. Compared to the OTTO scheme, the multi-pass refueling scheme needs 12.8% longer time to produce 1 SQ of plutonium and relatively the same time to get 1 SQ of LEU.

Table 3-2**. Average values of uranium and plutonium isotope masses per spent fuel pebble within the equilibrium phase of the multi-pass scheme (after one-year cooling). All values are within a confidence interval of 99%.**

Nuclides	**Multi-pass**	
	Mass (g)	**percentage***
Leftover ^{235}U	3.57E-01 ± 1.76E-03	8.1091%**
^{238}Pu	2.30E-04 ± 3.08E-06	0.4287%
^{239}Pu	3.75E-02 ± 1.48E-04	69.9530%
^{240}Pu	1.08E-02 ± 6.77E-05	20.2470%
^{241}Pu	3.90E-03 ± 3.32E-05	7.2731%
^{242}Pu	7.72E-04 ± 1.13E-05	1.4418%
^{241}Am	3.51E-04 ± 3.19E-06	0.6560%
Total Pu (g)	5.32E-02 ± 1.76E-03	1.2158%**
Number of cycles for 1 SQ of Pu***	511.2 ± 1.6 (5265.7 ± 16.5 days)	
Number of cycles for 1 SQ of LEU***	713.9 ± 3.5 (7353.2 ± 36.1 days)	

* based on the mean values.
** relative to initial uranium
*** for HTR-10

3.4. PR Evaluation

3.4.1. PR Evaluation using PRAETOR

Using the same methodology for calculating PR with PRAETOR described in Chapter 2, the PR values are calculated for the OTTO and the multi-pass refueling schemes to compare how significantly the multi-pass refueling scheme may change the PR value. Figure 3-18 shows the PRAETOR calculated PRs and all associated utility values can be found in Table A.2. The weights of all attributes are the same values as in Table A.1.

At burnup level of 75 and 80 GWd/MTU, Pu has a higher PR than ^{235}U. This is due to the low Pu quantity contained in the SFP, resulting in a high number of SFP needed to be collected to achieve 1 SQ of Pu. At 90 GWd/MTU, the PRs for Pu and ^{235}U are the highest.

The multi-pass scheme does not increase the PR of ^{235}U diversion at the same burnup level, since the multi-pass does not change the quantity of leftover ^{235}U in the SFP significantly. In fact, the total Pu quantities in both schemes are not significantly different. However, the PR of Pu in the multi-pass is slightly higher due to the higher fertile Pu isotope quantity that directly increase the radiation quantities of the SFP.

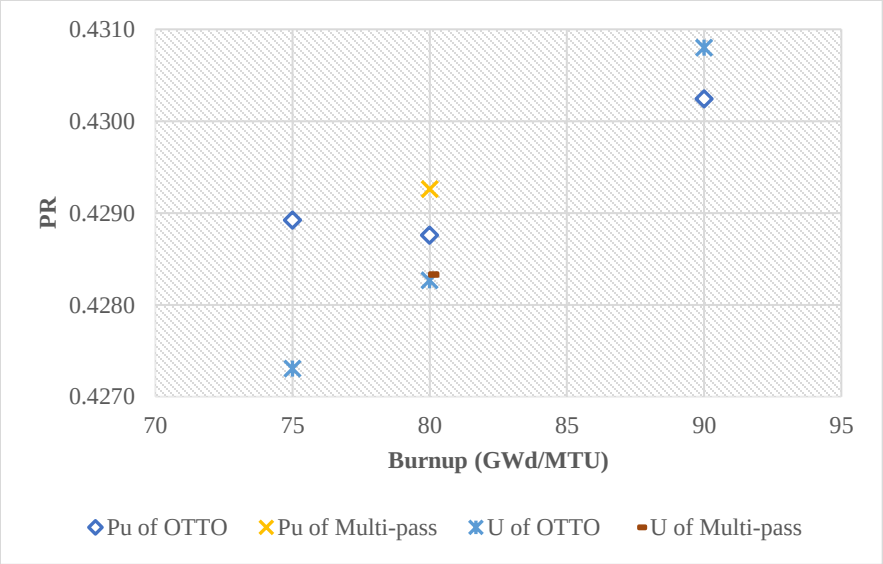

Figure 3-18. PR of HTR-10 with OTTO and multi-pass refueling schemes calculated using PRAETOR

3.4.2. PR Evaluation using the simplified MAUA method

Table 3 shows all the simulated parameters using the data from Tables 1 and 2. The simulation is only on the discharged spent fuel pebble of the OTTO and the multi-pass refueling scheme simulations. No spent fuel pebbles in the core are simulated for PR evaluation since the isotopic composition in the core varies greatly among the irradiated pebbles.

Table 3-3. PR parameters of a plutonium sphere

	OTTO 75 GWd/MTU	**OTTO 80 GWd/MTU**	**OTTO 90 GWd/MTU**	**Multi-pass 80 GWd/MTU**
Spontaneous Fission neutron rate ($neutrons.s^{-1}g^{-1}$)	9.27E+02 ± 1.07E-02	9.73E+02 ± 1.00E-02	1.04E+03 ± 1.07E-02	1.02E+03 ± 1.05E-02
Heating rate ($W.kg^{-1}$)	5.25E+00 ± 4.92E-07	5.92E+00 ± 5.82E-07	7.07E+00 ± 7.22E-07	6.09E+01 ± 6.02E-07
Radiation exposure ($R.h^{-1}$)	5.83E-02 ± 5.28E-05	6.12E-02 ± 5.58E-05	6.56E-02 ± 6.04E-05	7.67E-02 ± 1.35E-04
Rossi-α (s^{-1})*	-1.47E+06 ± 1.26E+03	-1.52E+06 ± 1.58E+03	-1.60E+06 ± 1.47E+03	-1.60E+06 ± 1.84E+03

*negative value is indicating a subcritical system.

The PR of the OTTO refueling scheme increases as the burnup increases (ref. Fig. 18), as expected, due to the increase of fertile plutonium isotopes content. Although the fissile isotope content also increases, the rate of fertile plutonium production is higher with higher burnup. At the same burnup of 80 GWd/MTU, the multi-pass refueling scheme increases the mean of its PR by 7.2%. However, within a confident interval of 99%, the PR of the multi-pass scheme is not statistically higher than the OTTO. Since MCNP does not have any capability to include the uncertainties in Table 3.2, the final uncertainty of the PR may change due to the unaccounted uncertainties.

The mean value of the multi-pass PR at the same burnup is higher than that of the OTTO due to its 6.44% higher fertile content and its 5.44% lower fissile content. These increase radiation emissions from the different plutonium isotopic composition of the multi-pass refueling scheme. The lower fissile content improves the PR value because of the reduction in the α value (more negative). This causes the material to need a longer

period to achieve prompt criticality, which will make it less attractive as a weapons material.

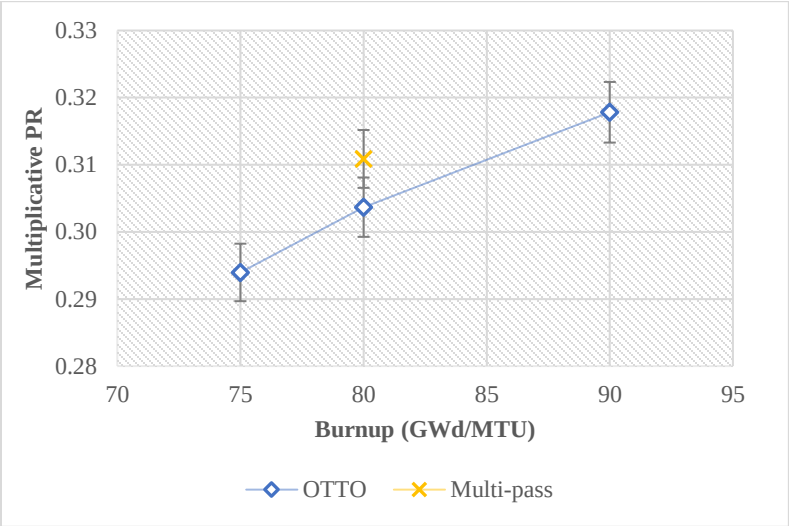

Figure 3-19. Plutonium PR of HTR-10 with the OTTO and multi-pass schemes calculated using the simplified MAUA.

Compared to PRAETOR's result, the simplified MAUA provides a consistent linear increment of PR with burnup. The PR at 75 GWd/MTU is calculated as much lower than by PRAETOR. As mentioned earlier, this is because the simplified MAUA only accounts for intrinsic parameters and is not being affected by the low Pu quantity in each spent fuel pebble.

4. PROLIFERATION RESISTANCE COMPARISION OF PRESSURIZED WATER REACTOR AND PEBBLE BED REACTOR TECHNOLOGIES

4.1. Introduction

As one of the generation IV reactors, the PBR is expected to be highly proliferation resistant. The best way to prove this is by performing a PR benchmark with other reactor technologies. Comparing the future to the current technologies provides a justifiable basis to provide a quantitative decision-making framework to choose the reactor technology itself or its associated fuel cycle. Since PR benchmarking needs a standard metric, the same tool or methodology must be applied uniformly as far as possible. This chapter aims to compare the PR of the PBR and PWR using the assessment methodology described in Chapter 2.

In this chapter, the Pebble bed modular reactor (PBMR-400) representing the PBR technology will be compared to the iPWR design of Babcox & Wilcox (Erighin 2012) representing the LWR technology, using the simplified PR assessment methodology, which provides a rapid way to calculate the PR of the two different technologies. Both reactor designs meet the criteria of an SMR requiring a long fuel cycle. The reduced need for refueling makes the SMR suitable for deployment at a remote area. Hence, the one-batch refueling scheme is suitable for the comparison. The PR assessment and comparison are based on the data generated by reactor physics simulations using MCNP performed on both reactor models.

A fair comparison should be made based on a comparable power level for both reactor types. The PBMR-400 is designed to produce a power output of 400 MWth, while

the iPWR design of Babcox & Wilcox is intended to produce a power output of 500 MWth. Due to a power discrepancy of 100 MWth, the PBR-400 design will be modified to compensate the power upgrade to 500 MWth, so that the comparison is on a uniform footing of rated power output. However, no modification will be made either to the fuel or to the reactor designs itself.

4.2. Methodology

The material quantity information needed for the PR calculations is generated by Monte Carlo simulations using MCNP 6.1 on modified PBMR-400 and B&W iPWR designs. Both designs will be simulated for a full 500MWth power without any interruption and without any reactivity control deployment. IAEA TECDOC 1694 provides a complete technical specification to develop the PBMR-400 model in MCNP 6.1. Kitcher and Chirayath (2016) provided sufficient information to simulate B&W iPWR operation within MCNP 6.1.

The PBMR-400 is modified to match the 500MWth power in terms of its fuel packing. Instead of using the BCC, a hexagonal closed packing (HCP) with a packing ratio of 74% is deployed to compensate for the power upgrade by adding more fissile loading. However, the fuel parameter is not changed. Hence, the HCP deployment will only increase the number of fuel pebbles in the core.

The PR comparison is made based on the leftover ^{235}U and Pu diversion scenarios in a one-batch refueling scheme on both PBR and PWR systems. Assuming no post-irradiation enrichment to both SNMs, the diversions are set to take place at several burnup values, including each reactor's respective discharge burnup. In each PR calculation, both

SNMs will be averaged over the whole material in the core. This means the PR of the two reactor types will be based on their core inventory as their discharged spent fuel in a one batch refueling scheme.

4.2.1. PBMR-400 design and its modification

The PBMR-400 is based on the evolutionary design of the German AVR, THTR and HTR-Modul designs. Its design started in 1996 and was supposed to be marketed by PBMR (Pty) Ltd. In general, the PBMR-400 design is similar to the HTR-10 except for some aspects. Similar to the HTR-10, the PBMR-400 design is based on a direct Brayton cycle and holds promise for higher efficiency. Because the direct cycle efficiency is very sensitive to the gas outlet temperature, the reactor outlet temperature is 900 ˚C, and the inlet temperature is 500 ˚C. The core diameter is 3.7 m, while the fuel zone height is about 11 m. The core is filled by graphite as a central neutron reflector that makes the core geometry have an annular shape. This central reflector is the significant difference in the PBMR-400 compared to the HTR-10, which is intended to avoid excessive neutron flux in the center of the core, since the PBMR-400 has a larger diameter core. The total number of pebbles in the core is approximately 452,000 with a packing fraction of 61%. Each pebble contains about 15,000 TRISOs totaling 9 grams of uranium with an initial uranium enrichment of 9.6 wt%.

The fuel pebble model used for the MCNP neutronics simulation described in the two previous chapters is used with some changes in the fuel parameters. Instead of containing 7,223 TRISOs, each pebble contains 15,011 TRISOs, using the same simple cubic (SC) configuration but with a lattice cube side size of 0.0778 cm. This is to configure

the pebble to contain the 9 grams of uranium. With this, each pebble has 10.28 g of UO_2 with a density of 10.46 g/cm^3. These only modify the occupancy density in the TRISO deployed zone but will not change the overall dimensions of the fuel pebble (ref. Fig. 2-1).

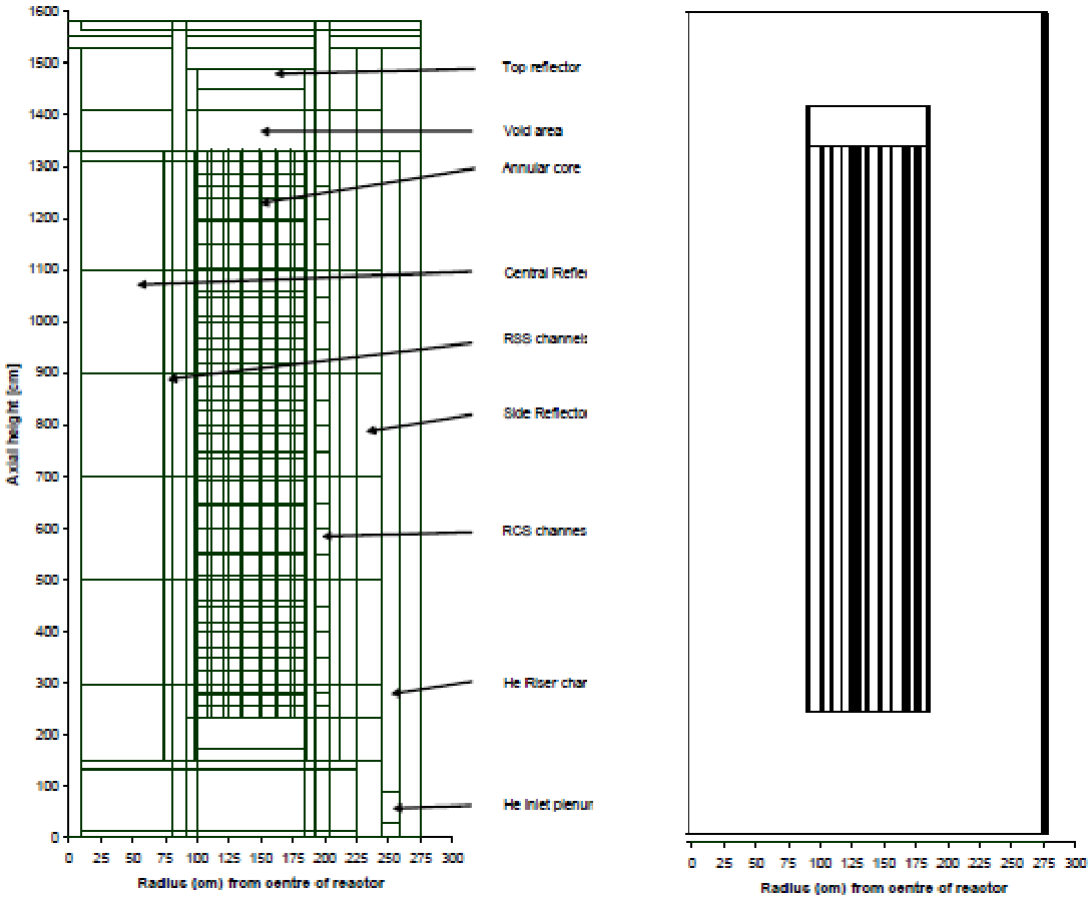

Figure 4-1. PBMR-400 core dimensions layout reprinted from IAEA TECDOC 1694 (left), and a simplified MCNP model using the available dimensions (right).

Fig. 4-1 shows the dimensions of the PBMR-400 obtained from IAEA TECDOC 1694. The core model in MCNP 6.1 is simplified by homogenizing all the graphite

structures and channels as a single material of graphite with a density of 1.78 g/cm^3. This includes the top and bottom reflectors.

Since the specified design of the PBMR-400 will be used for a 500 MWth simulation, the total number in the core will be increased to compensate the power upgrade. This is done by increasing the packing fraction of the pebbles in the core from its original value of 61%, which is considered as dense enough to pack the required number of pebbles. This can be done using the same BCC geometry that reaches a packing fraction of up to 68%. Instead of using BCC, this study uses the HCP configuration, which can reach a packing fraction of up to 74%.

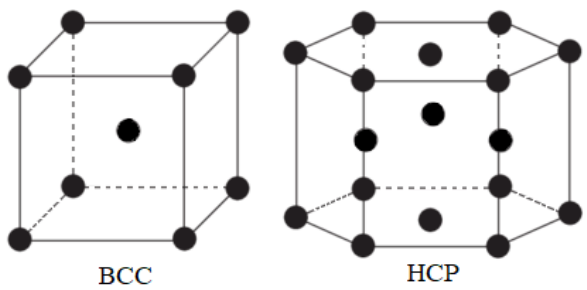

Figure 4-2. Geometry positioning used for pebble packing.

Figure 4-2 shows two pebble configurations: the BCC and the HCP lattices. These configurations are deployed in an infinite lattice simulation using MCNP 6.1. All the pebbles in all configurations are taken from the HTR-10 fuel design specifications presented in the previous chapters. At this step, all the fuel pebbles in the two deployed lattice configurations have the same initial uranium enrichment of 10wt%. Each contains a total UO_2 of 5 g with same number of TRISOs. The pebble dimensions of both are the same. The temperature of both is set at 1200K using ENDF/B-VIII nuclear data for all the

materials in the lattice. The only things that are different are the packing fraction, changing the pebble positioning, and the helium space between the pebbles. The BCC has a packing fraction of 61%, while the HCP is designated for a packing fraction of 74%. Each lattice is simulated at a constant power of 343 Wth per pebble.

The packing fraction of 74% in the PBMR's core with a height of 11.76 m increases the total number of loadable pebbles to 516,480. This does not change the overall core size, but it reduces the void area, since the effective cylindrical height with fuel increases by several tens of centimeters (IAEA TECDOC 1694). With these, the total uranium in the core becomes 4.68 tons. This much fissile loading should be able to provide an upgraded power of 457 MWth to achieve a similar discharge burnup of PBMR-400.

The modeling is carried out at a power of 500 MWth by assuming that the system (including fuel types, fuel enrichment, and fuel positioning) is sufficient to achieve neutron levels to maintain the criticality up to a certain burnup value. The neutron flux in the PBMR-500 is higher than in the PBMR-400. Exempting safety requirements, this assumption is valid since the neutron flux can have any value and the critical reactor can operate at any power. With the power of 500 MWth, the fuel is expected to reach a burnup value of 80 GWd/MTU within 743.7 days. However, as shown in Chapter 3, this may not be achievable using the one-batch operation because of the higher power deployment on the non-resized reactor. Figure 4-3 shows the model used in MCNP simulations.

The depletion simulation uses 3 million particles in 200 cycles of simulation to get a one-sigma stochastic standard deviation of less than 50 pcm in neutron reactivity. Since the packing ratio of the pebble lattice is maximized to 74% using HCP, no statistical

geometry using URAN is deployed. However, URAN is still used to statistically place the TRISOs within the pebble, since the packing fraction is only 13.9%. All the fuel pebble materials and helium coolant are at 1200K while all other reactor materials are at 600K and ENDF/B-VIII data is used within MCNP 6.1.

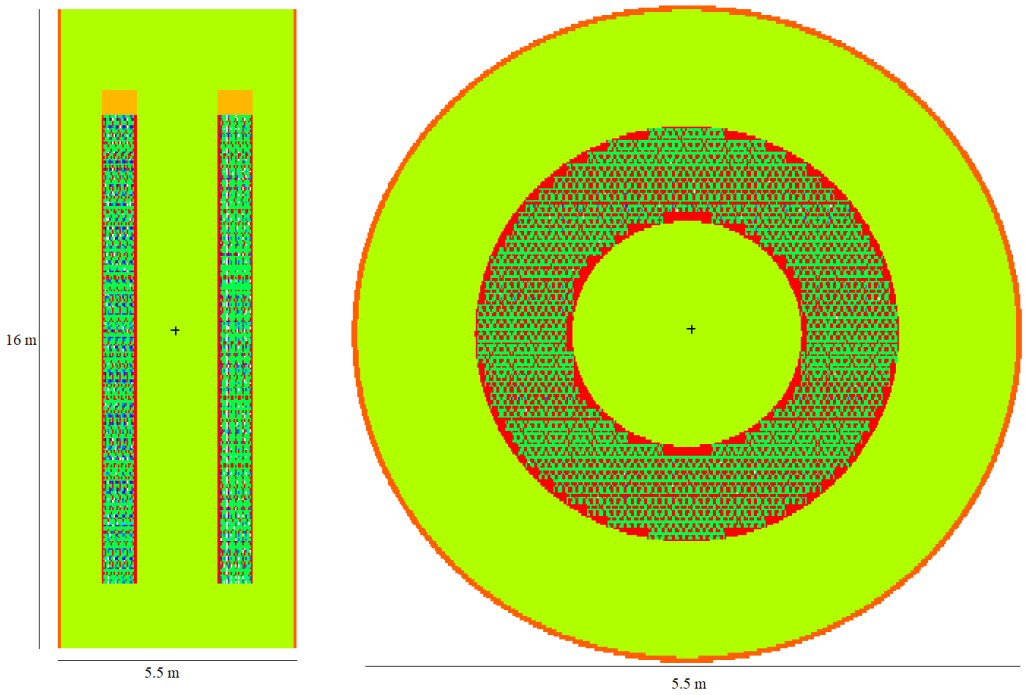

Figure 4-3. MCNP model of PBR: sideview (left) and top view (right).

4.2.2. PWR design

The iPWR design is a small and integral once-through steam generator with a rated power output of 500 MWth. The design is like the design of the AP-1000, producing 3000 MWth, but with a reduced number of shorter fuel assemblies. Each assembly comprises the typical 17x17 fuel rod assembly on a 21.5 cm pitch. The reactor is intended to provide power without interruption within a period of 48 months (Erighin, 2012). The integral design is intended to enhance its safety and reliability by placing primary circuit

components, such as the steam generator and pressurizer, within the reactor pressure vessel, eliminating the need for primary circuit pipework.

Table 4-1. iPWR technical specification

Parameters	Unit	Value
Fuel		
• effective length	cm	240
• radius	cm	0.392176
• ^{235}U enrichment		4.95wt%
• density	$g.cm^{-3}$	10.46
• Helium gap outer radius	cm	0.407924
• Helium density	$g.cm^{-3}$	0.0001604
• temperature	K	900
• cladding thickness	cm	0.05715
• cladding material		Zr-4
• cladding density	$g.cm^{-3}$	6.55
• lattice pitch	cm	1.26
Fuel Assembly		
• size		17 ×17
• number of fuel rod		264
• number of water channel		25
• pitch	cm	21.61728
• total number in the core		69
Water		
• density (upper to lower position)	$g.cm^{-3}$	0.62689 to 0.72460
• temperature	K	600
• axial reflector thickness (above and below fuel rod)	cm	20
• radial reflector thickness (outside core barrel)	cm	35
Core		
• height	cm	308.055
• barrel material		Stainless steel
• barrel density	$g.cm^{-3}$	7.92
• barrel inner radius	cm	120.8
• barrel thickness	cm	5
• pressure vessel material		Stainless steel
• pressure vessel density	$g.cm^{-3}$	7.92
• pressure vessel inner radius	cm	160.8
• pressure vessel thickness	cm	20
• temperature	K	300

Table 4.1. shows the fuel and core parameters used in the modeling (Kitcher and Chirayath, 2016). All the fuel assemblies have a uniform uranium enrichment, exempting any thermal hydraulics safety requirements. Using these parameters, an MCNP model can

be developed, as in Fig. 4-4. Total U in the core is 19.48 tons, which is 4.2 times more than in the PBMR-500, which is 4.68 tons. Both in the fuel and in the core size, the iPWR design is more compact than the PBMR.

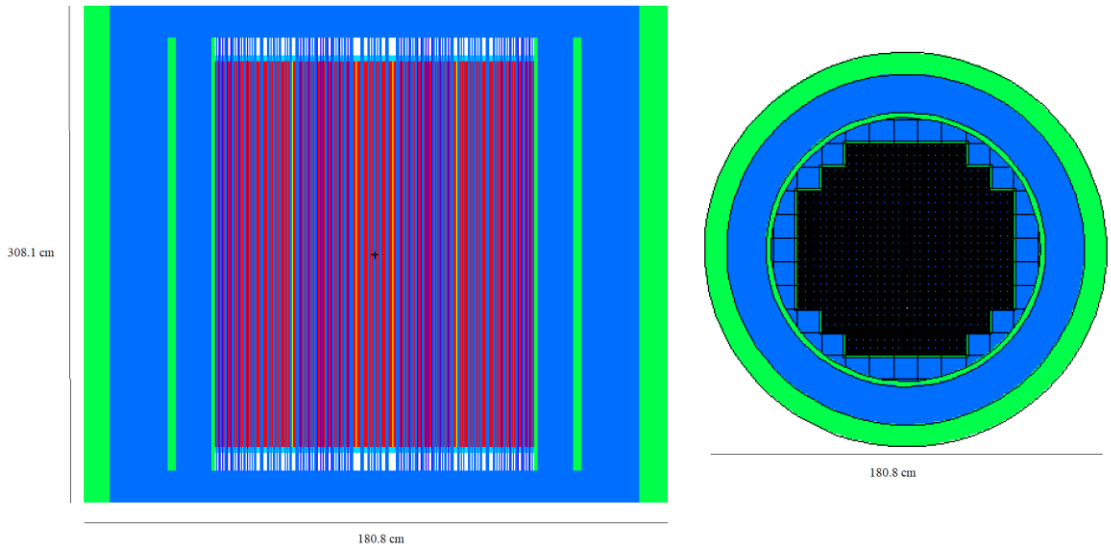

Figure 4-4. MCNP model of iPWR: sideview (left) and top view (right)

4.2.3. PR assessment

Following the simplified PR methodology provided in Chapter 2, the irradiated fuel of both rector types is cooled for 1 year, and the nuclide quantities are recalculated using MCNP 6.1. To calculate the PR of plutonium diversion, a sphere with a radius of 29.12 cm (for U) or 4.58 cm (for Pu) is used to calculate the spontaneous fission neutron rate, heat load, radiation load, and Rossi-α parameters. The PR assessment uses the multiplicative MAUA form of Eq. 2.2 only. These four parameters are used as inputs with a uniform weighting factor of 0.3 and a scaling factor of 4.268E-04 for the MAUA.

The calculated PR is not based on the minimum requirement of nuclear explosive device. This means that the quantity of the SNM is 1 SQ regardless of the produced

isotopic composition (or SNM quality). There are no changes to the PR calculation for Pu diversion, but the U spheres used for the PR calculations of U diversion are 75 kg of ^{235}U incorporated with other uranium isotopes. In this way, the PR measures how useful the SNM would be used as raw material for a nuclear explosive device. Hence, we are able to estimate the PR profiles by the simplified methodology not only for Pu diversion, but also for U diversion.

4.3. Results and Discussion

4.3.1. Effect of higher fuel pebble packing fraction.

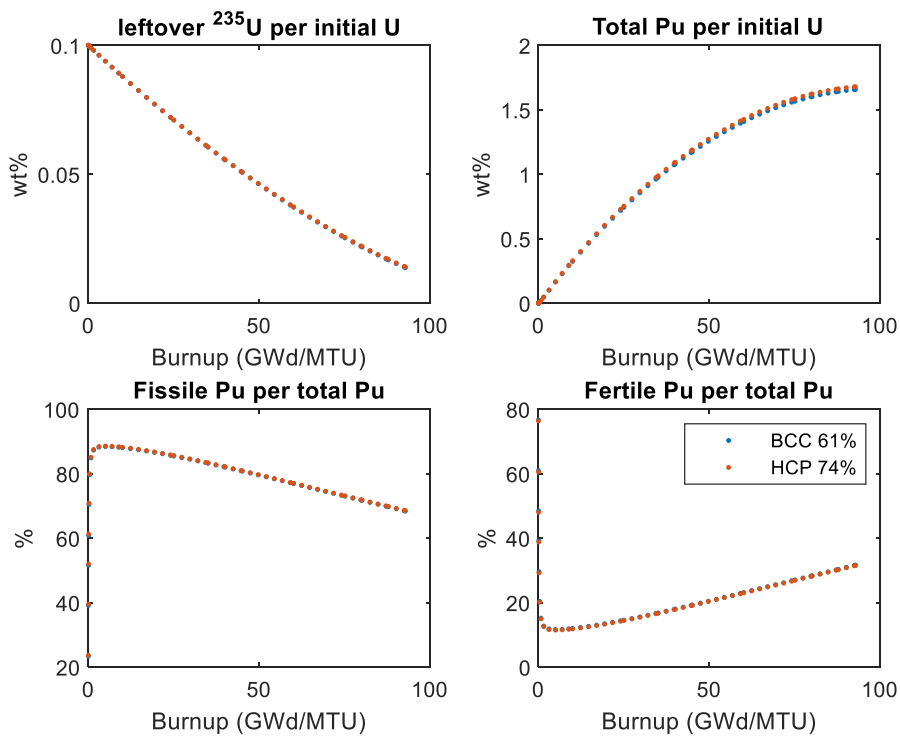

Figure 4-5. Simulated SNM quantities at different packing fractions normalized per mass of pebble.

The overall produced plutonium and leftover ^{235}U by the different packing fractions are not significantly different (ref. Fig 4.5). Almost all nuclides are produced in

a very similar quantity. The void between pebbles does not seem to affect the final SNM quantities. The difference in packing fraction slightly changes the total plutonium noticeably, but negligibly. Hence, the increase in packing fraction would not affect the PR value of the upgraded power of PBMR significantly.

4.3.2. Discharged burnup

All MCNP 6.1 simulations on both reactors deploy 3.75 million particles in 250 cycles. This achieves a one-sigma standard deviation of 36 pcm. The upgraded PBMR-400 cannot deplete the fuel to the burnup target of 80 GWd/MTU. Instead, it reaches subcriticality at an average discharged burnup of 64.14 GWd/MTU (which is very similar to that of the HTR-10 analyzed before) within 600 days (ref. Fig. 4-6). The reactor burns 65.2% of its ^{235}U to achieve the discharged fuel burnup. At this point, the core has a plutonium inventory of 77.69 kg and leftover ^{235}U of 156.4 kg. This is equal to 1.66 wt% and 3.34 wt% of the initial uranium loading, respectively. This also means that the reactor produces 5.91 SQ of plutonium and 1.27 SQ of LEU per year.

The iPWR system achieves subcriticality after about 1450 days of irradiation with an average discharged burnup of 39.5 GWd/MTU (ref. Fig. 4-7). This is two times longer than the PBMR, which is expected, since it has 4.2 times more U loading with ^{235}U enrichment occupying about half of the pebble fuel. At this point, the reactor has depleted the ^{235}U down to 1.52wt% or has lost 69.2%. This is somewhat comparable to the PBMR. After 1450 days, the iPWR produces 0.96% plutonium relative to the initial uranium loading. This is equal to 295.84 kg and 187.26 kg of ^{235}U and plutonium, respectively.

This implies that the iPWR produces 5.89 SQ of plutonium and 0.99 SQ of LEU in the spent fuel in the core per year.

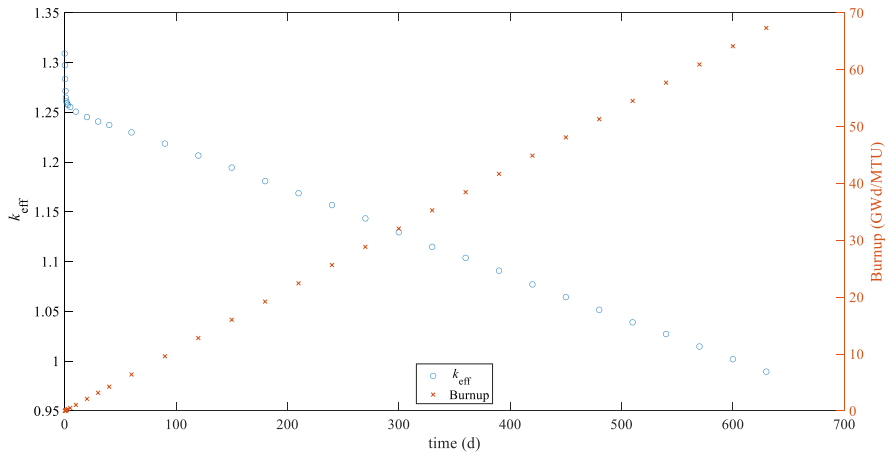

Figure 4-6. Effective neutron multiplication factor and burnup history of one batch simulation of the upgraded PBMR-400

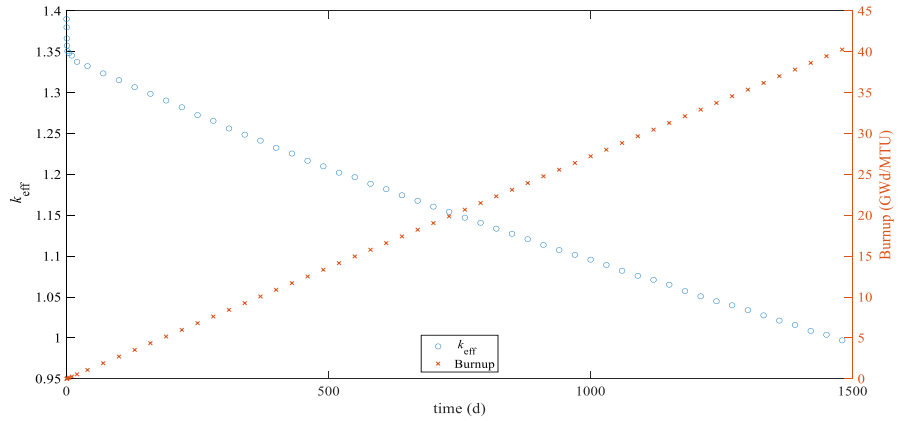

Figure 4-7. Effective neutron multiplication factor and burnup history of one batch simulation of the iPWR

4.3.3. SNM production mechanism

Compared to the iPWR, the PBMR produces very different amounts of SNMs. The amount of leftover ^{235}U is much more, since the initial ^{235}U enrichment is about twice

higher than in the PWR. The total plutonium produced by both reactors are similar at low burnup values (ref Fig. 4-8). However, above 20 GWd/MTU, the PBMR has a higher total plutonium quantity. At a similar simulated burnup value (approx. 38.5 GWd/MTU), the PBMR produces a total plutonium of 1.19wt% (relative to the initial uranium loading) and leaves the ^{235}U at the level of 5.44wt% (depleting 43.3% of the initial ^{235}U), while the iPWR produces a total plutonium of 0.95wt% and leaves the ^{235}U of 1.56wt% (depleting 68.5% of the initial ^{235}U). At their respective discharged burnup level (40 GWd/MTU for PWR and 65 GWd/MTU for PBR), the PWR produces a total Pu of 0.97wt%, while for PBR it is 1.66wt% relative to their respective initial uranium loading.

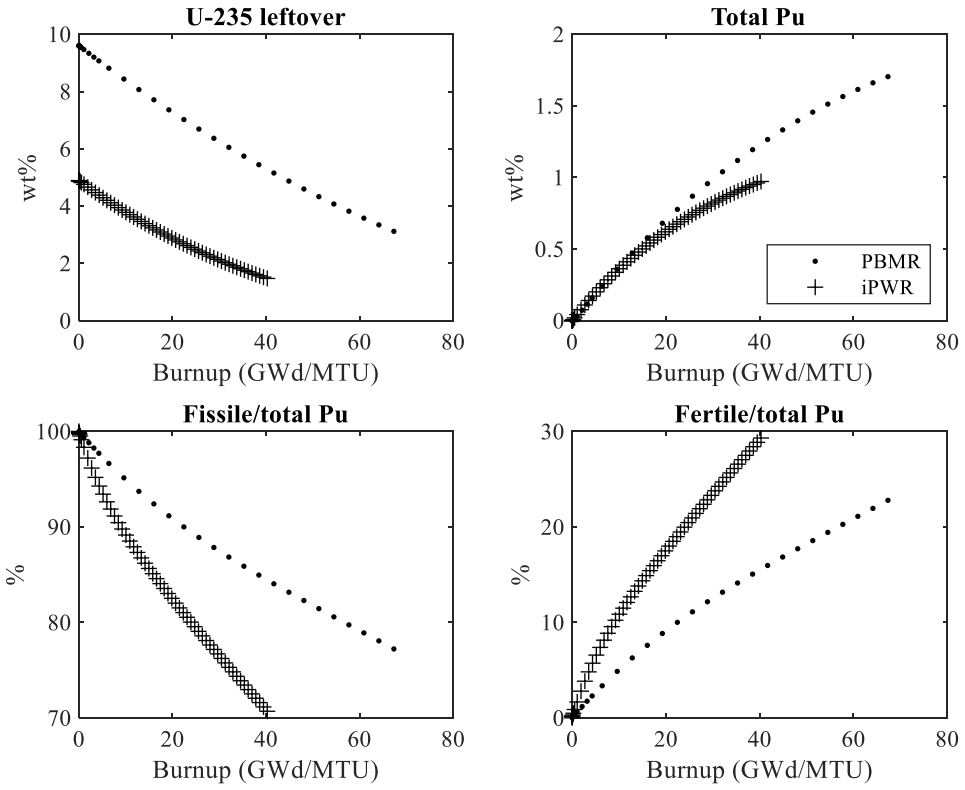

Figure 4-8. ^{235}U and plutonium in the spent fuel cooled after 1 year.

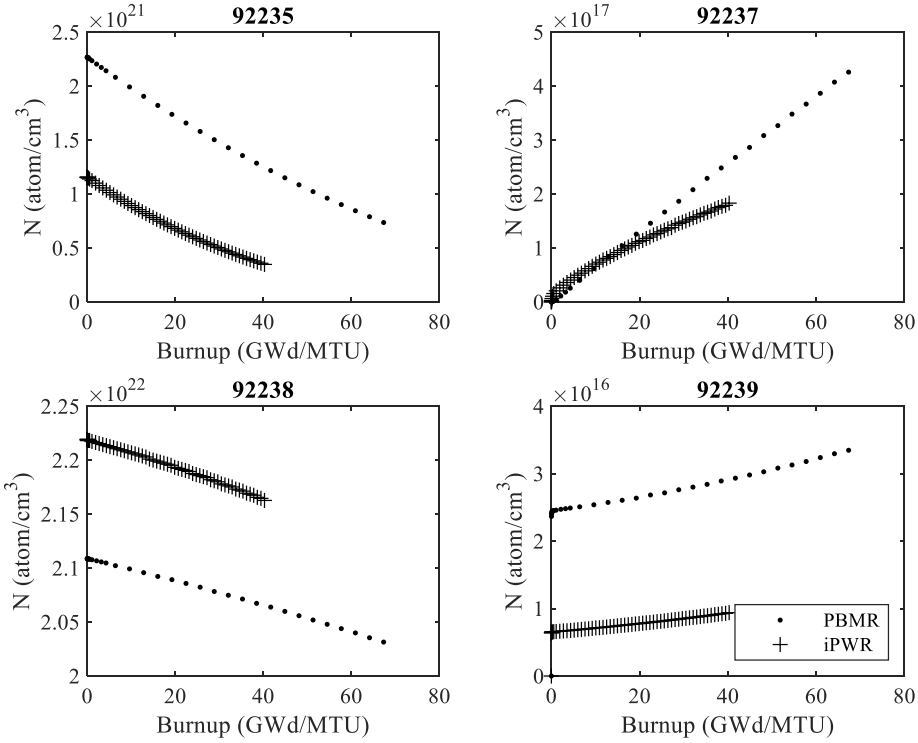

Figure 4-9. Uranium isotopes of core inventories of PBMR and iPWR

Table 4-2. Neutron cross sections (NEA 2021)

		Thermal neuron			Fast neutron		
		Scattering	**Capture**	**Fission**	**Scattering**	**Capture**	**Fission**
Moderator	^{1}H	20	2.0E-01	-	4	4.0E-05	-
	^{12}C	5	2.0E-03	-	2	1.0E-05	-
Structural materials, other	^{90}Zr	5	6.0E-03	-	5	6.0E-03	-
	^{56}Fe	10	2	-	20	3.0E-03	-
	^{16}O	4	1.0E-04	-	3	3.0E-08	-
Absorber	^{10}B	2	2.0E+02	-	2	4.0E-01	-
	^{113}Cd	100	3.0E+01	-	4	5.0E-02	-
	^{135}Xe	400	2.0E+06	-	5	8.0E-04	-
	^{115}In	2	1.0E+02	-	4	2.0E-02	-
Fuel	^{235}U	10	9.9E+01	5.8E+02	4	9.0E-02	1
	^{238}U	9	2	2.0E-05	5	7.0E-02	0.3
	^{239}Pu	8	2.7E+02	7.5E+02	5	5.0E-02	2

At any burnup value, the PBMR produces a higher amount of fissile plutonium (^{239}Pu and ^{241}Pu). At their discharged burnup level, the iPWR produces plutonium with a

fissile content of 71.14% of its total plutonium, while the PBMR produces plutonium with a fissile content of 78.06% of its total plutonium. In terms of uranium depletion, both reactors have a very similar depletion rate (ref. Fig 4.9). The only difference is their initial ^{235}U enrichments.

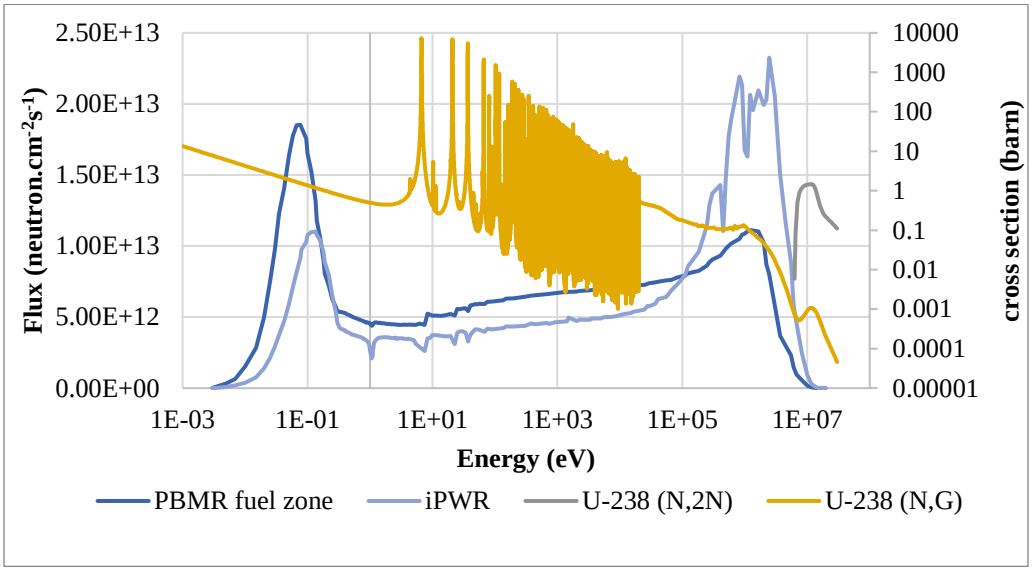

Figure 4-10. Neutron spectrums of PBMR and iPWR at their mid of life.

As in Fig 4.10, the PBMR has a lower fast neutron flux (above 100 keV) but has higher neutron fluxes within the thermal (0-0.625 eV) and intermediate energies (0.625 eV – 100 keV). This is due to the higher thermalization of PBMR through its utilization of graphite surrounding the fuel kernel. Graphite has a moderating ratio (MR) almost three times higher than light water. Although light water has a higher macroscopic scattering down power (MSDP), it also absorbs more neutrons than graphite does (ref. Table 4.2).

Since the fuel is placed as small fractions surrounded by graphite in the pebble, the PBMR fuel becomes more heterogeneous than the PWR. Neutrons slowdown in the

moderator region, which then increases the resonance escape probability. This causes the number of thermal neutrons absorbed in the fuel to grow and the one absorbed in any other reactor material to become smaller. This is supported by the lower neutron absorption of graphite compared to water. The heterogeneous setting also causes differences in the neutron flux in the fuel compared to the one in the graphite moderator due to the difference in neutron mean free path. With these, the k_{eff} of PBMR should be higher than the PWR. However, as in Fig 4.6 and Fig 4.7, the k_{eff} of PBMR is lower, since the total fissile loading is only about half of the iPWR. The resonance escape probability is also significantly affected by the fuel enrichment.

With less ^{238}U, approximately by half, the PBMR still produces ^{239}U at nearly 3 times the rate of the iPWR. Its neutron flux within the intermediate energies is stronger, causing more ^{238}U to absorb neutrons and to transmute them to ^{239}U. With a half-life of 23.45 minutes, ^{239}U decays β^- to ^{239}Np, which then also decays β^- with a half-life of 2.356 days to ^{239}Pu. This is the reason why ^{239}Np in the PBR system is much higher by almost 3.5 times (ref. Fig. 3-11) as the ^{239}Pu (ref. Fig. 3-12). This ^{239}Pu production is strengthened by the increased ^{237}U transmutation to ^{238}U through radiative capture rather than the other way through (n,2n) reaction. A typical thermal reactor produces ^{237}U by radiative capture of ^{236}U that do not fission and (n,2n) reactions of ^{238}U. However, the (n,2n) reactions within the PBMR is less likely to occur. As in Fig. 4-10, the PBMR has a much lower flux at energies above 6 MeV, making it less possible to have a such neutron reactions. This makes the ^{237}Np and ^{238}Np lower in the PBMR, which then causes the ^{238}Pu production to be much lower than in the iPWR (ref. Fig. 4-11).

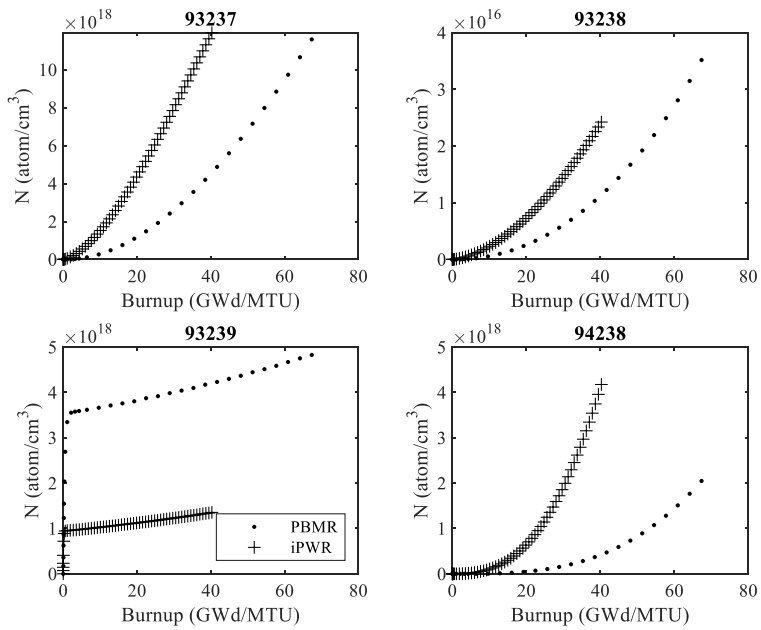

Figure 4-11. Neptunium and ^{238}Pu atomic densities of core inventories of the PBMR and the iPWR

The vast ^{239}Np production in the PBMR and its decay to ^{239}Pu should accumulate ^{239}Pu around the same multiplication number of 3.5 compared to the iPWR. However, the achieved number is only around two times higher (ref. Fig 3.12), and there is no sign that the ^{239}Pu loss is due to its transmutation to ^{240}Pu through radiative capture. The buildup rate of ^{240}Pu between the two reactors is very similar and the number in the iPWR is slightly higher. The most possible cause of this is the fission of ^{239}Pu contributing to the overall power production. With a higher thermalization factor, the PBMR is very likely to burn more ^{239}Pu than the iPWR. However, due to the high neutron flux within the intermediate energy zone, the accumulation of ^{239}Pu in the PBMR outnumbers the total ^{239}Pu being consumed in fission. This characteristic can be observed through the ^{239}Pu consumption, which is much higher at higher burnup values in both reactors as the curves

(Fig. 3-12) are approaching equilibrium. At higher burnup values, both reactor systems are using more ^{239}Pu to overcome the ^{235}U depletion, which is a characteristic of a thermal reactor.

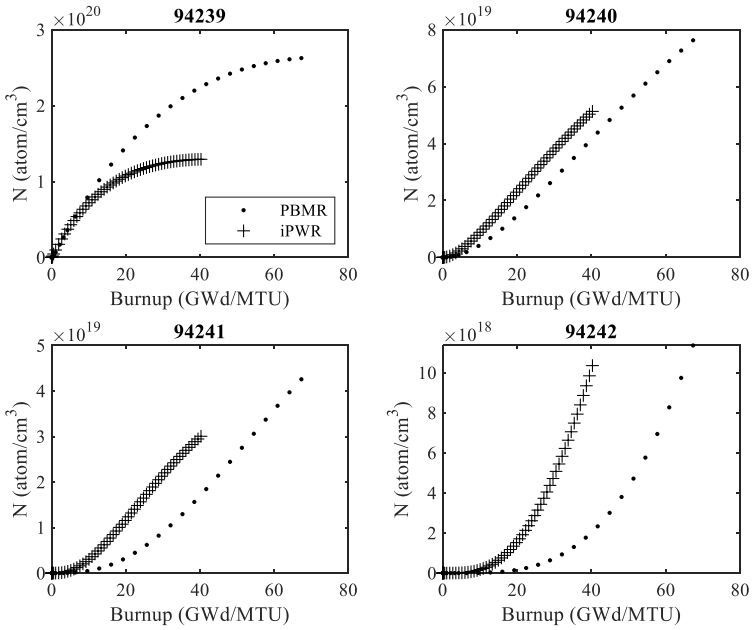

Figure 4-12. Plutonium isotopes of core inventories of the PBMR and the iPWR

4.3.4. PR evaluation

In general, the number of spontaneous fission neutrons produced by both the U and Pu spheres increase with the burnup level, since the amount of ^{235}U is decreasing and other U isotopes are increasing (ref. Fig. 4-14). This is due to the assumption of 1 SQ of LEU (75 kg of ^{235}U) in the sphere. The produced neutrons are mostly coming from ^{236}U and ^{238}U. A small fraction is also produced by ^{234}U. The spontaneous fission neutrons from the U sphere of PWR are more than for the PBR, since it has less ^{235}U and more of the other U isotopes. Table 4.3 lists the U isotope compositions produced by both reactors.

The composition also drives other parameters, e.g., the heat load (ref. Fig. 4-14) and the radiation load (ref. Fig. 4-15).

Table 4-3. Uranium isotope fractions from the spent fuel used for PR analysis.

PWR						
Burnup (GWd/MTU)	**4**	**10**	**16**	**25**	**38**	**40**
^{234}U	4.34E-07	9.81E-07	1.54E-06	2.58E-06	5.02E-06	5.21E-06
^{235}U	4.41E-02	3.83E-02	3.31E-02	2.58E-02	1.65E-02	1.60E-02
^{236}U	9.54E-04	2.08E-03	3.08E-03	4.44E-03	6.04E-03	6.11E-03
^{238}U	9.55E-01	9.60E-01	9.64E-01	9.70E-01	9.77E-01	9.78E-01

PBMR							
Burnup (GWd/MTU)	**4**	**10**	**16**	**25**	**38**	**48**	**65**
^{234}U	4.07E-08	9.09E-08	1.54E-07	2.63E-07	4.68E-07	7.00E-07	1.32E-06
^{235}U	9.13E-02	8.55E-02	7.89E-02	6.94E-02	5.74E-02	4.91E-02	3.65E-02
^{236}U	9.12E-04	2.01E-03	3.28E-03	5.07E-03	7.27E-03	8.78E-03	1.10E-02
^{238}U	9.08E-01	9.12E-01	9.18E-01	9.26E-01	9.35E-01	9.42E-01	9.53E-01

Table 4-4. Plutonium isotope fractions from the spent fuel used for PR analysis.

PWR						
Burnup (GWd/MTU)	**4**	**10**	**16**	**25**	**38**	**40**
^{238}Pu	3.23E-04	1.29E-03	2.94E-03	7.14E-03	1.78E-02	1.86E-02
^{239}Pu	9.35E-01	8.56E-01	7.88E-01	6.96E-01	5.83E-01	5.77E-01
^{240}Pu	5.53E-02	1.04E-01	1.38E-01	1.79E-01	2.22E-01	2.24E-01
^{241}Pu	9.00E-03	3.42E-02	6.03E-02	9.32E-02	1.24E-01	1.25E-01
^{242}Pu	2.15E-04	2.08E-03	6.25E-03	1.71E-02	4.24E-02	4.41E-02
^{241}Am	4.95E-04	2.14E-03	4.21E-03	7.44E-03	1.12E-02	1.14E-02

PBMR							
Burnup (GWd/MTU)	**4**	**10**	**16**	**25**	**38**	**48**	**65**
^{238}Pu	9.78E-06	6.01E-05	1.86E-04	5.29E-04	1.33E-03	2.25E-03	0.004546
^{239}Pu	9.78E-01	9.48E-01	9.13E-01	8.61E-01	7.96E-01	7.50E-01	0.68079
^{240}Pu	2.08E-02	4.64E-02	7.32E-02	1.06E-01	1.41E-01	1.61E-01	0.1869
^{241}Pu	9.61E-04	4.98E-03	1.29E-02	2.90E-02	5.33E-02	7.15E-02	0.097686
^{242}Pu	8.27E-06	1.13E-04	5.23E-04	2.05E-03	6.36E-03	1.17E-02	0.02526
^{241}Am	4.75E-05	2.46E-04	6.39E-04	1.43E-03	2.64E-03	3.53E-03	0.004827

Similarly, the isotopic composition of Pu (ref. Table 4.4) also drives the number of spontaneous fission neutrons, the radiation load, and the heat load. In the plutonium sphere, the fertile Pu isotopes control these parameters dominantly. They increase with the higher fuel burnup level.

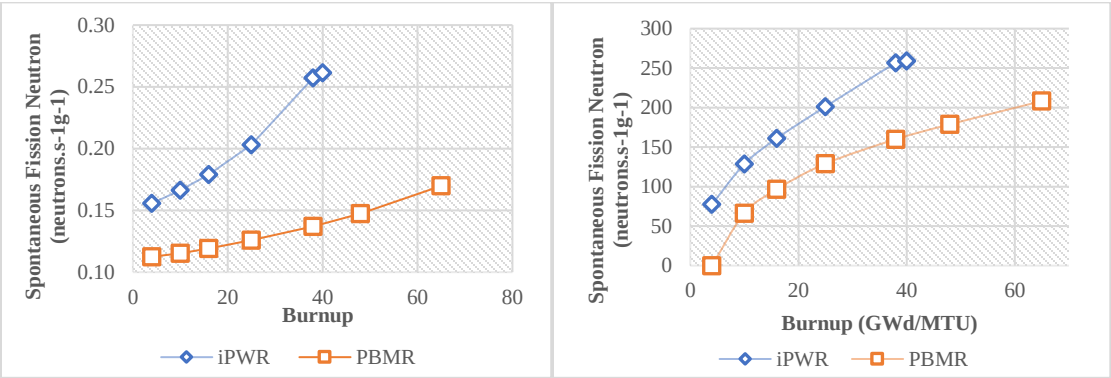

Figure 4-13. Spontaneous fission neutrons U sphere (left) and Pu sphere (right)

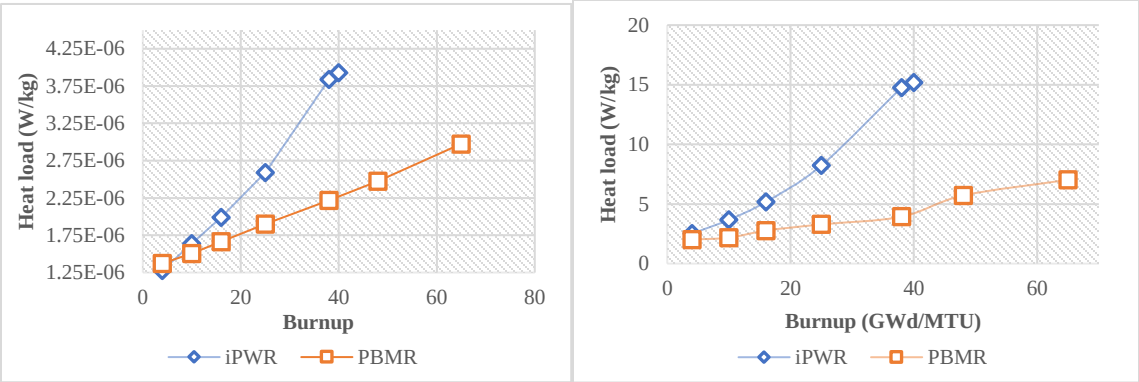

Figure 4-14. Heat load U sphere (left) and Pu sphere (right)

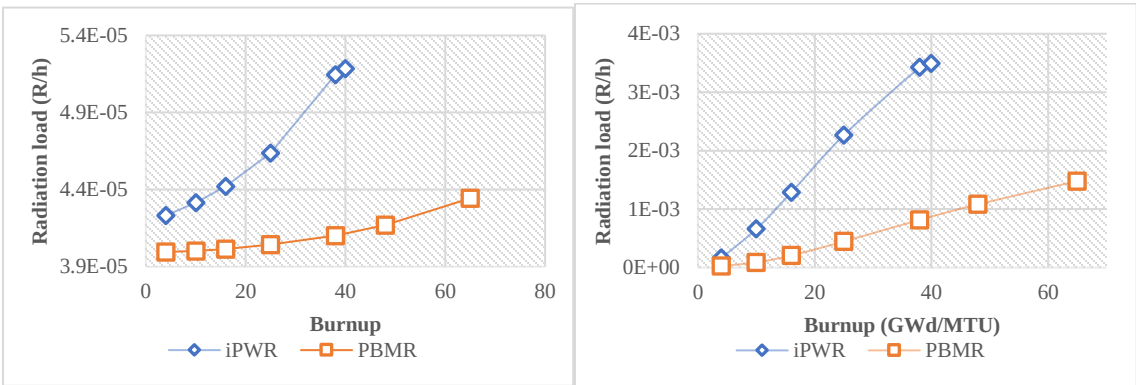

Figure 4-15. Radiation load U sphere (left) and Pu sphere (right)

The Rossi-α parameter indicates how fast a system can reach criticality. In a NED it should show as high as possible. The Pu system clearly has a higher Rossi-α value than the U system at their respective SQ (ref. Fig. 4-16). As the burnup level of the spent fuel increases, the Rossi-α value decreases, since the content of the fissile isotopes also decreases. Since the PBR produces more fissile Pu and leaves more ^{235}U, its values are higher than the iPWR at any respective burnup value. This applies generally to both Pu and U systems. However, within the iPWR, the Rossi-α value of the U system above 25 GWd/MTU is conversely increasing.

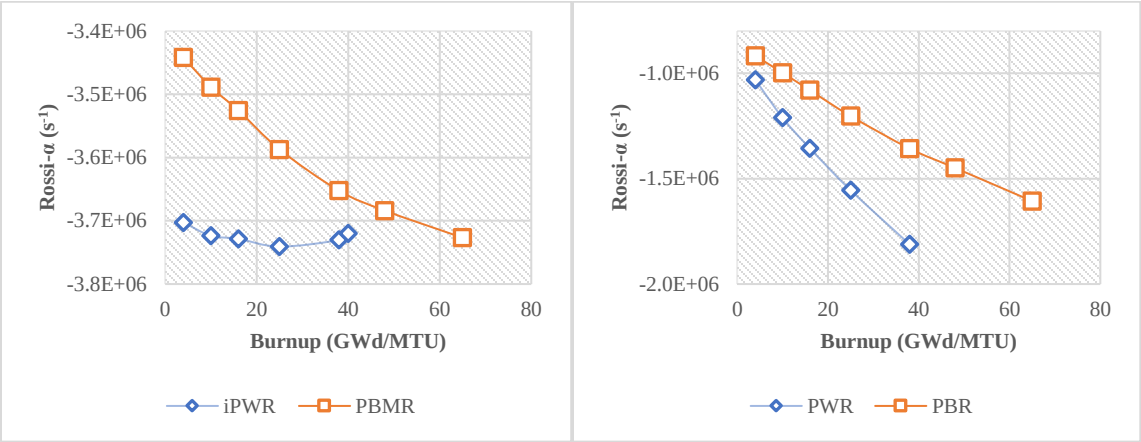

Figure 4-16. Rossi-α values of U sphere (left) and Pu sphere (right)

The increasing Rossi-α value above 25 GWd/MTU in the U system of iPWR is due to the increasing production of ^{234}U and ^{236}U with the increasing burnup. ^{234}U has a higher fission cross section than ^{235}U at higher neutron energies (ref. Fig. 4-17). Although ^{236}U has a lower fission cross section than ^{235}U, its quantity is 30% more than the ^{235}U itself at burnup levels above 25 GWd/MTU. These isotopes compete with ^{235}U in producing neutrons at high energy neutron spectrum.

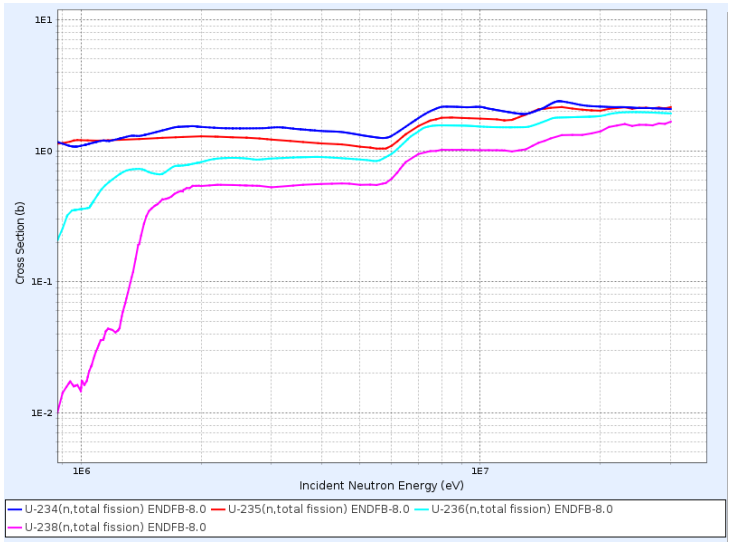

Figure 4-17. Fission cross section of uranium isotopes (KAERI 2021)

Figure 4-18 shows the PR values of the PBMR and the iPWR for ^{235}U and Pu diversions using the multiplicative form of MAUA. The multiplicative form uses a scaling factor of 4.27×10^{-4}. The iPWR has higher PR values for ^{235}U and Pu diversions than the PBMR, as expected. Ii is important to note that the calculated PR is derived from the mean values of nuclide quantities in the core. Since the neutron flux in the core will never be uniform at every position, the PR of the fuel portion in the lower neutron flux area is higher and the PR of the fuel portion in the higher neutron flux area is actually lower. MCNP's stochastic uncertainties in predicting the four parameters used for the PR assessment are propagated. However, the variance cannot be used to infer any material quantity uncertainty. The propagated uncertainties can be driven by deploying the number of particles used in the simulation. Since the number of particles in the simulation is around 100 million, the standard deviations in Fig. 4-18 are very small and, in the case of Pu diversion, they cannot be indicated on the graph.

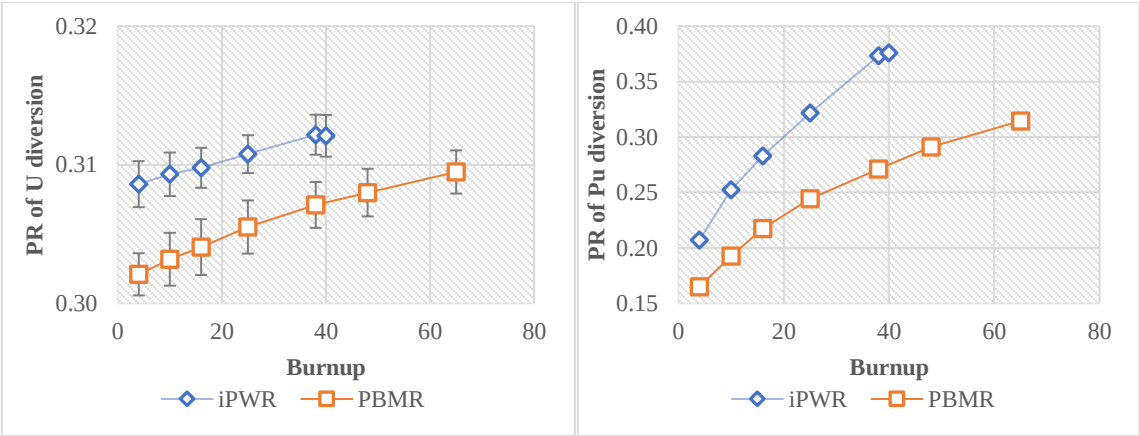

Figure 4-18. PR of ^{235}U and Pu diversions in iPWR and PBMR

Table 4.5 provides a summary of the PR comparison between the the iPWR and the PBMR at their respective fuel discharge burnup values. It is clear that the iPWR prevails over the PBMR. This means that the PBMR has a higher proliferation risk for both ^{235}U and plutonium in its spent fuel. The higher risk of the PBMR can be minimized through at least four ways of mitigation: lower fuel enrichment utilization; higher burnup target definition; multi-pass refueling deployment; and the deployment of adequate safeguards approach. However, they are not independent of each other. Any modification to one may change the others; hence an optimization is required.

Table 4-5. PR summary of PBR and LWR technologies

	iPWR	PBMR
Discharge burnup (GWd/MTU)	40	65
Operating period (days/cycle)	1,450	600
Spent fuel volume (m^3/cycle)	7.7	58.4
Initial enrichment	4.95wt%	9.6wt%
Initial U loading (tons)	19.48	4.68
leftover ^{235}U (kg/period)	295.84	156.40
leftover ^{235}U (SQ/y)	0.99	1.27
Produced Pu (kg/period)	187.26	77.69
Produced Pu (SQ/y)	5.89	5.91
Fissile Pu (of total Pu)	70.69%	78.06%
PR (U), multiplicative	0.263 ± 0.001	0.261 ± 0.001
PR (Pu), multiplicative	0.345 ± 0.002	0.282 ± 0.001

5. SAFEGUARDS APPROACH DEVELOPMENT

5.1. Introduction

The pebble bed reactor (PBR) produces spent fuel, which is attractive for nuclear proliferation as per the analysis presented in previous chapters. The proliferation risk is higher when fuel has higher initial ^{235}U enrichment and/or a lower fuel burnup. The PBR's online refueling feature allows it to discharge spent fuel pebbles (SFP), which are suitable for proliferation, at a desired fuel burnup. Hence, proliferation risk mitigation steps through nuclear safeguards for the PBR must be different from the item accountability practiced in the current fleet of light water reactors (LWRs).

Generally, in an LWR application, a reactor may typically be comprised of only one material balance area (MBA) for nuclear material control and accounting (NMC&A) purposes needed for nuclear safeguards monitoring. An MBA is an area established for NMC&A purposes so that the quantity of nuclear material in each transfer into or out of each MBA can be determined (NRC, 10 CFR). By using MBAs, the physical inventory of nuclear material in them can be determined when necessary, in accordance with special procedures. MBA development leads to key measurement point (KMP) determination at nuclear material input and output locations of each MBA. Since the PBR uses a semi-bulk fuel, it may need more than one designated MBA, unlike the current LWRs.

Since the PBR could produce high-quality plutonium and use a relatively high-assay low enriched uranium (HALEU) in its fuel compared to the LWR, a safeguards approach for the PBR should not be developed based solely on the quantity of SNM. The

high quality of the plutonium produced in the PBR should also be considered while developing a safeguards approach. With the online refueling feature in place in PBRs, plutonium quality in SFP can be optimized for proliferation. However, the risk of proliferation is lower if the online refueling is an OTTO scheme with a certain fuel burnup value and refueling period. The risk arises if the multi-pass scheme is applied, although it may decrease the quality of the plutonium produced in PBR. The safeguards approach development in this chapter will emphasize the multi-pass refueling scheme, although it is also applicable to the OTTO scheme.

A study on safeguards approaches for the PBR can be found in Durst et. al, 2009 and 2012. Their concept relies heavily on the current PWR safeguards system without providing any benchmark to measure the effectiveness of the proposed system. One challenge mentioned in this work, along with some other similar works, is the lack of realistic simulation and modeling of the PBR to determine the nuclear material content of its core fuel and spent fuel pebbles to design an adequate safeguards system. Therefore, those efforts did not lead to the development of a safeguards approach for PBR based on NMC&A principles.

In this chapter, a safeguards approach is developed enabling the mitigation of the proliferation risk associated with the operation of the PBR. This development is based on certain SNM diversion scenarios. Each diversion scenario relies on the material SNM flow and process information within the reactor that has been simulated, the results of which are presented in the previous chapters.

A proven concept of gamma radiation spectroscopy of SFP to identify U and Pu quantity and quality in the SFP is the basis for the safeguards approach developed and described in this chapter. The fuel burnup simulation results obtained using MCNP provided the data needed to produce and interpret the gamma spectroscopy data to help verify the declared parameters of SFP. Gamma spectroscopic analysis of the SFP paved the way for the development of a safeguards approach to mitigate the proliferation risk of diverting leftover ^{235}U and Pu in the SFP.

5.2. Methodology

The SNM diversion scenarios are developed based on SNM flow in the PBR. The scenarios developed assume that a state is the proliferator and not non-state actors (criminals, protestors, and terrorists). Since the SNM flow requires information on material quantity and quality, the simulated data in Chapters 2 and 3 are used in all the safeguards approach developmental steps. The scenarios are limited to ^{235}U and Pu diversions. The scenarios are intended to direct safeguards approach development and any deviation from them may require a modification to the developed approach.

5.2.1. Nuclear Material Accountancy (NMA) methodology

Nuclear material accountancy (NMA) is one of the components deployed by the international atomic energy agency (IAEA) to independently verify the correctness of the SNM accounting information produced by the facility operators and the State's system of accounting for and control of nuclear material (SSAC). In order to deploy a correct safeguards approach, the IAEA needs the design information to the extent possible without disclosing proprietary information. NMA requires the determination of MBAs, which are

designated areas for material accounting purposes. The inputs to and outputs from an MBA should be measured using equipment located at KMPs. A KMP is a physical location where nuclear material appears in such a form that it may be measured to determine material flow or inventory (NRC, 10 CFR). KMPs are vital to verify the material unaccounted for (*MUF*) of an MBA:

$$MUF = (P_B + I_{inc} - I_{dec}) - P_E \tag{5.1}$$

where P_B is the physical inventory at the beginning of a Material Balance Period (MBP), I_{inc} is the sum of increase to inventory, I_{dec} is the sum of decrease from inventory, and P_E is the ending physical inventory. An MBP corresponds to the IAEA's timeliness goal, which is 1 year for indirect use material (e.g., fresh fuel), 1 month for unirradiated direct use material (e.g., high-enriched uranium (HEU) and separated plutonium), and 3 months for irradiated direct use material (e.g., spent fuel containing plutonium and radioactive fission products).

The material flow model uses the data generated from the PBR fuel burnup simulations described in Chapter 3. The data is generated for an HTR-10 operating with a multi-pass (three-passes) refueling scheme. The data is expanded for the NMA application of HTR-PM with rated thermal power of 250 MWth. The HTR-PM is assumed to have 25 times the material quantity of the HTR-10. This material model is then used to conclude whether SNM diversion is detectable in a timely manner or not with the developed safeguards approach. To conclude that there is no material diversion in the system, the following rules must be satisfied within the timeliness goal (IAEA 2001):

$$|MUF| < 3\sigma_{MUF} \tag{5.2}$$

$$|MUF| < 1SQ \tag{5.3}$$

$$3\sigma_{MUF} < 1SQ \tag{5.4}$$

where one SQ for LEU is 75 kg of ^{235}U, for HEU it is 25 kg of ^{235}U, and for ^{233}U or for plutonium it is 8 kg. The MUF uncertainty (σ_{MUF}) is estimated based on the uncertainty of each method used in the approach by referring to the International Target Value (ITV) published by the IAEA (IAEA 2010).

The ITVs are developed to provide a guideline for facility operators, states, and international safeguards organizations to get achievable uncertainties in deploying their routine measurements. ITV is not intended to be used if any performance uncertainty is available from actual measurement results, especially when the uncertainty is much lower due to the use of a better measurement system. Instead, ITV may be used directly if there is no performance uncertainty available to calculate sampling plans, to set rejection limits, and to recalculate estimates of the combined uncertainties of inventories, throughput, and MUF. The ITV selection for the PBR system requires an adequate insight of measurement and verification systems.

Since the PBR with its online refueling requires a relatively fast safeguards system, non-destructive assay (NDA) will be the focus of this study. However, to verify the uranium loading of both FFP and SFP, mass measurement and pebble counting are also part of the developed approach.

Pebble mass measurement is important to verify that the fissile loading mass conforms with the declared mass. Mass measurement must be carried out at all KMPs, using an electronic balance measurement system or a load-cell based weighing system.

According to ITV, both systems have the same relative uncertainty value of 0.07%. Assuming the volume of the pebbles is constant with a diameter of 6 cm, that the UO_2 density is 10.4 g/cm^3, and that the UO_2 radius in the TRISO is 0.025 cm, the total SNM mass within a period at a KMP can be calculated as:

$$m_{SNM} = 0.8813\ \varepsilon\ N_p\ (1.0837 m_p - 212.0361) \tag{5.5}$$

where ε is the weight percent of SNM per pebble relative to the initial uranium mass per pebble, N_p is the number of pebbles per period, and m_p is the measured mass of the sampled pebble, which on an average is 200.27 g. The uncertainty related to the total mass of SNM within a period is:

$$\sigma_{m_{SNM}} = 0.8813 \sqrt{\begin{array}{c}(1.0837 m_p - 212.0361)^2 \left\{(N_p \sigma_\varepsilon)^2 + (\varepsilon \sigma_{N_p})^2\right\} \\ + \left(1.0837 \varepsilon N_p \sigma_{m_p}\right)^2\end{array}} \tag{5.6}$$

A pebble counter, regardless of its applied principle, must be deployed at the KMP to count the pebbles as items to provide the value of N_p. A simple electronic counter machine using ultrasonic or infrared waves may be easily deployed to count all of the pebbles passing through it. The counter will have an uncertainty component that contributes directly to the uncertainty of the total mass of SNM. However, since ITV does not list the uncertainty for this type of equipment, it is assumed to be 1%.

5.2.2. Gamma spectroscopy methodology

The ^{235}U measurements of the FFPs and the SFPs are important to verify the declared pebble's uranium enrichment and the leftover uranium in the SFPs. As described in previous chapters, PR is dependent on the initial ^{235}U enrichment, which, along with

fuel burnup, then determines the Pu content. Uranium enrichment measurements are relatively easy to perform on FFP compared to SFP and can be accomplished using spectroscopic gamma detectors, such as high purity germanium (HPGe) or sodium iodide (NaI), along with a multichannel analyzer (MCA). An HPGe measurement can provide a high-resolution gamma radiation spectrum that is able to provide peak-by-peak information for nuclide identification. If one can Assume that the ITVs of gamma spectroscopic measurements of LEU rods are applicable to pebbles then the ITV for NaI is 3.2% and for HPGe is 3.6%. The deployment of an HPGe detector with MCA enables both single and multiple peak identification because of its high-resolution capability. The safeguards approach in this study uses an HPGe detector to quantify the leftover ^{235}U and total Pu quantities.

Since no real FFP or SFP is available for this study, the analysis is based on simulated data for both the nuclide information and the gamma radiation spectroscopy. The spectroscopy simulation inputs are the FFP and the SFP models simulated in Chapter 2. The limitation to this method is the lack of background radiation, which would be found in the real measurement. In this case, the gamma radiation spectra can be considered as an ideal representation of the FFP and SFP. Hence, any application of this methodology to the real physical measurement should include a sensitivity study by considering background radiation. However, this study will provide a framework for an ideal interpretation.

An MCNP model of an HPGe detector, together with the pebble model, is developed within MCNP 6.1 (ref. Fig. 5-1). A detailed description of the HPGe model

used in this study can be found in a work completed by Conti, et al. (2013). The pebble model specification is the same as that described in Chapter 2. The gamma radiation source in the model is modelled as only coming from the UO_2 kernels, not from any other materials. The spectrum is calculated using the pulse shape estimator (F8 tally) of MCNP, which calculates the total count of particles interacting in the detector material per second.

The nuclide models simulated in Chapter 2 are generated under the tier 3 option in the BOPT of MCNP. This means the output nuclides are comprised of fission products in ENDF/B-VII.0 that have CINDER90 yield information. These nuclides can then be used to specify the gamma radiation emission lines as the source definition in MCNP. The gamma lines used in the source cover all related nuclide decay data that can be found in the IAEA nuclear data section. No minimum branching ratio are cut off. The gamma lines are then inserted manually as decay energies and their branching ratio to SDEF in MCNP. The lines are also used to multiply the normalized tally results.

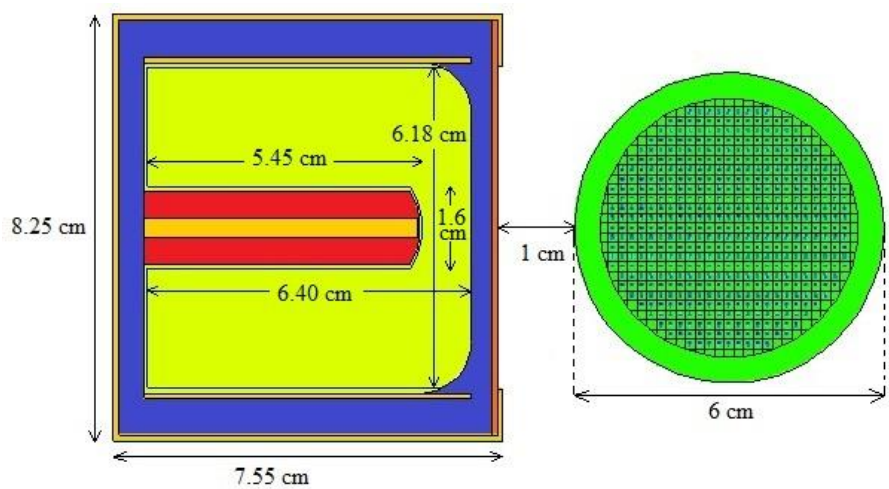

Figure 5-1. HPGe spectroscopy configuration model in MCNP 6.1

A simulated spectrum on the FFP will be used to identify the key peaks for initial ^{235}U enrichment identification. Since the FFP is assumed to contain only ^{235}U and ^{238}U in the form of UO_2, the most probable peak is the 185.7 keV of ^{235}U with a specific activity of 4.3E+04 gamma per second per gram of nuclide (Smith 1991).

The simulated spectrum data on the SFP will be used to define the leftover ^{235}U, as well as the Pu quantity and quality. They cannot be correlated directly with the peak of any spectrum. However, as described in previous chapters, burnup values correlate directly to the leftover ^{235}U and Pu quantities. In general application, fuel burnup can be verified using ^{137}Cs.

^{137}Cs is a fission product, and it has a very similar yield to uranium and plutonium (in thermal and in intermediate energies). The fission yields of ^{137}Cs for both ^{235}U and ^{239}Pu thermal fissions are similar (6.22% and 6.69%, respectively). Hence, the amount of ^{137}Cs should not be affected by the different ^{235}U enrichment in the pebbles. ^{137}Cs only loses by decay and does not lose much by neutron capture reaction. Therefore, its amount will reflect the number of fissions that occurred. It decays with a dominant peak at 661.7 keV that is easily recognized in an irradiated fuel spectrum. Its half-life of 30.17 years also enables its use in characterizing spent fuel that has been cooled at most for less than its half-life. The amount of ^{137}Cs produced in any fuel will be linear with exposure time.

To avoid complications regarding efficiency calibration associated with a single nuclide (^{137}Cs) measurement, ^{134}Cs to ^{137}Cs ratio measurements are preferred. However, ^{134}Cs has a short half-life of 2.06 years. The ratio of ^{154}Eu to ^{134}Cs concentrations also has a linear relationship with burnup and can also be used to verify fuel burnup directly. ^{154}Eu

has a longer half-life of 8.5 years, and hence requires less correction for its decay compared to ^{134}Cs. Since this study uses non-cooled and one-year cooled SFP data, these nuclides, but not limited to, are identified in the simulated spectrum to determine how they change within the SFP with respect to uranium enrichment and fuel burnup.

Fuel burnup correlates linearly with the leftover ^{235}U, total Pu, and the fissile Pu (^{239}Pu and ^{241}Pu). The leftover ^{235}U quantity and Pu quality (based on fissile Pu) depend on the initial ^{235}U enrichment and fuel burnup. The initial ^{235}U enrichment can be verified on the FFP. However, the spectrums of SFPs should also be able to define the initial ^{235}U enrichment using some suitable nuclide peaks.

The spectrum modeling on the SFP is performed on two sets of simulated data: without cooling and with one-year cooling. Each is comprised of data from three ^{235}U enrichments (4.95wt%, 10wt%, and 17wt%) at several burnup values from 5 to 90 GWd/MTU. As in Chapter 2, the 4.95wt% data will only have a maximum burnup of 45 GWd/MTU.

The non-cooled SFP gamma radiation spectra contains many peaks from many fission products, especially from the short half-life nuclides. These peaks may have a very tight energy difference to each other. The broadened spectrum, due to the decreased energy resolution of the HPGe system, may also convolve several adjacent peaks as one amplitude but still highlight the respective peak's height. Therefore, the interpretation of the peaks of interest may be done by reading its height as the count per second rather than the area of the peak. Meanwhile, the peak interpretation on the one-year cooled SFP spectrum may be done by calculating its area, since the SFP will have fewer gamma radiation peaks, as

the short half-lived fission products diminished. The identified peaks that relate to the leftover ^{235}U, total plutonium, and fissile plutonium must be applicable in the spectroscopy deployed in the safeguards approach.

5.3. SNM diversion scenario development

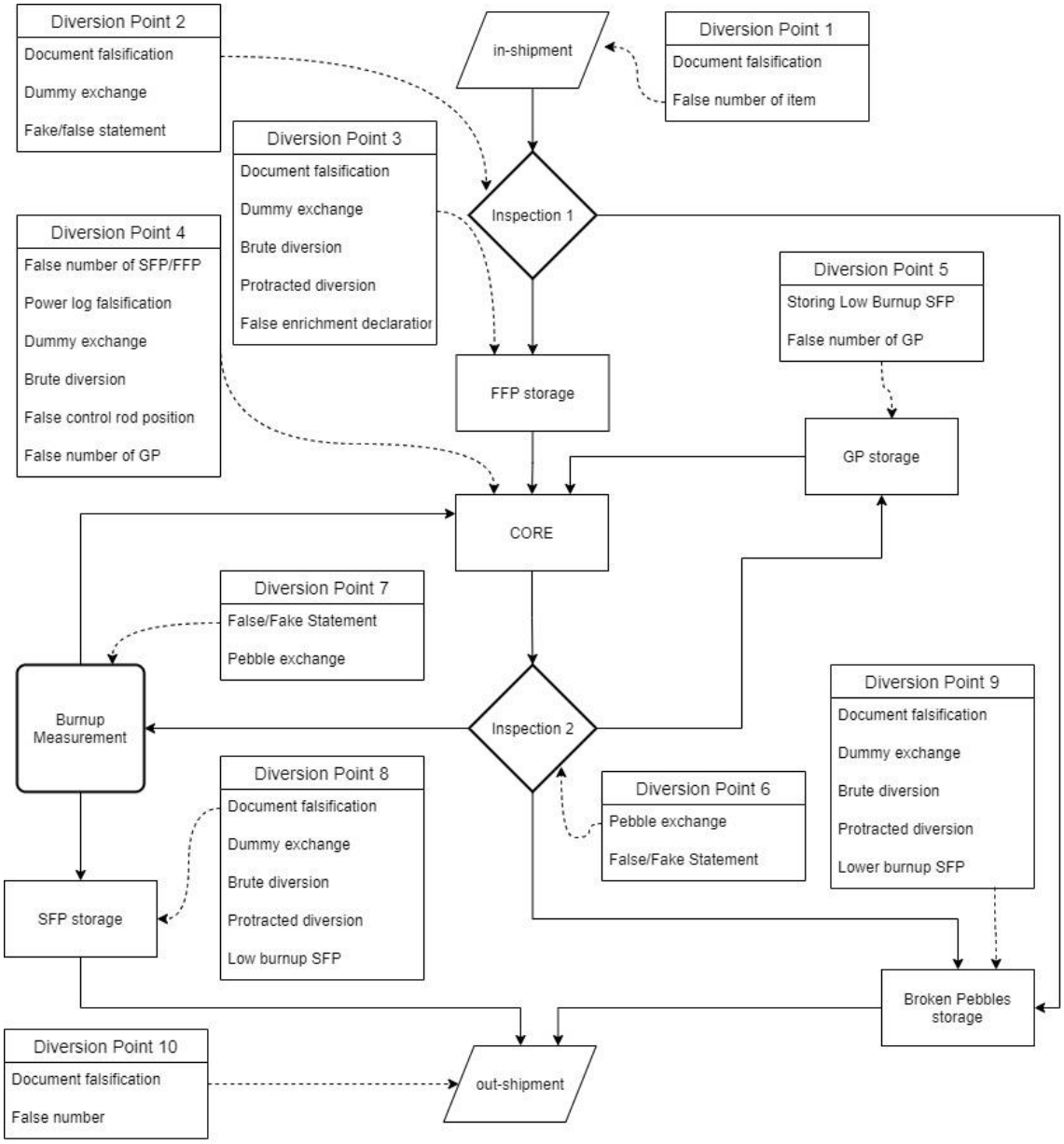

Figure 5-2. Points of uranium and plutonium diversion

The NMA implementation must be based on credible SNM diversion scenarios for an early optimization. They are needed to assure that the safeguards approach implemented in the facility effectively minimizes the proliferation risk. With a thermal reactor such as the PBR, a proliferator always targets ^{235}U and Pu, although there is also a possibility for ^{237}Np diversion. However, the analysis in this study is limited to ^{235}U and Pu only due to the interest of international safeguards practices.

As shown in the previous result, the ^{235}U diversion is optimum when the fuel has a high enrichment and a low burnup value. ^{235}U diversion may take place in almost any reactor process from the in-shipment to the out-shipment, which also may target the fresh fuel, not only the spent fuel. The in-shipment and the out-shipment processes are the interfaces of the reactor with the other fuel cycle phases, such as the fuel fabrication facility, permanent fuel storage, or reprocessing facility. Figure 5-2 lists the most probable points for SNM diversion. The scenario follows a possible reactor operation by enabling the online refueling feature of PBR.

The diversion scenario for plutonium is similar to that for uranium. However, the Pu diversion does not involve any fresh fuel. Hence, the FFP storage and the first inspection will not be of any concern for this scenario (ref. Fig. 5-2). The plutonium diversion has a different SQ target, so it may take place differently from uranium diversion. However, plutonium and uranium diversions should not be viewed as mutually exclusive. This is because the two may also happen at the same time, and this is very likely if the proliferator has access to material reprocessing and uranium enrichment facilities. In both plutonium and ^{235}U diversion, the counting of pebbles is of high importance.

Knowing the number of FFPs and SFPs in the core dictates the physical behavior in the reactor.

5.4. Nuclear Material Accounting analysis

With the simulated three-pass refueling scheme of the HTR-10, 294 FFPs are inserted and the same number of SFPs discharged within a refueling period of 10.3 days. 588 out of 882 discharged SFPs are reinserted into the core with an assumption that the 294 SFPs have achieved their target burnup. In the core, there are a total of 29,106 mixed fuel pebbles. With 5 grams of UO_2 per pebble enriched to 17wt%, the masses of inserted ^{235}U, the leftover ^{235}U, total Pu produced, and the produced fissile Pu per refueling period are 220 g, 105 g, 15.6 g and 12.2 g, respectively. These values are derived from the material depletion simulations in MBA-2, which contains the reactor core (ref. Fig. 5-3).

The other MBAs can be quantified based on the material flow in MBA-2, assuming that the quantity of defective FFP is 1% and that the defective quantity of the SFP is 1 % per refueling period. These quantities for each MBA are multiplied by a factor of 25 to get the same measurements for the HTR-PM, assuming the upscaling uses the same pebble fuel as the HTR-10.

MBA-1 contains only the FFPs. Once they are shipped into the reactor, the FFPs should be inspected for any physical impairment. Regardless of the number of defective FFPs, the number of pebbles taken out of storage to be irradiated in the reactor will be the same as the number of refueled SFPs. Since there is one input and two possible outputs, MBA-1 must be accounted using three KMPs (KMP-1, KMP-2, and KMP-3). The function of KMP-1 is to verify the shipped-in material, KMP-2 to verify the number

pebbles taken from the FFP storage, and KMP-3 to count the number of defective pebbles that are going to be stored in the broken pebble storage.

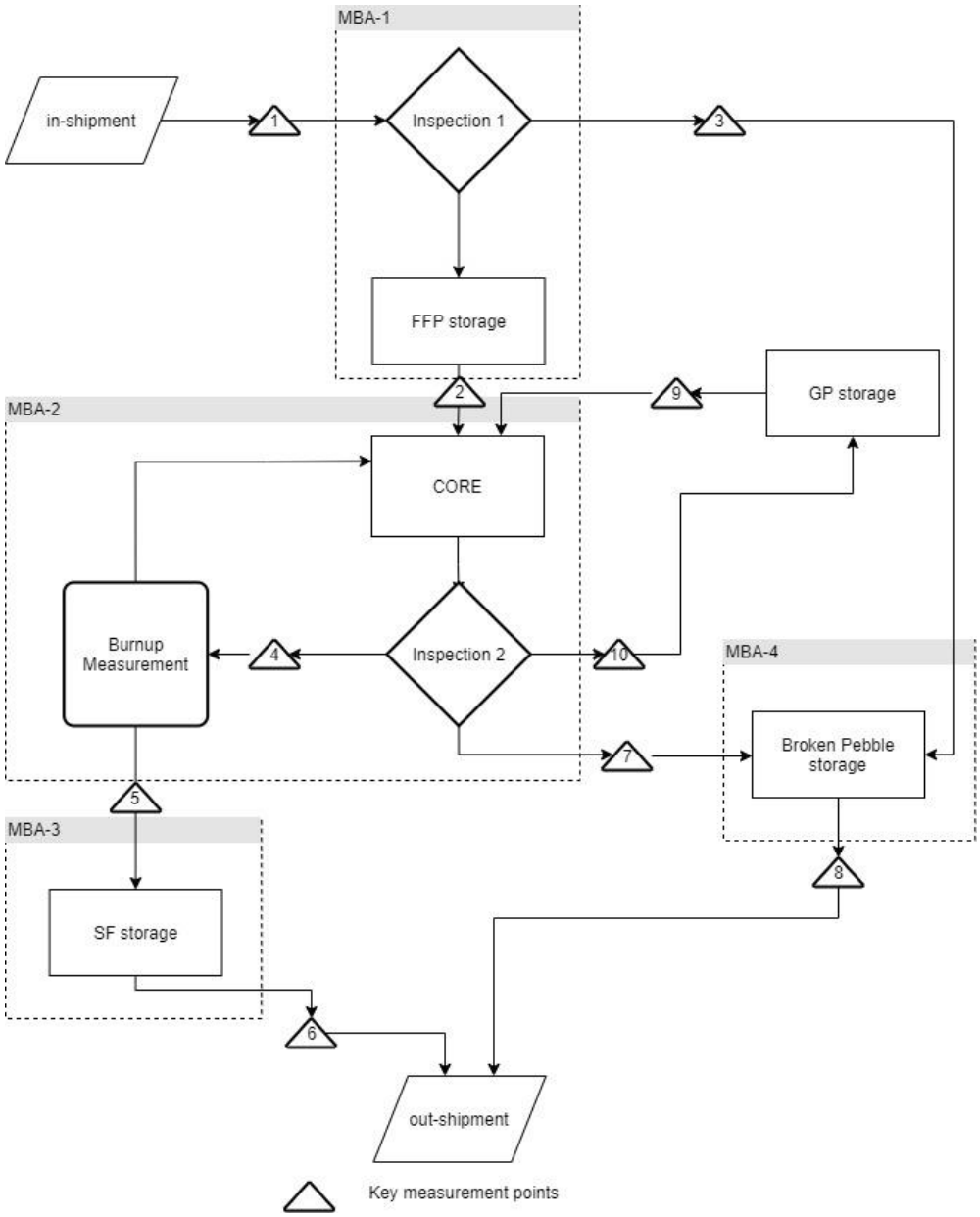

Figure 5-3. Material Balance Area and Key Measurement Points for PBR

MBA-2 accounts for all the materials going in and out of the reactor core. Materials sent into the core can be FFPs, graphite pebbles, or the SFPs that are reloaded to increase their burnup level. The number of FFPs going into the core must be verified using measurements at KMP-2. The number of graphite pebbles inserted into the core must be counted using measurements at KMP-9. Any pebble discharged from the core will be inspected to determine whether it has any defects. The defective pebbles will be passed to the broken pebble storage. The inspection also determines whether the pebble is fuel or graphite. Any non-defective graphite pebbles must be passed back to the graphite pebble storage, while the non-defective SFPs must be further measured in terms of their burnup level. In KMP-5, KMP-7, and KMP-10 the number of pebbles leaving the MBA-2 are verified. If the SFP has achieved its target burnup level, it will be kept in the spent fuel storage. If it has not achieved its target burnup level, it will be reloaded back into the core. KMP-4 and KMP-5 enable counting on the SFPs that are going to be wasted and that are going to be reloaded back into the core. This analysis assumes there is no SNM diverted by sending the fuel pebble to the graphite pebble storage.

MBA-3 is useful for accounting for all the SFPs that are cooling prior to their shipment to another facility to be stored or reprocessed. The needed cooling time will depend on the requirement issued by a regulatory body. Within the spent field storage, an arrangement must be designed in such a way that the SFPs are grouped based on their burnup level, which will enable a regular inspection for verifying the spent fuel parameters. MBA-3 must be accounted using measurements at two KMPs (KMP-5 and KMP-6).

MBA-4 contains all the defective pebbles, regardless of their types and parameters. It must be accounted using measurements at three KMPs (KMP-3, KMP-7, and KMP-8). Although the number of pebbles passed to the broken pebble storage would be far less than the pebbles passed to the MBA-3, MBA-4 contains a mix of pebble types (fuel and graphite) that complicates the accountancy. Therefore, like in MBA-3, the storage in MBA-4 must also be designed to store the pebbles based on their types and parameters. A regular inspection must be carried out to verify the quantity of materials contained in MBA-4.

Assuming there is no other way out of the graphite pebble storage, no MBA is required. However, two KMPs are needed to verify that there are no fuel pebbles passed into or out of this storage. This storage should also be inspected regularly to assure there is no fuel hidden by any means.

Table 5-1. Material flow quantity at each KMP (all units in kg/year)

MBA	KMP	HTR-10			HTR-PM		
		^{235}U	Total Pu	Fissile Pu	^{235}U	Total Pu	Fissile Pu
MBA-1	KMP-1	7.857	-	-	196.431	-	-
	KMP-2	7.779	-	-	194.486	-	-
	KMP-3	0.078	-	-	1.945	-	-
MBA-2	KMP-2	7.779	-	-	194.468	-	-
	Net in-core Production	-4.072	0.552	0.430	-101.801	13.812	10.748
	Reloaded	7.341	1.094	0.851	183.516	27.347	21.282
	KMP-4	11.011	1.641	1.277	275.274	41.021	31.922
	KMP-7	0.037	0.006	0.004	0.927	0.138	0.107
MBA-3	KMP-5	3.670	0.547	0.426	91.758	13.674	10.641
	KMP-6	3.670	0.547	0.426	91.758	13.674	10.641
MBA-4	KMP-3	0.078	-	-	1.945	-	-
	KMP-7	0.037	0.006	0.004	0.927	0.138	0.107
	KMP-8	0.115	0.006	0.004	2.872	0.138	0.107

Table 5.1 lists all material flow quantities at each KMP for both reactor scales (HTR-10 and HTR-PM). The flow quantities are determined by assuming that the MUF at each MBA is zero.

5.5. Gamma spectrum simulation results

5.5.1. FFP gamma spectroscopy

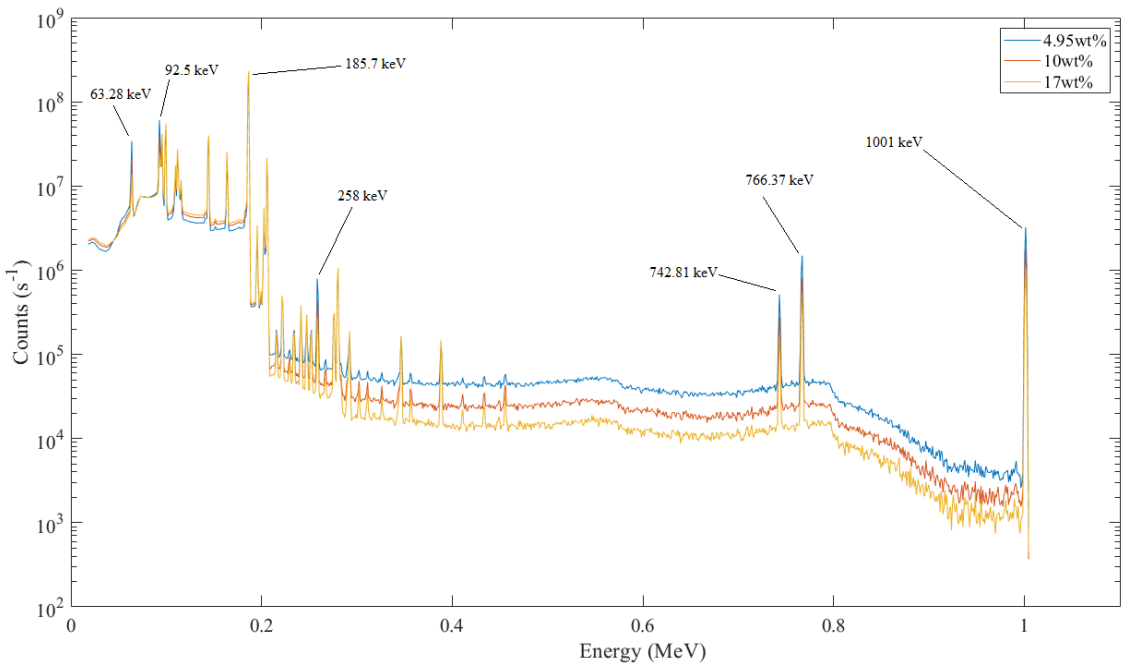

Figure 5-4. Gamma radiation spectra of FFP with different ^{235}U enrichments

Fresh fuel pebble with different enrichments can be distinguished using gamma spectroscopy based on their ^{235}U and ^{238}U properties. Both isotopes are not direct gamma emitters, but some of their daughters are. ^{235}U and ^{238}U decay primarily by emitting alpha particles with half-lives of 7.04×10^8 year and 4.47×10^9 years, respectively. In addition, ^{235}U emits gamma rays of energies 143.8 and 185.7 keV (prominent one). ^{238}U emits gamma rays of energies 63.28, 92.5, 258, 742.81, 766.37, and 1001 keV. The simulated

gamma radiation spectra of FFP (ref. Fig. 5-4) indicate these signals and can be used to interrogate the ^{235}U enrichment of the FFP (ref Fig 5.5).

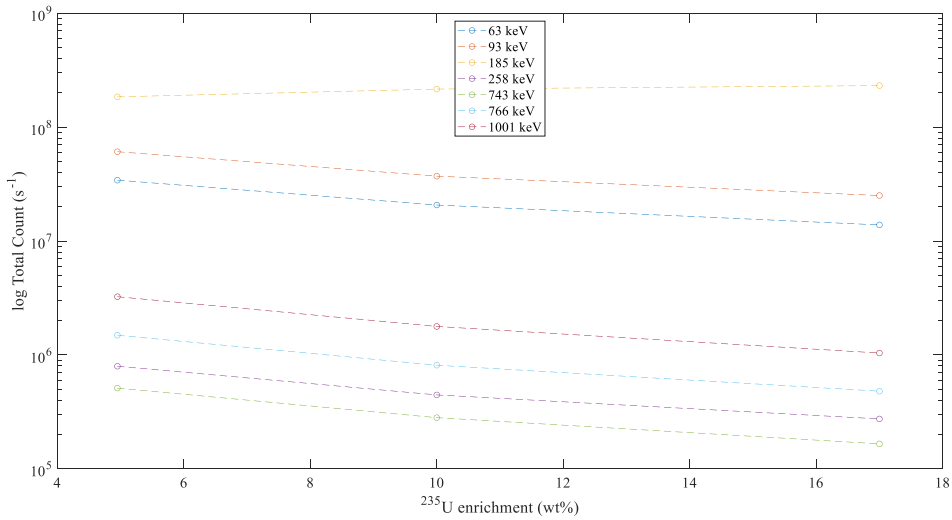

Figure 5-5. Total gamma radiation counts at several peaks of FFP spectra with different ^{235}U enrichments

5.5.2. One-year cooled SFP gamma spectroscopy

Nine gamma radiation spectra are obtained from simulation for each of the 10 wt% and 17 wt% one-year cooled SFP, along with five spectra for the 4.95wt% one-year cooled SFP. The spectral shapes for all SFPs are similar to Figure 5-6. The spectra of each SFP varies by its fuel burnup level. As the burnup changes, the change in isotopic composition also changes the emission intensity and hence the height of the gamma radiation peaks locally. This results in a relative change in the count ratio of a peak to the total count of a gamma spectrum. The relative count ratio of a spectrum is different from other spectra with different SFP parameter values.

Due to the relative peak ratio, the ^{137}Cs peak gathered from the spectroscopy is not directly linear with burnup as expected. At the same burnup, the ^{137}Cs signal is also different among different enrichment values. To deal with the relative peak ratio, a straight line with a maximum gradient from the ^{137}Cs spectral line (of the three pebbles) as a variation of the burnup level is used to correct all points in each spectrum.

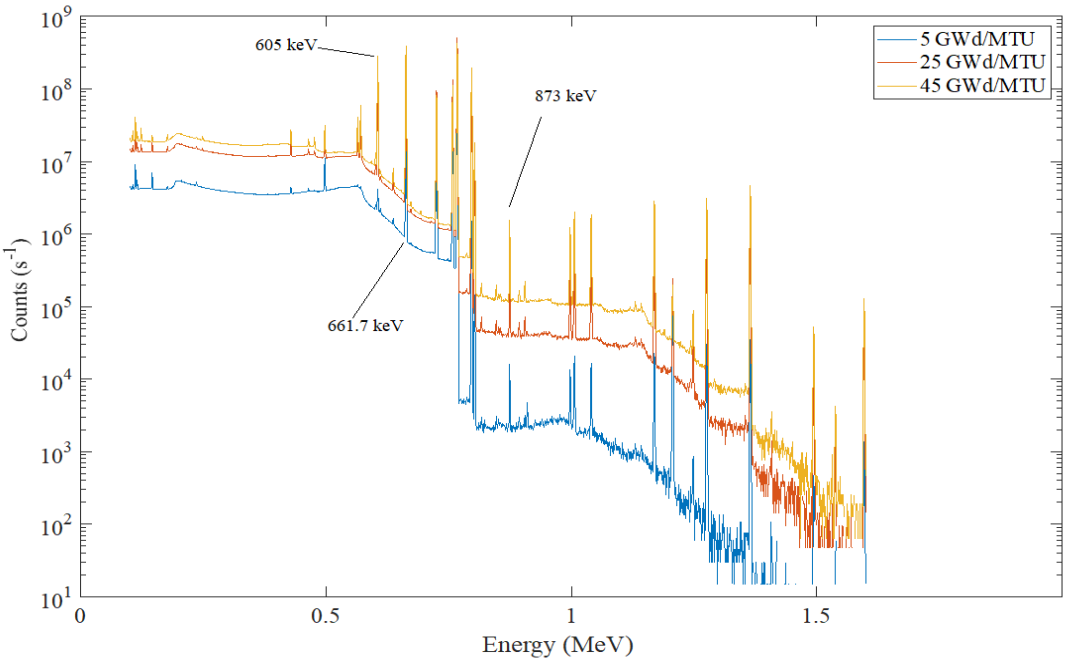

Figure 5-6. Spectrums of 1-y cooled 17wt% SFPs

Figure 5-7 shows the corrected total count of ^{137}Cs peak at 661.7 keV from three SFP types for varying burnup values. The total gamma radiation count profiles of ^{137}Cs are the same according to the atomic density profiles in the SFPs. All profiles have the same straight-line parameters regardless of their different initial ^{235}U enrichments. The corrected ^{137}Cs peak must be the first safeguards inspection checkpoint to verify the SFP's

burnup level, regardless of its initial ^{235}U enrichment. A similar yield of ^{137}Cs with uranium and plutonium fission makes this possible.

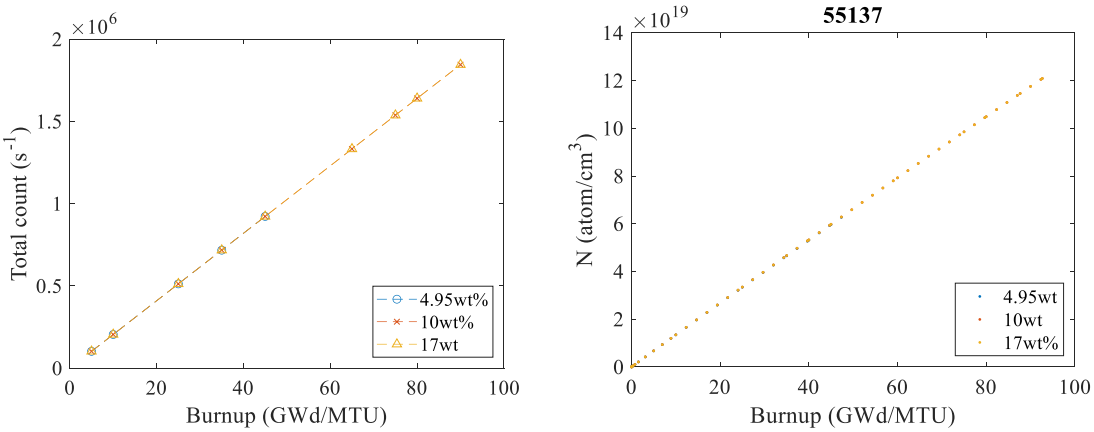

Figure 5-7. ^{137}Cs total count at 661.7 keV (left) and its density in the 1-y cooled SFP (right)

Other gamma energy peaks from ^{134}Cs are at energies 569, 605, 796, 802, 1039, 1168, and 1365 keV, ^{154}Eu at 873, 996, and 1005 keV have a different buildup behavior with fuel burnup. The response from these peaks varies with the initial ^{235}U enrichment values. Utilizing these peaks for SFP burnup verification is possible provided that the reactor is declared to use a certain FFP initial ^{235}U enrichment and that it can be verified before the FFP insertion into the core. The absence of this verification will result in a bias. Nevertheless, these peaks are very useful if they are used together with the ^{137}Cs peak to interpret the initial ^{235}U enrichment of the SFP once the fuel burnup has been determined using the ^{137}Cs peak.

The initial ^{235}U enrichment of the SFP can be determined using a total count ratio of either $^{134}Cs/^{137}Cs$ or $^{154}Eu/^{137}Cs$ (ref. Fig. 5-8). These ratios have a perfect straight-line linearity with fuel burnup. The gradient of the line represents the SFP's initial ^{235}U

enrichment. As the enrichment increases, the line will be less steep. The benefit of using these ratios is that they do not need the relative count correction, since the ratio will always be the same before and after the relative multiplier is applied. In practice, the isotopic ratio will need only a relative detector efficiency. Nevertheless, in PBR's multi-pass application, these ratios may not be used without or prior the SFP burnup level determination using the ^{137}Cs peak.

^{134}Cs is not a direct fission product. It is produced by the neutron capture reaction of a stable isotope of ^{133}Cs (with a cross section of approx. 30 barn) produced by the decaying of ^{133}Sb, ^{133}Te, ^{133}I, ^{133}Xe, and more, all of which are fission products. Hence, ^{134}Cs production needs at least 2 steps from the fissionable actinides. However, in general, its yield from ^{235}U is 1.27×10^{-5} and from ^{239}Pu is 9.89×10^{-4} (Phillips 1991). The higher yield from ^{239}Pu makes the ^{134}Cs quantity grow quadratically with increasing burnup. With a half-life of 2.06 years, ^{134}Cs would provide reliable information for spent fuel discharged from the core after one year.

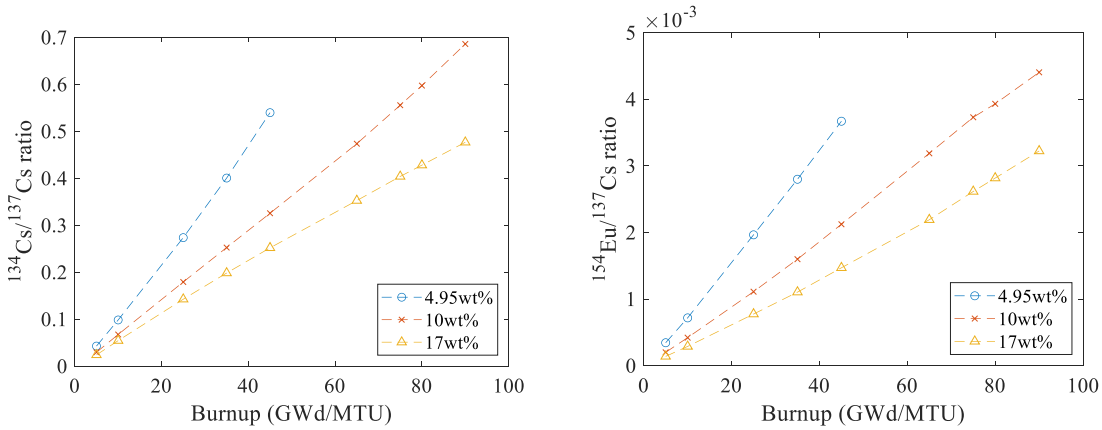

Figure 5-8. Count ratio of ^{134}Cs/^{137}Cs (left) and ^{154}Eu/^{137}Cs (right) of 1-y cooled SFP.

Like ^{134}Cs, ^{154}Eu is not a direct fission product. It is a product of a neutron capture reaction on ^{153}Eu, which is a direct fission product of uranium and plutonium. Hence, the signal characteristic generated by ^{154}Eu is very similar to ^{134}Cs. It is also yielded by plutonium more than by uranium. In the thermal spectrum, its yield from ^{239}Pu and from ^{235}U are 4.9E×10^{-7} and 1.95×10^{-9} per fission, respectively (IAEA 2021). Therefore, its value is increasing quadratically with burnup due to the increase of ^{239}Pu with fuel burnup. Its ratio with ^{137}Cs, as well as with ^{134}Cs, produces a straight-line relationship that can be used to distinguish the initial enrichment of SFP (ref. Fig. 5-8). With a half-life of 8.8 years, ^{154}Eu is applicable to characterize SFP stored for more than one year.

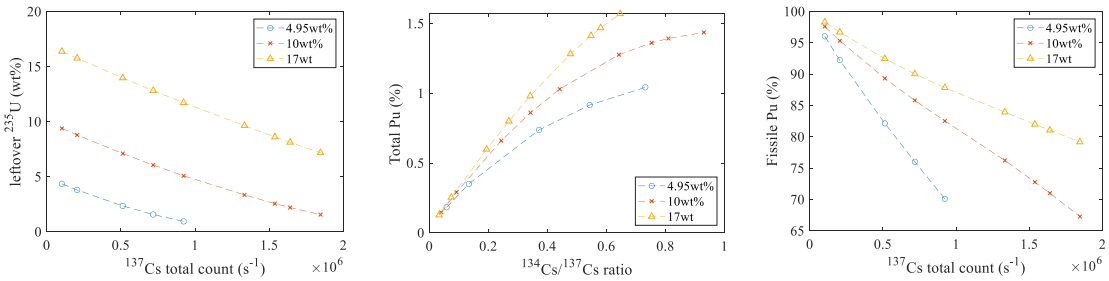

Figure 5-9. 661.7 keV and 605 keV peaks as the best leftover ^{235}U, total Pu, and fissile Pu indicators

When expressing the leftover ^{235}U and fissile Pu percentages, ^{137}Cs emerges as the best indicator, providing a clear and straightforward relationship between the quantities and the total count of 661.7 keV count. The total Pu percentages are found to be best indicated by the count ratio of ^{134}Cs to ^{137}Cs, which is similarly indicated by the count ratio of ^{154}Eu to ^{137}Cs. However, these indications cannot be implemented directly by measuring only ^{134}Cs and ^{137}Cs, since the determination of leftover ^{235}U, total Pu, and

fissile Pu percentages on a SFP must be preceded by the two work steps (burnup and ^{235}U initial enrichment determinations) explained previously.

5.5.3. Non-cooled SFP gamma spectroscopy

Since the SFP freshly discharged from the core contains many more fission products with short half-lives, its spectrum has many peaks that can be used to characterize the SFP (ref. Fig. 5-10). However, this could also be troublesome since a peak may be associated with more than one radionuclide. Also, a very close amplitude spacing between the peaks may introduce a neighborhood effect that distorts the peak of interest. Although the ^{137}Cs peak at 661.7 keV remains the best signature to identify the SFP burnup, the radionuclides used for identifying the SFP ^{235}U enrichment are quite different.

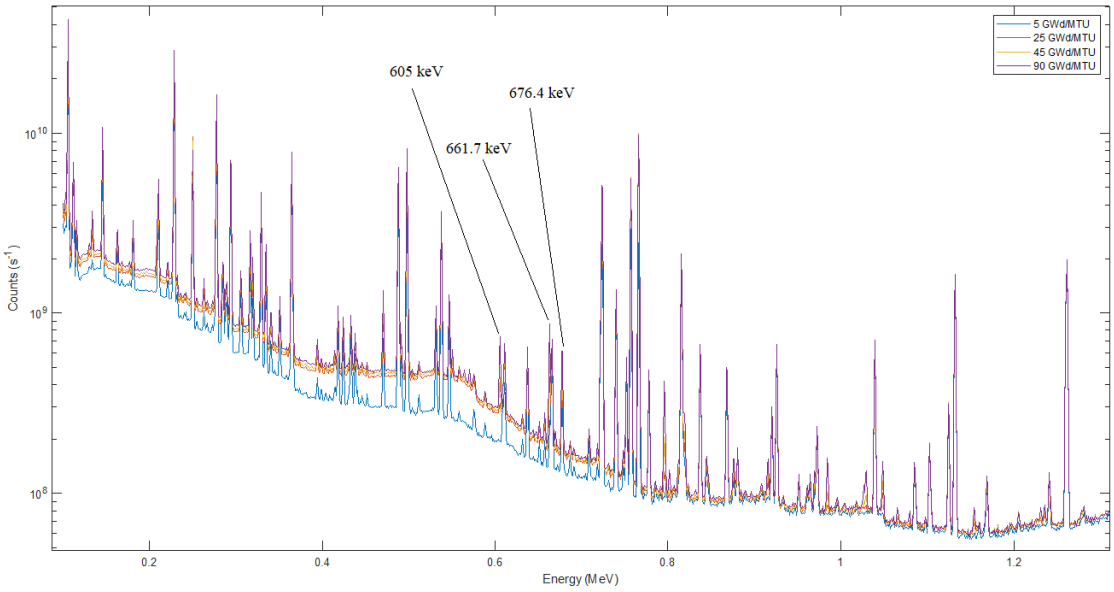

Figure 5-10. Spectrums of non-cooled 17 wt% SFPs

As opposed to the one-year cooled SFP gamma radiation spectra, the non-cooled SFP spectra cannot be used to identify the radionuclides from their peak area due the vast

number of radionuclides involved. The non-cooled SFP spectra do not have a significant relative signal strength issue due to their high total activities. Hence, they do not need the relative multipliers to correct the relative strength issue. The uncorrected profiles can distinguish the peak based on the ^{235}U enrichment of the fuel and the burnup value. The only issue with the spectra is selecting the peak height, due to the different in background activity of the spectra from different SFPs. This can be observed from the 661.7 keV peaks straight line profiles from different ^{235}U enrichments, which are different only by their intercepts (ref. Fig. 5-11). However, this happens locally at energies lower than 800 keV (ref. Fig 5.10). Hence, no global correction can be made to the non-cooled spectra. Without any correction, the count height of the peaks can be used to discriminate the SFP based on their ^{235}U enrichment and fuel burnup levels.

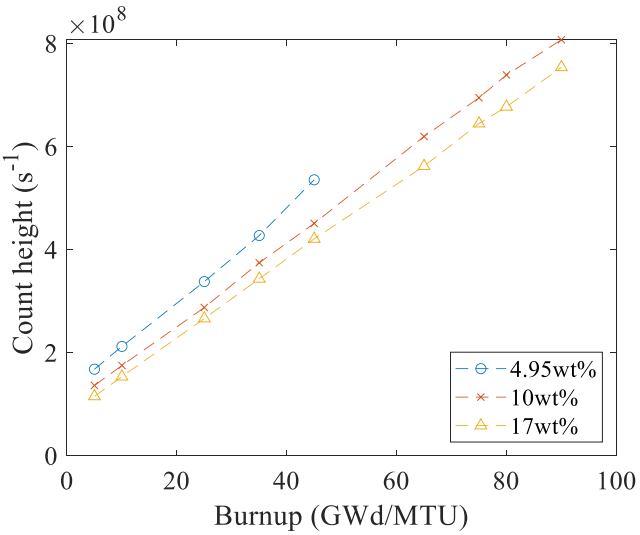

Figure 5-11. Uncorrected ^{137}Cs in the non-cooled SFP

A gamma energy peak of 676.4 keV can be identified as a signal from ^{105}Ru (ref. Fig. 5-12). The total counts within the spectra can distinguish the SFPs based on their ^{235}U enrichment and fuel burnup values. The fission yield for thermal neutron energy is

9.46×10^{-3} for ^{235}U and 5.76×10^{-2} for ^{239}Pu. Although its yield from ^{239}Pu is almost double, its half-life is only 4.44 hours. This causes its atomic density profile to become a straight-line with fuel burnup. However, its total count profile from the spectrometry provides valuable information about SFP burnup and ^{235}U enrichment, provided that its measurement is performed without any delay after the SFP is discharged. Since the fissile and fertile plutonium profiles have a straight-line relationship with fuel burnup (ref. Fig. 2.9), this relationship can also be used as a direct fissile or fertile plutonium indicator. As mentioned earlier, the estimation of initial uranium enrichment can be done if the fuel burnup has been already determined using the 661.7 gamma energy peak of ^{137}Cs.

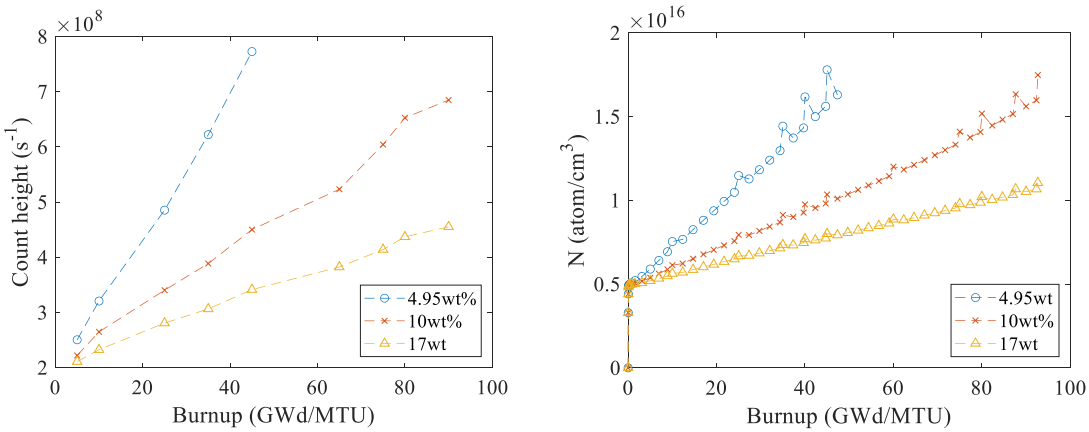

Figure 5-12. ^{105}Ru peak height at 676.4 keV (left) and its density in the non-cooled SFP (right)

The ratio of ^{134}Cs to ^{137}Cs gamma radiation peaks may still be used as a ^{235}U enrichment discriminator (ref. Fig. 5-13). Even though there are several gamma rays of different energies emitted by ^{134}Cs, the gamma radiation with energy 605 keV is the best gamma peak and can be identified relatively easily. However, the vast number of gamma energies involved in the non-cooled SFPs cause a signal-to-noise ratio that is poor and not

helpful in determining ^{235}U enrichment, especially at low fuel burnup. The ^{235}U enrichment cannot be identified properly in the spectra using ^{154}Eu peaks due to the same issue.

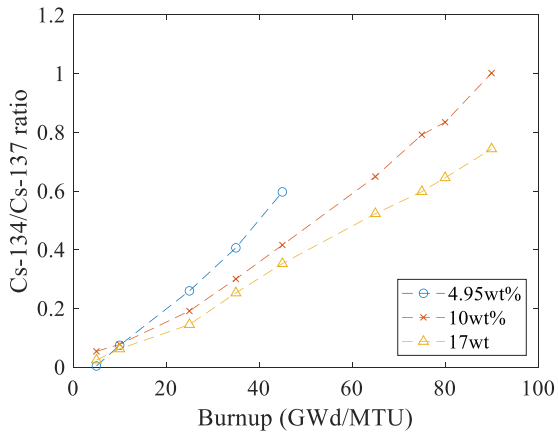

Figure 5-13. Count ratio of $^{134}Cs/^{137}Cs$ at ^{134}Cs peak of 605 keV from the non-cooled SFP

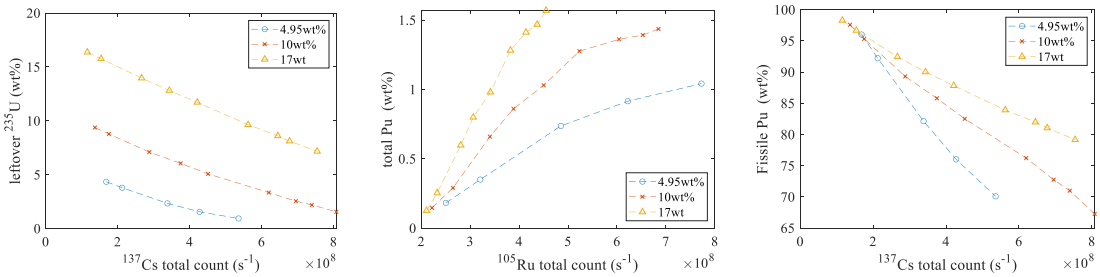

Figure 5-14. The best SNM indicators in the non-cooled SFPs

The 661.7 keV of ^{137}Cs is the best possible gamma peak to correlate directly to the leftover ^{235}U (ref. Fig. 5-14). However, the SFP initial ^{235}U enrichment must be determined prior to its use to avoid any bias of interpretation.

5.6. Online refueling monitoring system

The gamma spectroscopy system must be able to verify the FFP's initial ^{235}U enrichment, especially during an inspection of the fresh fuel storage. It must be done at

KMP-1, KMP-2, and KMP-3 if the facility uses fuels with various initial ^{235}U enrichments. However, since the risk of proliferation increases with the increase in initial ^{235}U enrichment, gamma spectroscopy should always be deployed at these KMPs to avoid a pebble replacement. Assuming that the same HTR-10 fuel parameters are also applied in HTR-PM, the initial enrichment of 17wt% must be estimated by the system with an uncertainty of 0.612wt% within one standard deviation, since the ITV for HPGe is 3.6%.

Table 5-2. Simulated measurement results and uncertainty in HTR-PM (uncertainties are within a level of confidence of 68%)

KMP	Simulated measurement results				uncertainty			
	Pebble Count (per year)	^{235}U (kg/y)	Total Pu (kg/y)	Fissile Pu (kg/y)	Pebble Count (per year)	^{235}U (kg/y)	Total Pu (kg/y)	Fissile Pu (kg/y)
KMP-1	262225	180.386			2623	9.688		
KMP-2	259625	178.597			2597	9.592		
KMP-3	2600	1.789			26	0.096		
KMP-4	771075	252.733	37.669	29.314	7711	13.577	2.023	1.574
KMP-5	257025	84.244	12.556	0.099	2571	4.526	0.525	0.525
KMP-6	257025	84.244	12.556	9.771	2571	4.526	0.525	0.525
KMP-7	2600	0.852	0.127	9.771	26	0.046	0.007	0.005
KMP-8	5200	1.704	0.254	0.198	52	0.092	0.014	0.011

The spectroscopy system should also be able to verify the initial ^{235}U enrichment, total plutonium, and fissile plutonium contained in a single SFP. The measurements of one-year cooled SFP can be deployed on the spent fuel storage only, which means it can only be done during inspection. However, the system on the non-cooled SFP can be deployed for the online operation. Based on the 3-passes simulation result, the system must be used to verify whether the SFP has leftover ^{235}U of 8.1wt% with an uncertainty of 0.292wt%, a total Pu content of 1.21wt% with an uncertainty of 0.043wt%, and a fissile Pu content of 0.94% with an uncertainty of 0.034wt%, which are all within one standard

deviation. All quantities are relative to the initial uranium metal load per pebble, which in this case is 4.407 g. These quantities may be different, depending on the fuel and operation parameters declared by the facility.

As mentioned earlier, all KMPs must include a pebble counter system to cope with the semi-bulk material in PBR. Assuming a uniform uncertainty of 1% for all counters, the total count of pebbles per year at each KMP and the respective SNM uncertainty is listed in Table 5.2. KMP-9 and KMP-10 are excluded, since the analysis is assuming there are no fuel pebbles sent into the GP storage.

The mass measurement system at each KMP is used to verify whether the pebble has the declared mass. The mass uncertainties in Table 5.2 are assuming that the measured pebble mass is declared as 200.2 g, including 5 g of UO_2. The *MUF* is assumed to be zero for all MBAs. Hence, the requirements of Eq. 5.2 and 5.3 are automatically fulfilled. However, in real application, the mass of all the pebbles will naturally not always be exactly the same and this will cause the MUF to be non-zero with more variants of the uncertainty. Meanwhile, the results in Table 5.2 can be used to determine whether uncertainties in mass measurements are less than one SQ to satisfy the nuclear material accountancy governing Eq. 5.4.

$$MUF_{MBA1} = m_{KMP1} - (m_{KMP2} + m_{KMP3})$$

$$MUF_{MBA2} = m_{KMP2} - m_{KMP5} - m_{KMP7} + m_{net\_incore}$$

$$MUF_{MBA3} = m_{KMP5} - m_{KMP6}$$

$$MUF_{MBA4} = m_{KMP3} + m_{KMP7} - m_{KMP8} \tag{5.7}$$

Equations 5.7 are used to calculate the MUF for each MBA derived from Eq. 5.1., where *m* is the measured mass at each KMP. Although the MUF for all MBAs is assumed to be zero, a measurement uncertainty within an MBA can be used to calculate its maximum allowable MUF based on Eq. 5.2. The uncertainties for these equations can be derived and calculated to calculate the maximum allowable MUF at each MBA per a timeliness goal of 3 months. In MBA-2, the increment and the decrement (the net mass in-core) of SNM within MBA-2 is not measurable but justifiable using KMP-2, KMP-5, and KMP-7, since the MUF is assumed as zero. The uncertainties for all MUF and allowable maximum MUF within each MBA for HTR-PM are listed in Table 5-3. Note that Eq. 5.4 requirement is met by all MBAs, which is a maximum of 75 kg for LEU and 8 kg for Pu, although no maximum requirement is applicable for the fissile Pu. The maximum MUF of ^{235}U in MBA-2 assumes that all pebbles are SFPs.

Table 5-3. Uncertainties and maximum allowable MUFs against SNM diversion scenario in HTR-PM

MBA	$3\sigma_{MUF}$ (kg/3-mo)			Maximum MUF (pebbles/3-mo)		
	^{235}U	Pu	Fissile Pu	^{235}U	Pu	Fissile Pu
MBA-1	10.23			13,650		
MBA-2	7.96	0.51	0.39	22,283	9,508	9,508
MBA-3	4.80	0.72	0.56	13,445	13,445	13,445
MBA-4	0.11	0.01	0.01	295	215	215

6. CONCLUSIONS

6.1. Summary

A high-fidelity model of a typical pebble bed reactor (PBR) core was developed, and multiple fuel burnup simulations were carried out using this model. The PBR model was developed using the Monte Carlo N-particle (MCNP) radiation transport code. The PBR fuel burnup simulations performed included variations in the enrichment of ^{235}U in the fuel (4.95, 10, and 17 wt%), as well as refueling schemes (one-batch, single-pass, and multi-pass). In the one-batch refueling scheme, the reactor is operated until it reaches subcriticality, at which point all the fuel pebbles in the core are replaced with fresh fuel. For the single-pass refueling scheme, the reactor core is divided into 33 axial fuel zones, or layers, and each of the 33 fuel-pebble-containing layers moves downward in the core with no fuel recirculation; instead, fresh pebbles are inserted at the top layer of the core. For the multi-pass refueling scheme, the core is divided radially into three zones in addition to 33 axial layers, and each pebble is passed through the core three times to achieve the target burnup.

To support nuclear safeguards approach development for the PBR, separate MCNP simulations were performed to produce the gamma radiation energy spectra of the fresh and spent fuel pebbles.

The results of multiple fuel burnup simulations provided quantitative estimates of the amounts of uranium, plutonium, and key fission products (^{137}Cs, ^{134}Cs, ^{154}Eu, and ^{105}Ru) present at various fuel burnup time steps, which is utilized for the proliferation

resistance (PR) assessment of a small and a large PBR. These estimates also form the basis for developing safeguards approaches for a typical PBR.

The PR assessments were carried out using an existing code, namely, PRAETOR (proliferation resistance analysis and evaluation tool for observed risk). However, PRAETOR was later found not to be suitable for performing a PR assessment of the PBR, and hence a new methodology was developed as part of this study. The PR values of the PBR were compared with those of a typical pressurized water reactor (PWR).

The new PR assessment methodology uses only four attributes (spontaneous fission neutrons, heat load, radiation load, and Rossi-α) compared to the 68 attributes used by the existing PRAETOR methodology. The calculated PR can be used to optimize the reactor system design to minimize the risk of nuclear proliferation at the design phase.

The PR assessment results for the PBR show that the relative PR of ^{235}U diversion is lower, since the ^{235}U enrichment falls under the high-assay low enriched uranium (HALEU) category. At a lower fuel burnup (5 GWd/MTU), ^{235}U diversion analysis showed a lower PR compared to Pu diversion by 4.8% (0.394 vs. 0.413). Conversely, at a higher fuel burnup (90 GWd/MTU), Pu diversion scenarios are found to have lower PR compared to ^{235}U diversions by 0.8% (0.399 vs. 0.402).

MCNP fuel burnup simulations of PBR show that, at the target burnup of 80 GWd/MTU, the 17 wt% fuel pebble produces Pu with a fissile isotope (^{239}Pu and ^{241}Pu) percentage of 81.1% relative to its total Pu, which is a reasonably good quality plutonium for use in a NED. At the same burnup level, the 10 wt% fuel pebble produces a fissile Pu portion of 71.13% relative to its total Pu. At 35 GWd/MTU, they become respectively

91.12% and 85.94% for the 17 wt% and the 10 wt% fuel pebbles. And with an initial enrichment of 4.95 wt%, the fissile plutonium portion is 82.42% at 35 GWd/MTU. Hence, the spent fuel of the PBR is attractive for proliferation if the fuel has sufficiently high ^{235}U enrichment and it is discharged at low burnup. Increasing the fuel burnup increases the total plutonium quantity.

A PBR with a 250 MWth output can yield 1.9 SQ of Pu and 1.73 SQ of LEU per year with a fissile Pu quantity of 82.9% at 65.9 GWd/MTU using a one-batch refueling scheme. By deploying an online refueling scheme, these numbers can be decreased. With a 15 MWd/MTU higher burnup, the OTTO online refueling scheme (at 80 GWd/MTU) may yield 1.78 SQ of Pu and 1.23 SQ of LEU per year with a fissile Pu quantity of 79.7%. The multi-pass refueling scheme does not decrease the numbers. In fact, at the same 80 GWd/MTU, the 250 MWth PBR with 3-pass refueling scheme may produce 1.73 SQ of Pu and 1.24 SQ of LEU. However, the quality of Pu decreases to 77.8%.

The OTTO refueling scheme uses more ^{235}U in the core. Moreover, although the amount of total plutonium is lower, its quality is 4.6% higher than the one-batch scheme based on the fissile content. However, this is not an issue with the discharged spent fuel. Since the OTTO refueling scheme can make the fuel pebbles reach a higher burnup level, the leftover ^{235}U and the fissile Pu decrease. At 75 GWd/MTU, the OTTO refueling scheme discharges the SFPs with a leftover ^{235}U portion of 8.86 wt% and a fissile Pu portion of 81.9% (of the total plutonium). These decrease with increasing burnup level.

In terms of the spent fuel discharged in the OTTO refueling scheme, the total plutonium content increases linearly with burnup, which reaches 1.18wt%, 1.25wt%, and

1.33wt% relative to the initial uranium loading for the 75, 80, and 90 GWd/MTU, respectively. However, its quality decreases with a burnup level at 80.97%, 79.40%, and 77.10%, respectively. As expected, the leftover ^{235}U decreases linearly with burnup at 8.86wt%, 8.18wt%, and 7.21wt% for the 75, 80, and 90 GWd/MTU, respectively. With this, the PR decreases as the fuel gains a higher burnup level, although the total plutonium increases. For safeguards purposes, this aspect can be monitored easily within the OTTO refueling scheme, since no fuel is sent back into the core, and the refueling rate can be used as a safeguards parameter. However, this would not be easy in the multi-pass refueling scheme, since the burnup among the pebbles may vary greatly and any pebble may be diverted by passing it through the core fewer times than it should.

By assuming a uniform refueling pattern, period, and the same number passes for the fuel pebble, the three-pass refueling scheme produces a lower fissile plutonium by 2.4% and a lower total plutonium by 3.3% in the SFP than the OTTO refueling scheme, although it leaves slightly higher ^{235}U by 0.3%. The multi-pass scheme reduces the quality of plutonium, since the utilization of ^{239}Pu for power production is higher than for the OTTO. Although these increase the mean of the PR, they do not significantly increase the PR of the three-pass scheme. At 80 GWd/MTU, the three-pass scheme has a mean value of PR 0.3109 ± 0.0043 compared to the 0.3037 ± 0.0044 of the OTTO within a confidence interval of 99%. This suggests that a higher number of fuel pebbles passes than the three-pass refueling scheme, which may increase the PR of PBR.

The developed PR assessment methodology provides a rapid way to assess an intrinsic proliferation barrier of a reactor design. It is feasible to use the outcomes of this

methodology to optimize the reactor design from a safeguards perspective. Coupled with a simulation code, it provides a relative measure to assess the intrinsic PR quantitatively. An infinite lattice fuel model is sufficient to optimize the fuel design, while a full core modeling would also enable an optimization on other reactor materials.

The comparison between the PBR and LWR systems shows that, at a power level of 500 MWth and a burnup level of 38.5 GWd/MTU, the PBMR produces a total plutonium of 1.19wt% relative to its initial uranium loading, which is more than the iPWR produces (0.95wt%). Due to its higher ^{235}U enrichment, the PBR produces spent fuel with a high ^{235}U content (5.44wt% from 9.6wt%), while the iPWR produces its spent fuel with a much lower ^{235}U content (1.56% from 4.95wt%). At this burnup level, the Pu of the iPWR contains fissile isotopes of 70.7%, while the PBR does 84.9%, respective to their total produced Pu. Therefore, the PBR system has more leftover ^{235}U, more total Pu, and more fissile Pu in its spent fuels, which leads to a higher risk of proliferation, either in ^{235}U diversion or in Pu diversion.

The high quantity and quality of SNM production in the PBR is due to a high overall neutron thermalization in the system, causing a high neutron fission and capture rate within the thermal and intermediate energies. A high ^{239}U transmutation is found in the PBR system, which leads to a high ^{239}Pu production. In addition, its fewer fast neutrons above 1 MeV causes a low ^{238}Pu production. These lead the PBR system to have a lower PR than the PWR system. Its proliferation risk is higher when the fuel pebbles have a lower burnup level. In the real practice, the multi-pass refueling scheme enables the operator to discharge a low burnup level SFP.

At its discharged burnup, the simulated SFP in the PBMR contains 156.4 kg of leftover ^{235}U per period, which amounts to1.27 SQ per year, while it is only 0.99 SQ per year in the iPWR. The Pu produced by the PBMR is 5.91 SQ per year with a fissile content of 78.06%. This is similar to the SFP in the iPWR system, which is about 5.89 SQ per year with a fissile content of 70.69%. In terms of Pu diversion, the intrinsic PR of the PWR system (0.345 ± 0.002) is higher than for the PBR system (0.282 ± 0.001). However, the PR of U diversion for both reactor systems is the same (PWR: 0.263 ± 0.001 vs. PBR: 0.261 ± 0.001).

With this result, the PBR system cannot be proven to pose a lower proliferation risk than the current PWR technology. However, with its safety advantages, the PBR is still a feasible option for implementation in an energy system. The proliferation risk can be mitigated by implementing a proper safeguards approach. The proposed minimum safeguards approach is found to be sufficient for the modelled material flow within a 250 MWth core module of the PBR. The developed safeguards approach is found to mitigate the proliferation risk associated with PBR system, especially the one associated with its online refueling issue. Focusing on the SNM quantities, the initial ^{235}U enrichment, and the SFP burnup level, gamma spectroscopy is found to be a suitable means for verification in the safeguards approach. Gamma spectroscopy enables the values of those parameters to be verified during a safeguards inspection with or without the multi-pass scheme.

The ^{137}Cs gamma energy peak measurement (661.7 keV) is a powerful signature to quantify the burnup level of SFPs. Its independence with respect to ^{235}U enrichment

allows the SFP gamma measurement to enable the burnup level measurement consistently in a multi-pass refueling scheme.

On a one-year cooled SFP, once the burnup level has been determined, gamma energy lines of ^{134}Cs, ^{154}Eu, and lines ratio of ^{134}Cs/^{137}Cs and ^{154}Cs/^{154}Eu can be used to quantify the SFP's initial ^{235}U enrichment. On a non-cooled SFP, gamma energy lines of ^{105}Ru and a ratio of ^{134}Cs/^{137}Cs are found to be useful to distinguish the SFP's initial ^{235}U enrichments. These lines can act as direct SNM quantity indicators, provided that the initial ^{235}U enrichment and the burnup level of SFP has been determined. A relationship to the weight fraction of the SNM is preferred to the SNM quantity to accommodate the various masses of the pebbles due to the loading difference in the number TRISOs in each pebble. In practice, the pebble mass can be determined using a typical mass measurement.

6.2. Key contributions

Key contributions of this dissertation study include:

- Estimated the burnup-dependent masses of uranium, plutonium, and key fission products in the fuel through high-fidelity MCNP simulations of a typical PBR by considering variations in ^{235}U enrichments in the fuel as well as refueling schemes.
- Developed a new methodology for intrinsic PR assessment of nuclear fuel cycle systems to rank various uranium and plutonium diversion scenarios.
- Carried out PR assessments of the PBR for the aforementioned core simulation attribute (^{235}U enrichment and refueling scheme) variations

and the PR values generated for the PBR case were compared with that of a PWR. PR comparison showed that PBR is not better than PWR.

- Proposed a new nuclear safeguards approach for the PBR, which consists of multiple material balance areas (MBAs), key measurement points (KMPs), and the corresponding material balance periods (MBPs). This new safeguards approach utilizes the mass measurements of the pebbles and gamma spectroscopy of key fission product isotopes (^{137}Cs, ^{134}Cs, ^{154}Eu, and ^{105}Ru) to estimate fuel burnup, uranium enrichment, left over masses of uranium and plutonium in the spent fuel pebble.

6.3. Suggested future work

Due to the unavailability of a physical spent fuel sample, the proliferation risk quantification in this study is based on simulated data using stochastic radiation transport simulation. Computationally, the data on isotopic estimates of SFP generated by MCNP is reliable, but verification with measured data is needed to validate the proposed nuclear safeguards approach.

Real gamma spectroscopic measurements of SFPs with various burnups and cooling periods will be extremely useful for the NMA aspect of the PBR. Not all gamma radiation signal information can be fully captured manually from the spectroscopic measurements. This will be an issue in the real round-the-clock application. An artificial intelligence technique, such as a neural network, may be studied and implemented to use all the information within a gamma radiation spectrum.

The developed safeguards approach involves an item counter that has not been developed for pebble counting. A statistical analysis on how the counter performs should be investigated.

REFERENCES

Acir, A., and H. Coskun. "Neutronic analysis of the PBR-400 full core using thorium fuel mixed with plutonium or minor actinides." *Annals of Nuclear Energy 48* (Annals of Nuclear Energy 48, 45-50), 2012: 45-50.

Aoki, T., S.S. Chirayath, and H. Sagara. "Proliferation Resistance Evaluation of an HTGR Transuranic Fuel Cycle Using PRAETOR Code." *Annals of Nuclear Energy 141*, 2020: 107325.

Brown, F.B., and W. R. Martin. "Stochastic Geometry Capability in MCNP5 for The Analysis of Particle Fuel." *Annals of Nuclear Energy 31*, 2004: 2039-2047.

Charlton, W.S., et al. "Proliferation Resistance Assessment Methodology for Nuclear Fuel Cycles, Nuclear Technology." *Nuclear Technology 157*, 2007: 143-156.

Chirayath, S.S., C.R. Schafer, and G.R. Long. "A New Methodology to Estimate Stochastic Uncertainty of MCNP-Predicted Isotope Concentrations in Nuclear Fuel Burnup Simulations." *Annals of Nuclear Energy 151*, 2021: 107911.

Chirayath, S.S., et al. "Proliferation Resistance Analysis and Evaluation Tool for Observed Risk (PRAETOR)—Methodology Development." *Journal of Nuclear Materials Management XLIII No.2*, 2015.

Conti, C.C., I.C.P Salinas, and H. Zylberberg. "detailed procedure to simulate an HPGE detector with MCNP5." *Progress in Nuclear Energy 66*, 2013: 35-40.

Dudley, T., P. Villiers, W. Bouwer, O. Tsaoi, and E. Mulder. "The Reactor Core Neutronic Model for The Pebble Bed Modular Reactor." *Nuclear Engineering and Design 238*, 2008: 3002-3012.

Durst, P.C. *INL/EXT-12-26561 Safeguards-by-Design: Guidance for High Temperature Gas Reactors (HTGRs) With Pebble Fuel.* Idaho National Laboratory, 2012.

Durst, P.C., et al. *INL/EXT-09-16782: Nuclear Safeguards Considerations for the Pebble Bed Modular Reactor (PBMR).* Idaho National Laboratory, 2009.

Ensslin, N. "Principles of Neutron Coincidence Counting." In *NUREG/CR-5550 LA-UR-90-732: Passive Nondestructive Assay of Nuclear Materials Manual*. U.S. Nuclear Regulatory Commission, 1991.

Erighin, M.A. "A 48-month extended fuel cycle for the B&W mPower Small Modular Nuclear Reactor." *PHYSOR 2012 – Advances in Reactor Physics.* American Nuclear Society, 2012.

Fensin, M. L, and M Umbel. "Testing actinide fission yield treatment in CINDER90 for use in MCNP6 burnup calculations." *Progress in Nuclear Energy 201585*, 2015: 719-728.

Fensin, M. L., M. R. James, and J. D. Galloway. "Performance Upgrades to the MCNP6 Burnup Capability for Large Scale Depletion Calculations." *Progress in Nuclear Energy 83*, 2015: 186-190.

IAEA. *Cummulative Fission Yields.* 2021. https://www-nds.iaea.org/sgnucdat/c3.htm (accessed May 27, 2021).

—. *IAEA-TECDOC-1382: Evaluation of high temperature gas cooled reactor performance: Benchmark analysis related to initial testing of the HTTR and HTR-10.* Vienna: International Atomic Energy Agency, 2003.

—. *IAEA-TECDOC-1694: Evaluation of High Temperature Gas Cooled Reactor Performance, International Atomic Energy Agency.* Vienna: International Atomic Energy Agency, 2013.

—. *International Nuclear Verification Series No 3: IAEA Safeguards Glossary.* Vienna: International Atomic Energy Agency, 2001.

—. *Nuclear Data Section.* July 15, 2020. https://www-nds.iaea.org/relnsd/vcharthtml/VChartHTML.html.

—. *STR-368 International Target Values 2010 for Measurement Uncertainties in Safeguarding Nuclear Material.* Vienna: International Atomic Energy Agency, 2010.

Ion, S., D. Nicholls, R. Matzie, and D. Matzner. "Pebble bed modular reactor – the first-Generation IV reactor to be constructed." *Nuclear Energy 43 No. 1*, 2004: 55-62.

KAERI. *Table of Nuclides.* March 20, 2021. http://atom.kaeri.re.kr/nuchart/.

Kaplan, A.C., et al. "Determination of total plutonium content in spent nuclear fuel assemblies with the differential die-away self-interrogation instrument." *Nuclear Instruments and Methods in Physics Research Section A: Accelerators, Spectrometers, Detectors and Associated Equipment Vol. 764*, 2014: 347-351.

Kepisty, G., P. Stanisz, and J. Cetnar. "Monte Carlo burnup in HTR system with various TRISO packing." *Annals of Nuclear Energy 92*, 2016: 419-430.

Kiedrowski, B.C., F.B. Brown, and P.P.H. Wilson. "Calculating Kinetics Parameters and reactivity Changes with Continuous-energy Monte Carlo." *PHYSOR 2010 – Advances in Reactor Physics to Power the Nuclear Renaissance.* American Nuclear Society, 2010.

Kitcher, E.D. "Performance and Safety Analysis of Generic Small Modular Reactor." *MS Thesis at Texas A&M University*, 2012.

Kitcher, E.D., and S.S. Chirayath. "Neutronics and thermal hydraulics analysis of a small modular reactor." *Annals of Nuclear Energy 97*, 2016: 232-245.

Lamarsh, J. R, and A. J. Baratta. *Introduction to Nuclear Engineering 3rd edition.* Prentice Hall, 2001.

Metcalf, R.R.M. *New Tool for Proliferation Resistance Evaluation Applied to Uranium and Thorium Fueled Fast Reactor Fuel Cycles.* MS Thesis , College Station: Texas A&M University, 2009.

Mulyana, D., and S.S. Chirayath. "Investigation of Nuclear Safeguards Attributes Through Neutronic Simulation of Pebble Bed Reactor Core." *ANS Transactions Volume 121 Number 1* (ANS Transactions, Volume 121, Number 1), 2019: 1063-1066.

Nakano, Y., and T. Okubo. "Plutonium isotopic composition of high burnup spent fuel discharged from light water reactors." *Annals of Nuclear Energy 38*, 2011: 2689-2697.

NEA. *The Joint Evaluated Fission and Fusion File* . January 1, 2021. https://www.oecd-nea.org/dbdata/jeff/jeff33/index.html.

Pelowitz, D.B. et al. *LA-CP-13-00634: MCNP6 User's Manual Version 1.0 Rev. 0.* Los Alamos National Laboratory, 2013.

Phillips, J.R. "Irradiated Fuel Measurement." In *NUREG/CR-5550 LA-UR-90-732: Passive Nondestructive Assay of Nuclear Materials Manual*. U.S. Nuclear Regulatory Commission, 1991.

Rosales, J., A. Munoz, C. Garcia, C. Brayner, J. Perez, and A. Abanades. "Computational Model for the Neutronic Simulation of Pebble Bed Reactor's Core Using MCNPX." *International Journal of Nuclear Energy*, 2014.

Simnad, M. T. "The easy history of high-temperature helium gas-cooled nuclear power reactors." *Energy vol 16 Issues 1-2*, 1991: 25-32.

Smith, H.A. "The measurement of uranium enrichment." In *NUREG/CR-5550 LA-UR-90-732: Passive Nondestructive Assay of Nuclear Materials Manual*. U.S. Nuclear Regulatory Commission, 1991.

Stewart, J.E. "Principles of Total Neutron Counting." In *NUREG/CR-5550 LA-UR-90-732: Passive Nondestructive Assay of Nuclear Materials Manual*. U.S. Nuclear Regulatory Commission, 1991.

Teuchert, E., and K.A. Haas. "Nonproliferation Issue of the Pebble Bed High-Temperature Reactor, Nuclear Technology." *Nuclear Technology* 72, no. 2 (1986).

Tran, N. T., and V. K. Hoang. "Neutronic characteristic of an OTTO refueling PBMR." *Nuclear Engineering and Design Vol. 253*, 2012: 269-276.

Turkmen, M., and U. Colak. "Effect of pebble packing on neutron spectrum and the isotopic composition of HTGR fuel." *Annals of Nuclear Energy 46*, 2012: 29-36.

Wang, M.J., R.J. Sheu, J.J Oeir, and J.H Liang. "Criticality calculations of the HTR-10 pebble-bed reactor with SCALE6/CSAS6 and MCNP5." *Annals of Nuclear Energy 64*, 2014: 1-7.

Wu, S.R., S.C. Wu, D.S. Chao, and J. H. Liang. "Burnup computations of online-refueling process for pebble bed reactors using layer-mixed-shell fuel movement model." *Applied Radiation and Isotopes 147*, 2019: 1-6.

Wu, Z., D. Lin, and D. Zhong. "The design features of the HTR-10." *Nuclear Engineering and Design 218*, 2002: 25-32.

Xu, Y., S. Hu, F. Li, and S. Yu. "High temperature reactor development in China." *Progress in Nuclear Energy 47 (1-4)*, 2005: 260-270.

APPENDIX A

PRAETOR INPUT

Table A.1. PRAETOR input attributes, their weights and designated utility values for the infinite-lattice simulation

i	Attribute	u_i value	Weight (k_i)
Stage 1. Diversion			0.333
	Subgroup 1.1: Material handling difficulty during diversion		0.175
1	Mass per SQ	κ_1 (kg)	0.178
2	Volume per SQ	κ_2 (m^3)	0.170
3	Number of items per SQ	κ_3	0.162
4	Material form	Solid	0.080
5	Radiation level in term of dose	κ_4 ($Sv.hr^{-1}$)	0.186
6	Chemical reactivity	With air: no, with water: no, with steel (fast): no, with plastic (fast): no, with steel (slow) no, with plastic (slow): no	0.076
7	Temperature of the source process	25 ^oC	0.089
8	Heat load of material	κ_5 ($W.cm^{-3}$)	0.060
	Subgroup 1.2 Difficulty in evading detection, material accounting & control system		0.173
9	Uncertainty in accountancy measurements	1 SQ/yr	0.281
10	expected vs. actual material unaccounted for	10 SQ	0.281
11	Frequency of measurements	Never	0.203
12	Amount of material available	1.5 SQ (^{235}U) and 4.8 SQ (Pu)	0.234
13	Probability of detection	0.1%	1.000
	Subgroup 1.3 Difficulty of covertly making facility modification		0.157
14	Is there any space for modification?	0 (No)	0.173
15	Number of people for modifications	20 count	0.173
16	Whether remote handling tools required?	0 (No)	0.126
17	Whether specialization tools required	0 (No)	0.126
18	Whether the process need to be halted?	0 (No)	0.135
19	Risk of modification with respect to safety	0	0.126

i	Attribute	u_i value	Weight (k_i)
20	Risk of penetrating containment	100%	0.143
	Subgroup 1.4 Difficulty of evading IAEA with covert facility modifications & process monitoring		0.173
21	Probability of getting caught by IAEA Accounting	0.001	0.500
22	Probability of detection by process monitoring	0.001	0.500
	Subgroup 1.5 Physical Protection Threat Spectrum		0.175
23	Nuclear material containment and surveillance	Category 2, No surveillance, no seals, no remote or attended monitoring	1.000
24	Computerized accounting system presence	None	1.000
25	Perceived adversary Design Basis Threat (DBT)	0 (No DBT with high adversary capabilities)	1.000
26	Physical protection system for outsider threats	0 (least)	1.000
27	Physical protection system for insider threats	0 (least)	1.000
Stage 2. Transportation			0.186
	Subgroup 2.1 Material handling difficulty during transportation		0.510
28	Mass per SQ	κ_1 (kg)	0.1901
29	Volume per SQ	κ_2 (m^3)	0.182
30	Material form	solid	0.124
31	Radiation level in term of dose	$\kappa 4$ ($Sv.hr^{-1}$)	0.207
32	Heat load of material	$1.5\kappa_5$ ($W.cm^{-3}$)	0.094
33	Chemical reactivity	With air: no, with water: no, with steel (fast): no, with plastic (fast): no, with steel (slow) no, with plastic (slow): no	0.053
34	Immediate chemical toxicity	1 ppm (highest)	0.070
35	Time averse chemical toxicity	1,000 ppm (least)	0.078
	Subgroup 2.2 Difficulty of evading detection during transportation		0.490
36	Mass of material and transportation container	$0.5\kappa_1$ (kg)	0.189
37	Volume of material and transportation container	$0.5\kappa_2$ (m^3)	0.151
38	Heat load of material	$1.5\kappa_5$ ($W.cm^{-3}$)	0.104
39	Shield thickness required to reduce radiation field to 10mR/hr	κ_6 (m)	0.104
40	Host country size	1,904,569 km^2	0.160
41	Number of declared nuclear facilities	34 count	0.151
42	IAEA imagery analysis rate	0 count/month	0.142
Stage 3. Transformation			0.277

i	Attribute	u_i value	Weight (k_i)
	Subgroup 3.1 Facilities and equipment needed to process diverted material		0.338
43	Number of process steps to metallic form	8 count-table	0.340
44	Number of export control equipment/materials required	107 counts	0.377
45	Minimum electrical requirement	1 MWe	0.282
	Subgroup 2: Workforce required for transformation		0.357
46	Number of unskilled workers required	120 person-years	0.125
47	Number of skilled workers required	30 person-years	0.273
48	Number of advanced degree workers required	10 person-years	0.308
49	Number of technical experts required	5 person-years	0.294
	Subgroup 3.2: Difficulty of evading detection of transformation activities		0.301
50	IAEA Additional Protocol in force?	no	0.144
51	Long-range environmental sampling rate	0 sampling/month	0.119
52	Sensitivity of IAEA equipment	0%	0.156
53	Isotopic signatures	2 (uranium target) 4 (Plutonium target)	0.150
54	Facility size	2500 m^2	0.136
55	Heat load of transformation process	0.0001 MWth	0.062
56	Sonic load	0 dB	0.056
57	Radiation load	κ_7 ($R.hr^{-1}SQ^{-1}$)	0.050
58	Volume of non-naturally occurring gases emitted	κ_8 ($Ci.y^{-1}SQ^{-1}$)	0.067
59	Volume of undiluted radioactive liquid emissions	643(Ci/yr) after one-year cooling	0.062
Stage 4. Weaponization			0.223
	Subgroup 1: Difficulty associated with design		0.353
60	Spontaneous fission neutron emission rate	κ_9 ($n.s^{-1}g^{-1}$)	0.197
61	Radiation exposure at one meter	κ_{10} ($R.hr^{-1}SQ^{-1}$)	0.159
62	Heating rate of weapons material	κ_{11} ($W.kg^{-1}$)	0.137
63	Whether ballistic assembly methods can be used?	no	0.199
64	Number of phases in nuclear material phase diagram	7 count	0.308

i	Attribute	u_i value	Weight (k_i)
	Subgroup 2: Handling difficulty and skills for design		0.272
65	Radiation level in terms of dose	κ_{12} (Sv.hr^{-1}SQ^{-1})	0.337
66	Chemical reactivity	With air: no, with water: no, with steel (fast): no, with plastic (fast): no, with steel (slow) no, with plastic (slow): no	0.359
67	Radiotoxicity	1 (very high)	0.304
68	Knowledge and skills needed to design and fabricate	0 for uranium target, 1 for plutonium target	1.000

Table A.2. PRAETOR utility values for various refueling schemes.

i	Attribute	u_i value							
		leftover ^{235}U diversion				Pu diversion			
		1p-29d	1p-31d	1p-35d	3-passes	1p-29d	1p-31d	1p-35d	3-passes
1	mass per SQ (kg)	16813.83	18419.65	20620.74	18350.96	13608.08	12694.29	11997.52	13141.34
2	volume per SQ	21.74949	23.82669	26.6739	23.73784	17.6027	16.42067	15.51936	16.99894
3	number of items per SQ	192307.7	210674.2	235849.1	209888.5	155642	145190.6	137221.3	150303.6
4	material form	All in solid							
5	radiation level in terms of dose (Sv/h/SQ) TOTAL	0.20	0.26	0.36	0.28	0.17	0.18	0.21	0.20
6	chemical reactivity	n n n n n n							
7	temperature of the source process	25							
8	heat load of material	7.14E-04	7.14E-04	7.93E-04	7.14E-04	7.14E-04	7.14E-04	7.93E-04	7.14E-04
9	uncertainty in accountancy measurements	1							
10	expected vs material unaccounted for (MUF)	0							
11	frequency of measurements	never							
12	amount of material available	1							
13	probability of detection	0.001							
14	Space for modification	0							
15	number of people for modification	0.00001							
16	remote handling tools requirement	0							
17	special tool requirement	0							
18	process suspension	0							
19	safety risk of modification	0							
20	risk of penetrating containment	100							
21	Probability of getting caught by IAEA	0.001							
22	probability of detection by process monitoring	0.001							
23	Nuclear material containment and surveillance	2nnn				2nnn			
24	Computerized accounting system presence	none							
25	Perceived adversary Design Basis Threat [DBT]	0							

i	Attribute	u_i value							
		leftover ^{235}U diversion				Pu diversion			
		1p-29d	1p-31d	1p-35d	3-passes	1p-29d	1p-31d	1p-35d	3-passes
26	Outsider threats for physical protection system	0							
27	Insider threats for physical protection system	0							
28	mass per SQ	16813.83	18419.65	20620.74	18350.96	13608.08	12694.29	11997.52	13141.34
29	volume per SQ	21.75	23.83	26.67	23.74	17.60	16.42	15.52	17.00
30	material form	All in solid							
31	radiation level in terms of dose TOTAL Sv/hr/SQ	0.20	0.26	0.36	0.28	0.17	0.18	0.21	0.20
32	heat load of material	1.07E-03	1.07E-03	1.19E-03	1.07E-03	1.07E-03	1.07E-03	1.19E-03	1.07E-03
33	chemical reactivity	n n n n n n							
34	immediate chemical toxicity	1							
35	time averse chemical toxicity	1000							
36	mass of material and transportation container	8406.92	9209.83	10310.37	9175.48	6804.04	6347.15	5998.76	6570.67
37	volume of material and transportation container	10.87	11.91	13.34	11.87	8.80	8.21	7.76	8.50
38	heat load of material	1.07E-03	1.07E-03	1.19E-03	1.07E-03	1.07E-03	1.07E-03	1.19E-03	1.07E-03
39	shield thickness to reduce radiation (m)	6.46E-02	6.66E-02	6.93E-02	6.73E-02	6.28E-02	6.35E-02	6.47E-02	6.45E-02
40	host country size	1904569							
41	number of declared nuclear facilities	34							
42	IAEA imagery analysis rate	0							
43	number of steps to metallic form	8							
44	number of export-controlled equipment	107							
45	minimum electrical equipment	1							
46	number of unskilled workers required	120							
47	number of skilled workers required	30							
48	number of advance degree worker	10							
49	number of technical experts	5							
50	is additional protocol in force?	0							
51	long range environmental sampling rate	0							

i	Attribute	u_i value							
		leftover ^{235}U diversion				Pu diversion			
		1p-29d	1p-31d	1p-35d	3-passes	1p-29d	1p-31d	1p-35d	3-passes
52	sensitivity of IAEA equipment	0							
53	isotopic signatures	2				4			
54	facility size	2500							
55	heat load of transformation process	0.0001							
56	sonic load	0							
57	radiation load R/h	63.23	77.86	101.68	84.02	51.18	53.66	59.16	60.17
58	volume of non-naturally occurring gasses emitted	4170913	5011192	6330135	5020994	3375681	3453569	3682988	3595592
59	undiluted volume of liquid emission	643							
60	spontaneous fission product rate n/s/g	3.55E-03				187.67	194.78	210.10	204.80
61	radiation exposure at one-meter R/h/SQ	1.21E-05				1.30E-03	1.52E-03	1.86E-03	1.56E-03
62	heating rate of weapons material	4.34E-05				5.25	5.92	7.07	6.09
63	whether ballistic assembly method can be used?	0							
64	number of phases in phase diagram	7							
65	radiation level in terms of dose	1.21E-07				1.3E-05	1.52E-05	1.86E-05	1.56E-05
66	chemical reactivity	n n n n n n							
67	radio-toxicity	1							
68	knowledge and skill level for weapon type alternatives	1				1			

APPENDIX B

MCNP INPUT SCRIPTS

```
PBR Infinite lattice model
1    1  -10.4 -1  VOL=6.54498E-05 u=1 imp:n=1         $ UO2 kernel VOL=6.54498E-05
2    2 -1.05  1 -2                u=1 imp:n=1         $ Buffer coating
3    2 -1.9   2 -3                u=1 imp:n=1         $ IPyC coating
4    3 -3.18  3 -4                u=1 imp:n=1         $ SiC coating
5    2 -1.9   4 -5                u=1 imp:n=1         $ OPyC coating
6    4 -1.73  5                   u=1 imp:n=1         $ Graphite matrix
7    0 -6  7 -8  9 -10  11  lat=1 u=2 imp:n=1 fill=1  $ SC
8    0 -12                        u=3 imp:n=1 fill=2  $ active fuel sphere of fuel ball
9    4 -1.73  12 -13              u=3 imp:n=1         $ graphite shell of fuel ball
10   0 -21                        u=3 imp:n=1 fill=2  $ 1/8 fuel ball in lattice [ 1  1  1]
11   0 -22                        u=3 imp:n=1 fill=2  $ 1/8 fuel ball in lattice [ 1  1 -1]
12   0 -23                        u=3 imp:n=1 fill=2  $ 1/8 fuel ball in lattice [ 1 -1 -1]
13   0 -24                        u=3 imp:n=1 fill=2  $ 1/8 fuel ball in lattice [ 1 -1  1]
14   0 -25                        u=3 imp:n=1 fill=2  $ 1/8 fuel ball in lattice [-1  1  1]
15   0 -26                        u=3 imp:n=1 fill=2  $ 1/8 fuel ball in lattice [-1  1 -1]
16   0 -27                        u=3 imp:n=1 fill=2  $ 1/8 fuel ball in lattice [-1 -1 -1]
17   0 -28                        u=3 imp:n=1 fill=2  $ 1/8 fuel ball in lattice [-1 -1  1]
20   4 -1.73 21 -41               u=3 imp:n=1         $ 1/8 fuel ball in lattice [ 1  1  1]
21   4 -1.73 22 -42               u=3 imp:n=1         $ 1/8 fuel ball in lattice [ 1  1 -1]
22   4 -1.73 23 -43               u=3 imp:n=1         $ 1/8 fuel ball in lattice [ 1 -1 -1]
23   4 -1.73 24 -44               u=3 imp:n=1         $ 1/8 fuel ball in lattice [ 1 -1  1]
24   4 -1.73 25 -45               u=3 imp:n=1         $ 1/8 fuel ball in lattice [-1  1  1]
25   4 -1.73 26 -46               u=3 imp:n=1         $ 1/8 fuel ball in lattice [-1  1 -1]
26   4 -1.73 27 -47               u=3 imp:n=1         $ 1/8 fuel ball in lattice [-1 -1 -1]
27   4 -1.73 28 -48               u=3 imp:n=1         $ 1/8 fuel ball in lattice [-1 -1  1]
18   5 -0.0001604 13 21 22 23 24 25 26 27 28
                     41 42 43 44 45 46 47 48 u=3 imp:n=1     $ Helium fill
19   0 31 -32 33 -34 35 -36 fill=3 imp:n=1
31   0 -31:32:-33:34:-35:36  imp:n=0         $ outside world

1  so 0.025 $ UO2 kernel
2  so 0.034 $ Porous buffer, thickness = 95 micron
3  so 0.038 $ IPyC, thickness = 40 micron
4  so 0.0415 $ SiC,  thickness = 35 micron
5  so 0.0455 $ OPyC, thickness = 40 micron
6   px  0.099389 $ [ 1  0  0]
7   px -0.099389 $ [-1  0  0]
8   py  0.099389 $ [ 0  1  0]
9   py -0.099389 $ [ 0 -1  0]
10  pz  0.099389 $ [ 0  0  1]
11  pz -0.099389 $ [ 0  0 -1]
c -------------Fuel pebble and lattice----------------------------------------
12  so  2.5 $ fuel region radius
13  so  3.0 $ Ball radius
21  s   3.592147675  3.592147675  3.592147675  2.5 $[ 1  1  1]
22  s   3.592147675  3.592147675 -3.592147675  2.5 $[ 1  1 -1]
23  s   3.592147675 -3.592147675 -3.592147675  2.5 $[ 1 -1 -1]
24  s   3.592147675 -3.592147675  3.592147675  2.5 $[ 1 -1  1]
25  s  -3.592147675  3.592147675  3.592147675  2.5 $[-1  1  1]
26  s  -3.592147675  3.592147675 -3.592147675  2.5 $[-1  1 -1]
27  s  -3.592147675 -3.592147675 -3.592147675  2.5 $[-1 -1 -1]
28  s  -3.592147675 -3.592147675  3.592147675  2.5 $[-1 -1  1]
41  s   3.592147675  3.592147675  3.592147675  3 $[ 1  1  1]
42  s   3.592147675  3.592147675 -3.592147675  3 $[ 1  1 -1]
43  s   3.592147675 -3.592147675 -3.592147675  3 $[ 1 -1 -1]
44  s   3.592147675 -3.592147675  3.592147675  3 $[ 1 -1  1]
45  s  -3.592147675  3.592147675  3.592147675  3 $[-1  1  1]
46  s  -3.592147675  3.592147675 -3.592147675  3 $[-1  1 -1]
47  s  -3.592147675 -3.592147675 -3.592147675  3 $[-1 -1 -1]
48  s  -3.592147675 -3.592147675  3.592147675  3 $[-1 -1  1]
*31  px -3.592147675
*32  px  3.592147675
*33  py -3.592147675
*34  py  3.592147675
*35  pz -3.592147675
*36  pz  3.592147675

mphys on
kcode 15000 1 40 200
```

```
c ksrc  0 0 0
sdef pos=0 0 0 axs=0 0 1 rad=d1  ext=d2 erg=2
si1 0 3
sp1 -21 1
si2 -3 3
sp2 -21 1
URAN     2 0.0538 0.0538 0.0538         $ Applying stochastic geometry to fuel
burn  time=.3 .3 .4 .5 1 2.5 5 10 20 24.1286899 25 25 14.1286899 30
           30 30 30 30 30 12.3860697 30 30 30 30 8.257379802 30 30
           4.128689901 30 30 4.128689901 30 30 30 30 30 30 12.3860697
           30 30 30 30 30 30 12.3860697 30 30 4.12868990130 30 30 30
           8.257379802 30 30 4.128689901 $in days
      pfrac=1 1 1 1 1 1 1 1 1 1 1 1 1 1 1 1 1 1 1 1 1 1 1 1 1 1 1 1 1
            1 1 1 1 1 1 1 1 1 1 1 1 1 1 1 1 1 1 1 1 1 1 1 1 1 1 1 1 1
      power=0.000687144 $ (MWth)
      mat=1
      matvol=0.961538462 $ in cm3
      bopt=1.0 -24 1.0
m1   92235.83c -0.1498225      $ Uranium dioxide 80%, density = 10.4 g/cc
      92238.83c -0.7314863     $ enrichment = 17%
      8016.83c  -0.1186872
      5010.83c  -7.37235e-07
      5011.83c  -3.26275e-06
m2    6000.83c   1 $ Carbon coatings
mt2 grph.10t
m3   14028.83c  -0.64561
      14029.83c  -0.03269
      14030.83c  -0.0217
      6000.83c  -0.3 $ SIC coating
m4    6000.83c   1             $ Graphite matrix & shell
mt4 grph.10t
m5  2003.83c -0.00000137
     2004.83c -0.99999863     $ Helium
```